FROM microRNAS TO MITOCHONDRIA IN THE MACROPHAGE RESPONSE TO *MYCOBACTERIUM TUBERCULOSIS*

(AND INFLAMMASOME ACTIVATION IN COVID-19)

by
Monika Marie Looney

A dissertation submitted to Johns Hopkins University in conformity with the requirements for

the degree of Doctor of Philosophy

Baltimore, Maryland
March 2021

Abstract

Tuberculosis (TB) and COVID-19 are two major infectious disease problems. While TB is caused by a slow growing bacterium, *Mycobacterium tuberculosis* (*Mtb*), and COVID-19 is caused by a virus, severe acute respiratory syndrome coronavirus 2 (SARS-CoV-2, SARS-COV-2), both diseases have widespread impact on human health and share many common pathologies. Outcome of infection with both pathogens is heavily influenced by the response of host macrophages. Here we use a combination of unbiased and targeted approaches, including transcriptomics, methylomics, and cytokine analysis to evaluate immunological responses in human macrophages exposed to *Mtb* and SARS-CoV-2. Using *in vitro* macrophage exposure models and both unbiased and targeted analysis approaches, we find that the macrophage response to *Mtb* is shaped by changes in the production of small non-coding RNAs, including microRNAs (miRNAs) and tRNA-derived fragments (tRFs), gene expression, methylation, mitochondrial responses, while host responses to SARS-CoV-2 are shaped by macrophage-mediated viral sensing and inflammasome activation.

Using next generation sequencing, we show that certain miRNAs are consistently dysregulated in *Mtb* infection. These miRNAs target a number of differentially expressed genes involved in processes central to the anti-TB response, including immune cell activation, macrophage lipid metabolism, and blood vessel development. Many genes involved in immune cell activation and metabolic reprogramming were also subject to changes in methylation. Additionally, we investigate dysregulation of tRFs, a novel form of small non-coding RNA that have never before been studied in the context of bacterial infections. We find that tRFs are significantly dysregulated in infection with *Mtb* and that dysregulated tRFs derive primarily from the host mitochondrial genome. Fluorescent imaging shows that increased abundance of

mitochondria-biased tRFs is linked to recruitment of a tRF cleaving enzyme Angiogenin (ANG) and the apoptotic suppressor x-linked inhibitor of apoptosis protein (XIAP) to host mitochondria. Finally, we investigate the role of the inflammasome in SARS-COV-2 infection and find that SARS-COV-2 stimulates activation of the NLRP3 inflammasome through MyD88-mediated direct sensing of extracellular virus in macrophages, but not nasal or lung epithelial cells.

Taken together, our studies show that the macrophage plays a central role in the host response to both *Mtb* and SARS-COV-2 infection and that macrophage responses are shaped by a network of pre- and post-transcriptional molecular regulatory factors.

Primary Reader and Advisor: Petros C. Karakousis

Secondary Reader: William Bishai

Preface

I would like to acknowledge my thesis advisor, Dr. Petros Karakousis, my thesis committee members, Drs. William Bishai, Anne Hamacher-Brady, and Marc Halushka, the director of my PhD Program, Dr. Lee Martin, and my many colleagues at the Center for Tuberculosis Research for their mentorship and guidance throughout the course of my PhD. I would also like to thank our administrators, namely Stacey March, for their help with ensuring the completion of all of my degree requirements. I also acknowledge the blood donors from the Blood Donor Center at the Anne Arundel Medical Center who have helped make this work possible. Finally, I would like to thank my friends and family for their undying support and encouragement.

Dedication

This dissertation is dedicated to my family and friends who have always been my biggest supporters and who have encouraged me to achieve my ambitions.

Quotes

“TB is the biggest baddest bug out there.” – Gyanu Lamichhane

“The only good TB bug is a dead one.” – Jacques Grosset, Petros Karakousis

“Don’t worry about COVID. Things will be back to normal in a couple months.” – Petros Karakousis

Contents

List of Tables

List of Figures

Chapter 1: Introduction

1.1 *Mycobacterium tuberculosis* and SARS-CoV-2, the old and new of pandemic-causing diseases

Tuberculosis (TB) and COVID-19 were the most deadly infectious diseases caused by single infectious agents in 2020 [1, 2]. While caused by very different pathogens, these diseases are inherently linked as pandemic-causing respiratory infections that disproportionately affect those living in poverty [1].

In 2019, TB caused 1.4 million deaths and approximately 10 million new illnesses [1]. TB incidence is heavily influenced by health disparities and ~95% of TB cases occur in low and middle income countries [1, 3]. While TB incidence has been steadily declining in recent years, estimates from the WHO indicate that global TB deaths may increase by an additional 200,000 – 400,000 in 2020 alone and that new TB cases may increase by an additional one million per year between 2020 and 2025 [1]. These increases are largely attributed to disruptions and reprioritizations of TB tracking, health services, and economic resources during the COVID-19 pandemic. While *Mycobacterium tuberculosis* (*Mtb*), the bacterium that causes TB, has been the top cause of death due to a single infectious agent since 2015, in 2020, it was surpassed by severe acute respiratory syndrome coronavirus 2 (SARS-CoV-2), the virus that causes COVID-19 [4]. By the end of 2020, COVID-19 had caused 1.8 million deaths worldwide, and the number continues to increase rapidly [2]. Like TB, rates of COVID-19 are higher in economically disadvantaged communities and for people of color [5, 6].

Due to its sudden and appearance and enormous impact on human health and daily life, COVID-19 has received worldwide attention that has resulted in an unprecedented response from

governments, industry, academic science, medicine, and public health organizations. This response has led to the rapid development of novel vaccines and treatments for COVID-19 that have and will continue to prevent severe disease and save lives. However, the "COVID problem" is far from solved. Many unknowns regarding the pathobiology of SARS-COV-2 infection and COVID-19 disease remain. Even as vaccines and treatments become more widely available, it is critical that research continues to learn about the fundamental mechanisms that drive development of COVID-19 disease and impact outcome of infection.

In contrast to COVID19, TB constitutes a persistent public health crisis that has caused disease in humans for thousands of years [1, 7]. Despite its long-standing impact on human health, the TB problem remains unsolved due to significant gaps in dedicated resources and the complexity of the disease itself. Though vaccines and treatments to prevent and cure TB exist, they are not sufficient for eradicating the disease from the world population and are becoming less effective over time. The Bacille Calmette-Guérin (BCG) vaccine has been in use as an anti-TB vaccine since the early 1920s and has limited efficacy in preventing TB in adults, but remains the only approved vaccine for TB. [8, 9]. However, multiple new candidates, including the M72/AS01$_E$ vaccine and intravenous BCG are in development, yielding promising results [1, 10, 11]. Similarly to the BCG vaccine, the main antibiotic components of the first-line regimen for treating drug-susceptible TB (isoniazid, rifampin, pyrazinamide, and ethambutol) have remained unchanged for decades. However, major developments for second line treatments have been made and new candidates are moving through clinical trials [1, 12]. Despite this progress, the COVID19 pandemic has significantly derailed TB control efforts around the world. While many COVID19 response measures were modeled after or built upon existing TB management infrastructure, the COVID19 pandemic will undoubtedly delay the achievement of the Sustainable Development

Goals for ending TB [1]. Especially in the wake of this most recent pandemic, elimination of TB will require a revitalization of integrated efforts similar to those seen in the response to COVID19.

On a biological level, *Mtb* and SARS-COV-2 may seem entirely unrelated. *Mtb* is a slow-growing bacterium which can survive and proliferate both intra- and extracellularly [13]. SARS-COV-2 is a positive-sense single-stranded RNA virus which can survive outside of a host for short periods of time, requiring invasion of host cells to replicate and cause disease [14, 15]. *Mtb* primarily infects innate immune cells, such as macrophages [13]. SARS-COV-2 relies on infection of nasopharyngeal and lung epithelial cells for producing new viable viral particles, however infection with SARS-COV-2 also stimulates a response from uninfected immune cells [13, 16, 17]. Despite these differences, *Mtb* and SARS-COV-2 display various similarities in their pathogenesis. Both organisms can be spread via aerosol transmission, which leads to infection of the respiratory tract and lungs. While it is suspected that most people who are exposed to either *Mtb* or SARS-COV-2 will not develop active disease symptoms, those individuals who develop disease can experience a spectrum of symptoms ranging from mild cough to death [13-16]. Worse outcomes are associated with a dysregulated immune responses that cause severe respiratory symptoms and long term residual tissue damage [13, 16].

For TB and COVID19, the biological factors that determine which individuals mount an effective response to clear the infection and which go on to develop severe disease remain largely unknown. Research aimed at investigating how host responses shape disease progression are critical for understanding infection outcome and for driving development of effective vaccines and treatments required for eradication of both TB and COVID19. The following thesis details my efforts to improve our understanding of the innate immune responses to infection with *Mtb* and SARS-COV-2.

Chapter 2: Regulation of the Macrophage Response to *Mycobacterium tuberculosis* infection

2.1 Background

2.1.1 Altered microRNA expression and DNA methylation during *Mtb* infection

Macrophages, phagocytic innate immune cells, are the primary cell type infected by *Mtb.* The host's ability to control *Mtb* infection is dependent upon regulation of various cellular processes, including activation of macrophages which carry out cell-mediated killing of *Mtb*, formation of lipid-laden "foamy macrophages" via alteration of metabolism and lipid synthesis, and cell-to-cell signaling to coordinate innate and adaptive immune responses [18-21]. However, *Mtb* has evolved virulence mechanisms to dysregulate such host responses and promote its own survival [19, 22]. While it is known that *Mtb* infection drives changes in expression of host genes involved in these pathways, mechanisms by which *Mtb* alters host transcriptional responses to subvert macrophage-mediated killing are not well understood.

Many key host transcriptional pathways are controlled by microRNAs (miRNAs) and epigenetic changes (primarily methylation of promoter regions). *Mtb* infection has been shown to dysregulate miRNA expression and alter methylation patterns in infected host cells [23, 24]. However, most of the published studies in this area suffer from two critical limitations: 1) biased or limited scope of analysis, and 2) reliance on cancer-derived cell lines [25-30]. Previous studies on miRNA and epigenetic regulation focus primarily on specific entities pre-selected as being "of interest" based on their known function in TB disease [25-29]. Although targeted approaches are very powerful for examining the role of specific miRNAs and methylation changes in *Mtb*-host interactions, they are unable to provide a global understanding of transcriptional networks

regulating host defenses against *Mtb* infection and cannot identify novel host regulatory factors involved in these processes. Furthermore, transcriptional and epigenetic analysis of immortalized cell lines is limited by the observation that such cells at baseline display dysregulation of small regulatory RNAs, epigenetic markers, and messenger RNA (mRNA) [25, 30].

2.1.2 Transfer RNA-derived fragments in human disease

Like miRNAs, tRNA-derived fragments (variably termed tRFs, tDRs, tiRNAs, or tRNA halves), are a diverse class of small non-coding RNAs, which are generated in response to host cell stress across a variety of disease states [31-33]. The term "tRFs" encompasses various subtypes of tRNA-derived molecules, including tRF-1, tRF-3, tRF-5, i-tRF, and tiRNAs. These tRFs may derive from the cell's nuclear or mitochondrial genome. The human nuclear genome encodes 433 tRNAs and the mitochondrial genome encodes 22 mitochondrial tRNAs (mtRNAs), each of which serves as a source of tRFs [34]. tRFs block translation by interfering with the eIF4F complex and polysomes [35, 36]. As in the case of miRNAs, they may also complex with Argonaute machinery to regulate protein expression via translational repression and mRNA target degradation [37-40]. Several studies reported increased tRF formation in cancer [41, 42] and viral infection [43]. However, the potential role of tRFs has not been studied during infection with *Mtb* or other bacterial pathogens.

2.1.3 Mitochondrial responses to *Mycobacterium tuberculosis*

Many of the innate signaling pathways that determine outcome of infection are also influenced by mitochondrial responses [44, 45]. During infection with *Mtb*, mitochondria play a particularly important role by determining if a cell will undergo apoptosis or necrosis. When infected with avirulent mycobacteria, macrophages tend to initiate apoptosis, which is characterized by the recruitment of BAX/BAK pore-forming proteins to the outer mitochondrial

membrane (OMM), release of cytochrome C from the mitochondrial intermembrane space into the cytoplasm, formation of an apoptosome, and activation of proteolytic caspase enzymes [46]. This process is associated with containment of bacteria, clearance of infection, and minimal activation of inflammatory processes [47]. Given the overall outcome, in this context, apoptosis can be classified as a host-beneficial response. Alternatively, during infection with virulent *Mtb*, macrophages may undergo necrosis, a proinflammatory programmed cell death pathway characterized by retention of cytochrome C in the mitochondria, swelling of the mitochondria, and eventually rupture of the OMM and degradation of macrophage cell membranes [46, 47]. Largely due to the breakdown of macrophage membranes, necrosis leads to bacterial escape, which allows previously contained *Mtb* to infect neighboring cells, or replicate extracellularly within granulomas [47]. Some mitochondria-dependent pathways, including apoptosis, can be regulated by miRNAs, so it is possible that they may also be associated with tRF production [25].

2.2 Key macrophage responses to infection with *Mycobacterium tuberculosis* are co-regulated by microRNAs and methylation

We hypothesized that *Mtb* alters transcriptional responses in infected macrophages to favor intracellular bacillary survival by modulating the expression of miRNAs and the methylation patterns of key host defense genes. Using unbiased next-generation sequencing (NGS) and high-throughput DNA methylation profiling, we provide an integrated analysis of dysregulated small RNAs, methylation patterns, and transcriptional pathways during *Mtb* infection of human monocyte-derived macrophages (MDMs).

2.2.1 Methodologies

Ethics

The use of MDMs from human donors for this study was approved by the Johns Hopkins University Institutional Review Board (JHU IRB). All samples were de-identified by the Blood Donor Center of the Anne Arundel Medical Center, Maryland, USA prior to use in these studies. The authors did not have any contact with donors. All experiments using donor-derived MDMs were deemed non-human subjects research by the JHU IRB.

Bacterial cultures

The virulent *Mtb* strain H37Rv-*lux* was used for all studies. H37Rv-*lux* contains the full bacterial luciferase operon, *luxAB*, which constitutively expresses luciferase and its substrate luciferin, thus producing a robust luminescent signal measured in relative light units (RLU), which serves as a reliable and instantaneous readout for colony forming units (CFU) [48]. H37Rv-*lux* was cultured in 7H9 + 10% OADC + 0.05% Tween-80 + 0.2% glycerol at 37°C in a shaking incubator or made into frozen stocks kept at -80°C in 7H9 + 10% OADC + 0.05% Tween-80 + 10% glycerol. Three frozen stocks were thawed and used to confirm a viable bacterial density of $1x10^8$ CFU/ml. These frozen stocks were used directly for infection of primary human MDMs.

Isolation of primary human MDMs

Primary human peripheral blood mononuclear cells (PBMCs) were isolated from platelet-depleted whole blood from healthy human donors using standard Ficoll-paque density gradient centrifugation (GE Healthcare, Cat# 17144003). Monocytes were isolated from the buffy coat using passive plastic adherence to cell culture plates at 37°C, 5% CO_2, for 4 hours in serum-free media (RPMI-1640 + 4mM L-glutamine). After a 4-hour incubation, non-adherent lymphocytes

and erythrocytes were washed away five times in 1X phosphate buffered saline (PBS). Adherent monocytes were allowed to differentiate into macrophages over a period of one week at 37°C, 5% CO_2, in complete media containing 10% non-heat inactivated fetal bovine serum (FBS) (RPMI 1640 + 4mM L-glutamine + 10% FBS). Media was changed every 2-3 days.

Infection of MDMs with *Mtb*

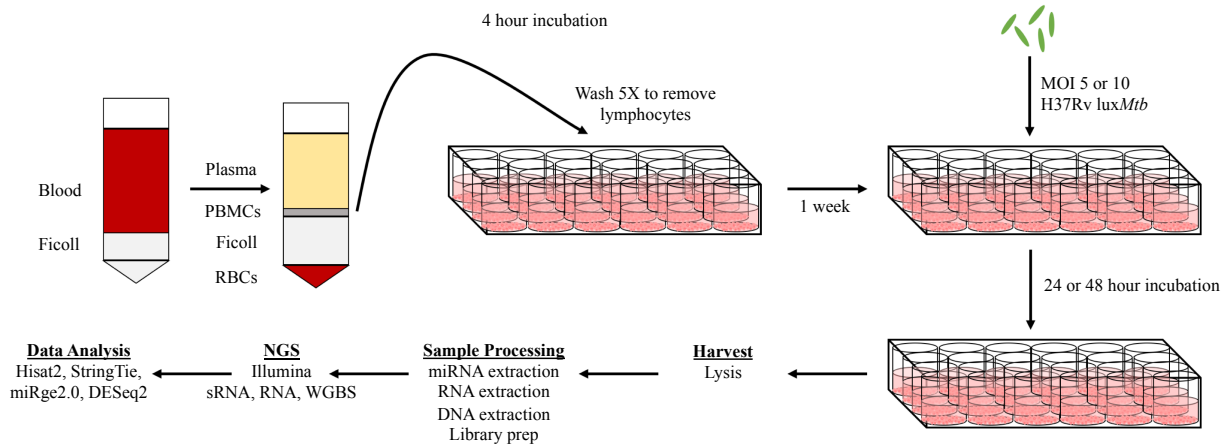

Figure 1. Experimental workflow diagram.
Platelet-depleted whole blood from healthy human donors was used for isolation of primary human monocytes. Peripheral blood mononuclear cells (PBMCs) were isolated using Ficoll-paque gradient separation. PBMCs were incubated in serum-free media for four hours to allow for monocyte adherence to cell culture plates. After incubation, non-adherent lymphocytes were washed away with 1X PBS. Monocytes were allowed to differentiate in complete media containing 10% FBS for 1 week, and then infected with luminescent Mtb (H37Rv-lux) for 24 or 48 hours. At each time point, cells were lysed in TRIzol for RNA extraction, library preparation, and sequencing. Sequencing analysis was performed using miRge2.0 and DESeq2 packages in R.

After 7 days of differentiation, primary human MDMs were infected with *Mtb* H37Rv-*lux* at a multiplicity of infection (MOI) of 5 or 10 for 24 or 48 hours. Infected cells and uninfected controls were incubated in complete cell culture media (described above) at 37°C, 5% CO_2 (**Figure 1**). At each time point post-infection, MDM viability was measured by 3-(4,5-dimethylthiazol-2-yl)-5-(3-carboxymethoxyphenyl)-2-(4-sulfophenyl)-2H-tetrazolium) (MTS) assay (**Figure 2**) and

measured for bacterial burden by single tube luminometer (**Figure 3**) [49]. Matched wells for each sample were also harvested for RNA isolation in TRIzol reagent (ThermoFisher).

Assessment of MDM viability

MDM viability was determined by MTS assay (Promega, CellTiter 96® AQueous One Solution Cell Proliferation Assay, Cat # G3582). At 24 and 48 hours post-infection, triplicate wells were incubated with MTS reagent for 4 hours, following manufacturer protocol. Reactions were read in a BMG Labtech Optima Fluorescence Microplate Reader (**Figure 2**).

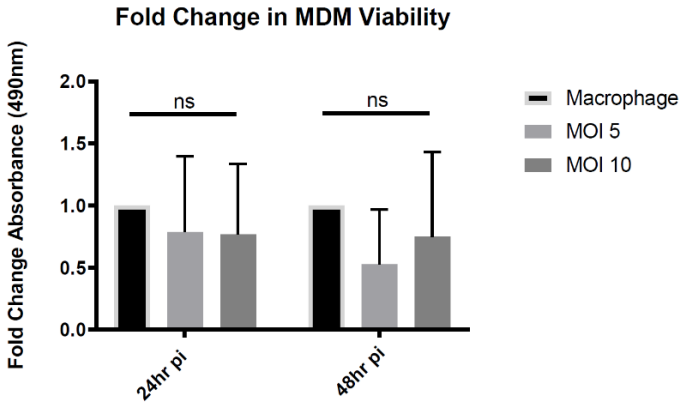

Figure 2. Assessment of host cell viability in *Mtb*-infected primary human MDMs. Macrophage viability of primary MDMs infected with H37Rv-*lux* for 24 or 48 hours at MOI of 5 or 10. Viability measured by MTS assay at 24 or 48 hours post-infection (p.i.). *n*=4. Significance determined by two-way ANOVA and Tukey's multiple comparisons test. ns = not significant.

Assessment of bacterial burden

H37Rv-*lux* contains an integrated bacterial luciferase operon (*LuxAB*), including genes encoding the enzyme luciferase and its substrate luciferin under control of a constitutive promoter [48]. Therefore, relative luminescent units (RLUs) can be used as a real-time readout for bacterial burden, which is directly proportional to colony-forming units (CFUs). Triplicate MDMs for each

donor were lysed in 0.05% sodium dodecyl sulfate (SDS) and immediately read in a single tube luminometer (Promega GloMax 20/20) (**Figure 3**).

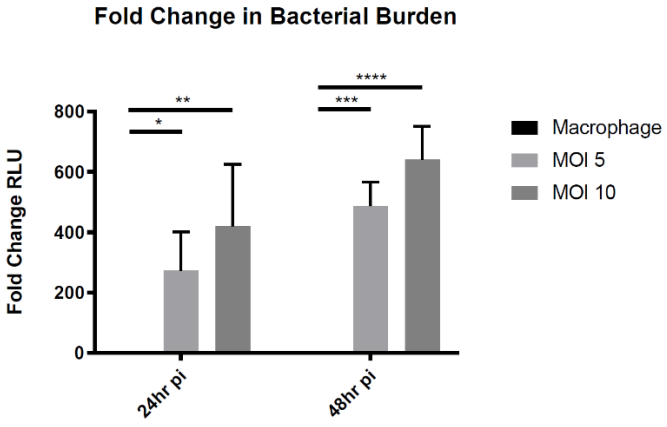

Figure 3. Assessment of bacterial burden in *Mtb*-infected primary human MDMs.
Primary human MDMs from four human blood donors were infected at either an MOI of 5 or 10 for 24 or 48 hours post-infection (p.i.). Bacterial burden measured as luciferase signal (Relative Light Units, RLU) from live H37Rv-*lux*. *n*=4. Significance determined by two-way ANOVA and Tukey's multiple comparisons test. * p = 0.0316, ** p = 0.0018, *** p = 0.0006, **** p = <0.0001.

Small RNA isolation, library preparation, sequencing, and analysis

Total RNA, including small RNA, was isolated from samples frozen at –80°C in TRIzol using the Qiagen miRNeasy mini kit (Qiagen, Cat#217004) according to manufacturer instructions. Quality of total and small RNA were assessed using a fragment analyzer at the Johns Hopkins University DNA Services Core Facility.

RNA was converted into small RNA libraries for small RNA sequencing (sRNA-seq) using the Qiagen QIAseq miRNA Library Kit (Qiagen, Cat# 331505). Quality, size, and concentration of small RNA libraries were then assessed using a fragment analyzer at the Johns Hopkins University DNA Services Core Facility. Libraries were pooled to 1ng/µl and sequenced in a single run on a NextSeq 500 instrument to a depth of at least 1 million reads per sample at the JHU TSC.

sRNA-seq raw data were aligned using miRge2.0, a bioinformatic sequencing analysis tool designed specifically for processing sRNA-seq data [50]. Differential expression of miRNAs was compared using the DESeq2 package, including Benjamini Hochberg correction, in R. miRNA target analysis was performed using miRNet2.0 [51]. Pathway enrichment analysis of differently expressed miRNA targets was generated using the R package gprofiler2 [52, 53].

Total RNA isolation, library preparation, sequencing, and analysis

Total RNA was isolated with the Qiagen AllPrep DNA/RNA Mini Kit (Qiagen, Cat # 80204) following manufacturer instructions. Quality of RNA was assessed using a fragment analyzer at the Johns Hopkins University Transcriptomics and Deep Sequencing Core Facility (JHU TSC).

Purified total RNA was submitted to the JHU TSC for library preparation and sequencing. RNA was converted into total RNA libraries using Illumina TruSeq Stranded Total RNA Library Prep Kit (Illumina, Cat # 20020597). RNA library quality, size, and concentration were assessed using a fragment analyzer at the JHU TSC. Libraries were pooled to 2nM and sequenced in a single run on a NextSeq 500 instrument by single-end sequencing to a depth of approximately 50 million reads per sample with a read length of 75 base pairs. Reads were aligned using the Hisat2, Stringtie, Ballgown pipeline described previously [54]. Differential expression was assessed using the DESeq2 package in R. Benjamini Hochberg correction was used.

DNA isolation, whole genome bisulfite sequencing library prep, sequencing and analysis

Genomic DNA was isolated in parallel with total RNA from identical samples using the Qiagen AllPrep DNA/RNA Mini Kit (Qiagen, Cat# 80204). Purified DNA was submitted to the JHU TSC and sent to Novogene Co., Ltd. for quality control check, bisulfite conversion, library

preparation, and whole genome bisulfite sequencing, and preliminary analysis. DNA was fragmented with a Covaris S220 to generate fragments of 200-300bp in length. Adapter ligation and library preparation was performed using the EZ DNA Methylation Gold Kit (Zymo Research, Cat # D5005). Quality control was performed using a Qubit2.0 and Aligent 2100 bioanalyzer and samples were pooled to a concentration of 2nM. Libraries were sequenced on an Illumina HiSeq platform using paired-end sequencing. Data analysis pipeline involved alignment to the Ensemble *Homo sapiens* reference genome version GRCH83 release 92 and quantification using Bismark [55]. Analysis of differentially methylated regions (DMRs) was performed using DSS [56-58]. Gene ontology enrichment analysis of DMRs was using GOseq [59]. Integration with sRNA-seq and RNA-seq was performed in R.

2.2.2 Results

miRNAs in primary human MDMs are dysregulated by *Mtb* infection

To investigate *Mtb*-driven changes in miRNA expression of primary human macrophages, we isolated MDMs from healthy donors and infected them *ex vivo* with *Mtb* strain H37Rv-*lux,* which produces a bioluminescent signal that serves as a real-time immediate measure of bacterial burden [48]. At each time point (24 or 48 hours post-infection (h.p.i.)), the cells were assessed for viability and bacterial burden (**Figure 2, 3**). Matched wells were used to harvest RNA for library preparation and sRNA-seq (**Figure 1**).

Consistent with the published literature in cell lines [30], we found that some miRNAs in primary human MDMs were significantly dysregulated following infection with virulent *Mtb* (**Figure 4**). Additionally, we found that the number of dysregulated miRNAs and the magnitude

of dysregulation increased both with time post-infection and MOI, suggesting that miRNA dysregulation increases with severity of infection.

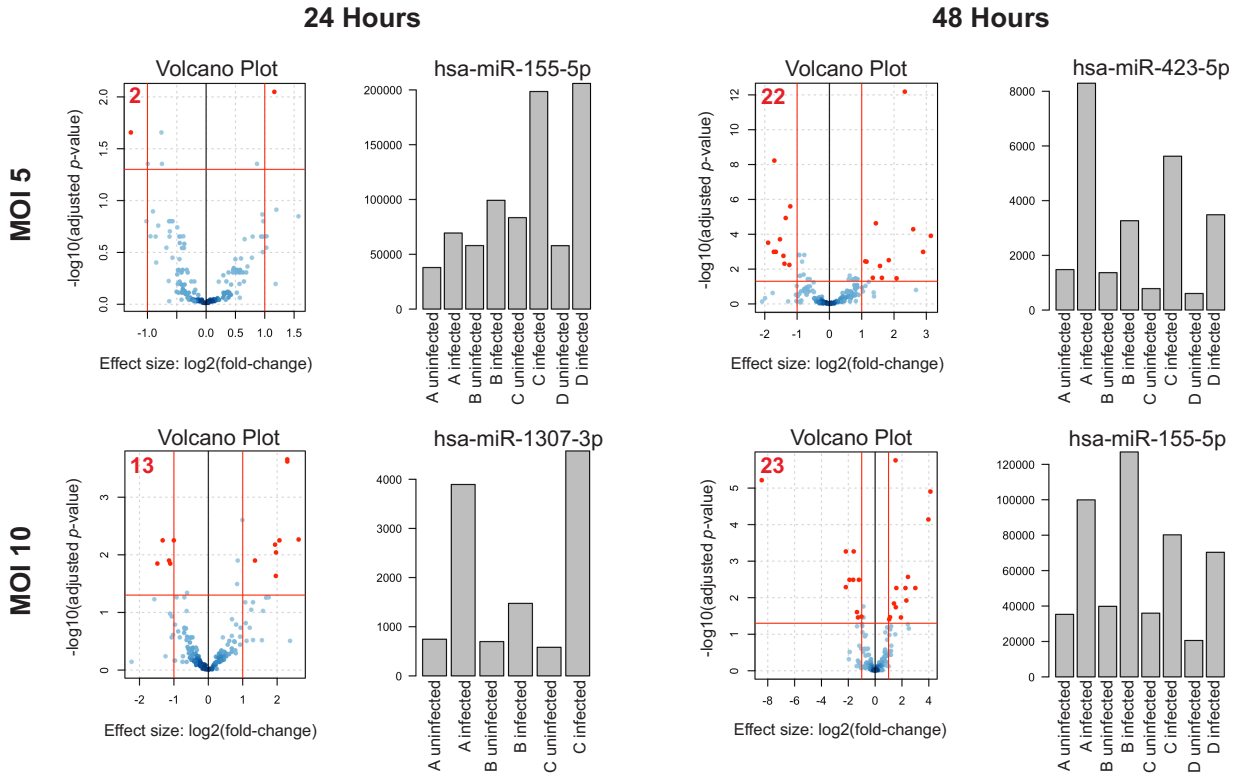

Figure 4. miRNA dysregulation increases with time post-infection and MOI.
Volcano plots of differentially expressed miRNAs in each condition. n = 4 independent human donors. Red lines represent significance thresholds, red numbers represent total number of significantly DE miRNAs. Bar plots to the right of each volcano plot show the most significantly dysregulated miRNA for that condition. A, B, C, and D in bar plots refer to individual biological replicates (individual blood donors). y-axis on bar plots is number of normalized reads.

In the mildest infection condition (MOI= 5 at 24 h.p.i.), there were only two miRNAs which were significantly dysregulated. In contrast, 22 miRNAs were significantly differentially regulated at 48 h.p.i. At MOI= 10, the number of dysregulated miRNAs increased from 13 at 24 hours to 23 at 48 h.p.i. (**Figure 4, Volcano plots; Table 1**).

Table 1. Significantly down and upregulated miRNAs for each condition.

MOI	Time Post Infection	Downregulated miRNAs	Upregulated miRNAs
5	24 hours	miR-340-5p	miR-155-5p
5	48 hours	miR-340-5p miR-374a-5p miR-30b-5p/30c-5p miR-22-5p miR-374b-5p miR-22-3p miR-15a-5p miR-660-5p miR-365a-3p/365b-3p miR-21-5p	let-7a-5p/7c-5p miR-1307-3p miR-3615-3p miR-155-5p miR-148a-3p miR-191-3p miR-486-5p miR-328-3p miR-423-5p miR-1275 miR-122-5p miR-12136
10	24 hours	miR-19b-3p miR-374a-5p miR-15a-5p miR-30b-5p/30c-5p miR-34a-5p	miR-423-3p miR-486-5p miR-328-3p miR-3615-3p miR-423-5p miR-1307-3p miR-501-3p miR-12136
10	48 hours	miR-1307-5p miR-374a-5p miR-340-5p miR-365a-3p/365b-3p miR-22-3p miR-30b-5p/30c-5p miR-374b-5p miR-21-5p miR-185-5p miR-23a-3p/23b-3p	let7b-5p miR-132-5p miR-148a-3p miR-155-5p miR-501-3p miR-1307-3p miR-664a-5p miR-423-5p miR-191-3p miR-486-5p miR-1275 miR-122-5p miR-12136

We also examined which miRNAs were the most significantly dysregulated in each infection condition. We found that miR-155-5p was consistently and significantly upregulated in both the least (MOI of 5, 24 hours) and most severe (MOI of 10, 48 hours) conditions **(Figure 4, Bar plots).** miR-155-5p was also significantly upregulated at MOI of 5/48 hours, although miR-

423-5p was the most statistically significantly different in this condition. miR-1307-3p, the most significantly dysregulated miRNA in the MOI of 10 at 24-hour condition was also upregulated, although it was not significantly dysregulated in other conditions.

Taken together, these results suggest that the degree of miRNA dysregulation is driven by severity of *Mtb* infection and that miRNAs which are dysregulated in more than one condition, such as miR-155-5p, may be important regulators of the macrophage response to *Mtb*.

Bioinformatic analysis and literature review allowed identification of 10 candidate miRNAs for further analysis

In order to gain a deeper understanding of how dysregulated miRNAs may be altering the macrophage response to infection with *Mtb,* we developed the following set of criteria for prioritizing miRNAs for further study: 1) dysregulation of the miRNA must be significant in more than one of the four infection conditions, and must be consistently dysregulated in the same direction (i.e., consistently up- or down-regulated); 2) dysregulation of the miRNA must trend with MOI or time post-infection; 3) the miRNA itself must be known to be abundant in human macrophages (as determined by MiRgeneDB [60]); 4) known, experimentally validated, targets of the miRNA must also be abundant in human macrophages (as determined by The Human Protein Atlas [61] to ensure stoichiometric probability of miRNA-target interaction in our cell type of interest); and 5) miRNAs which have been previously described as being involved in other forms of infectious cell stress are given special consideration as positive controls (**Figure 5**).

miRNA candidate selection criteria:

1. Dysregulated in same direction in more than one condition
2. Dysregulation trends with MOI and/or time post-infection
3. Abundant in human macrophages
4. Validated targets abundant in human macrophages
5. (Bonus) previously described in other infections

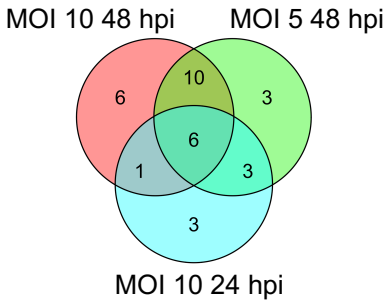

Figure 5. Selection of miRNA candidates for pathway analysis.
NGS analysis and literature review led to selection of 10 candidate miRNAs and their respective targets. Left) Selection criteria for candidate miRNAs. Right) Venn Diagram showing 20 differentially expressed miRNAs shared between the three conditions in which we observed the most significant miRNA dysregulation (top 3).

From our own sRNA-seq dataset, we identified 6 significantly dysregulated miRNAs fitting our selection criteria. These miRNAs were miR-155-5p, miR-191-3p, miR-22-3p, miR-21-5p, miR-30b-5p, and miR-30c-5p. Due to their high degree of sequence similarity, miR-30b-5p and miR-30c-5p are combined for sequencing alignment in miRge2.0. However, as they have some distinct gene targets, for integrated network analysis, miR-30b-5p and miR-30c-5p were separated and analyzed as distinct entities.

We added 4 additional candidate miRNAs based on criterion #5, which we included as controls known to be involved in altering cellular responses during infection: miR-223-5p, miR-29a-3p, miR-27a-3p, miR-125b-5p [25-28]. These additional four candidate miRNAs were each dysregulated in a consistent direction in more than one condition, but did not meet our conservative thresholds for significance ($\log_2$(fold-change) > 1 ; adjusted p-value < 0.01). These 10 miRNAs became candidates for further functional pathway analysis (**Table 2**).

Table 2. List of candidate miRNAs to be used for further analysis.

Source	miRNA
NGS	miR-155-5p miR-30b-5p miR-30c-5p miR-191-3p miR-22-3p miR-21-5p
Das et al. *2016. [25]* Dorhoi *et al*. 2013. [26] Sharbati *et al*. 2012. [27] Rajaram *et al*. 2011. [28]	miR-29a-3p miR-223-5p miR-27a-3p miR-125b-5p

Final selection of miRNA candidates for ongoing mechanistic analyses. 6 miRNAs that met selection criteria were selected from 20 miRNAs differentially expressed in more than one "top 3" condition. 4 additional candidates were selected as positive controls based on their representation in relevant literature [25-28].

Many mRNAs dysregulated in *Mtb*-infected MDMs are targets of candidate miRNAs

To assess dysregulation of host cell pathways at the mRNA level, we performed RNA-seq of total RNA extracted from uninfected vs. infected MDMs. A total of 815 mRNAs were significantly dysregulated in *Mtb* infection ($\log_2$(fold-change) > 1 ; adjusted p-value < 0.05) (**Figure 6A**). We compared these significantly dysregulated genes to a comprehensive list of all known targets of each of the 10 candidate miRNAs (via miRTarBase v8.0)[51] to generate a profile of 158 genes which are both targeted by at least one candidate miRNA and were significantly dysregulated in our RNA-seq dataset (**Figure 6B**). The number of dysregulated genes that were also targets of at least one candidate miRNA ranged between miRNAs. For instance, miR-155-5p had the most with 54 target genes that were dysregulated during *Mtb* infection, while miR-191-3p only had two (**Figure 6B**). All miRNA candidates had at least two significantly dysregulated targets.

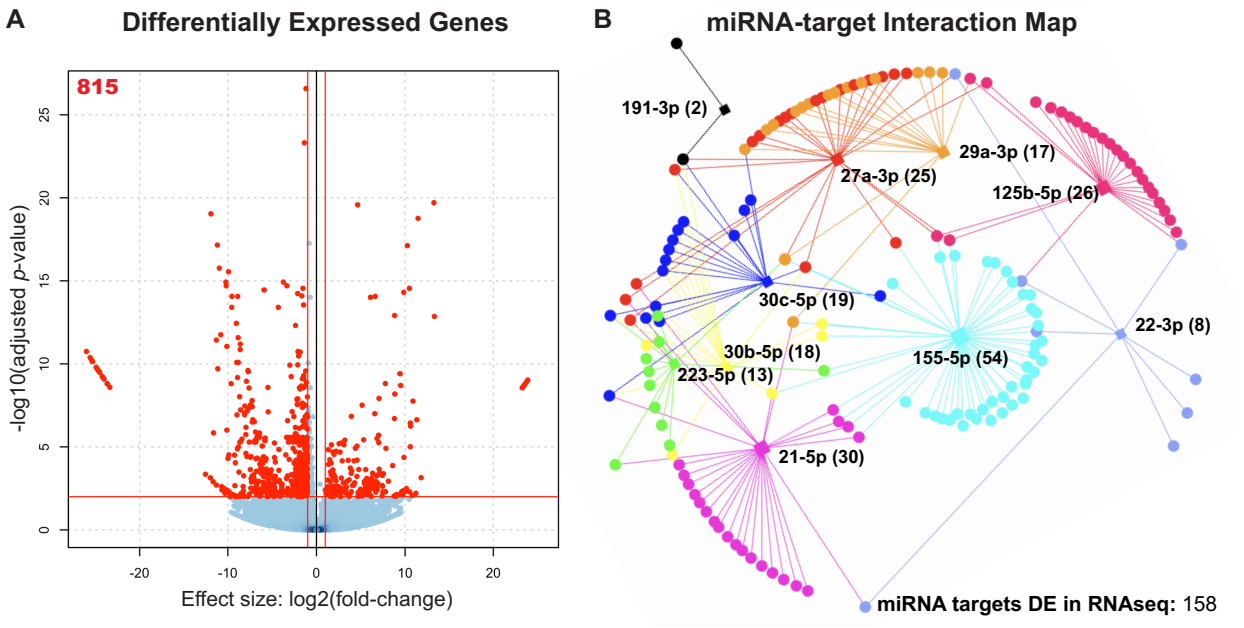

Figure 6. Association of significantly dysregulated miRNAs with differentially expressed cognate mRNAs during *Mtb* infection of human MDMs.
A) Volcano plot showing all differentially expressed mRNAs during *Mtb* infection. n = 4 independent human donors. Red lines represent significance thresholds, red number represent total number of significantly DE mRNAs. B) Interaction map showing network of candidate miRNAs and their respective targets. Square nodes represent each candidate miRNA (labeled). Circular nodes and points represent differentially expressed gene targets (targets identified by miRTarBase v8.0 and miRNet). Numbers in parentheses beside each miRNA label represent the number of gene targets that are also significantly dysregulated in the RNAseq results. Each miRNA node is uniquely color-coded. Edges that extend between miRNA nodes and gene and gene target nodes are coded to the same color of their respective miRNA regulator.

We found that 119 out of the 158 dysregulated target genes were downregulated (75.3%), however, each miRNA had both down and upregulated targets in *Mtb* infection, suggesting direct and indirect regulation (**Figure 6B**). Therefore, it is likely that those genes which are dysregulated in the opposite direction of their associated miRNA are more likely to be targeted by that miRNA during *Mtb* infection [62]. To determine if the genes dysregulated in our RNA-seq dataset were enriched for candidate miRNA targets, we performed a Chi-square analysis with Yates correction using a two by two contingency table. We found that the set of 815 differentially expressed genes is enriched for targets of our 10 miRNAs of interest ($X^2 = 14.86$, $z = 3.86$, $p = 0.0001$), suggesting

that it is unlikely that dysregulation of miRNA candidate genes would occur solely due to random chance (**Table 3**). Odds ratio calculation shows that it is 1.42 times more likely for dysregulated mRNAs to be candidate miRNA targets compared to non-targets.

Table 3. Contingency table for enrichment of dysregulated miRNA targets.

	Non-miRNA Targets	**miRNA Targets**	**Total**
Not dysregulated	17083	2886	19967
Dysregulated	657	158	815
Total	17740	3044	20784

Metric	**X^2**	**z-score**	***p*-value**
Results	14.86	3.86	0.0001

Chi-square analysis with Yates correction to determine if dysregulated genes are statistically enriched for miRNA targets. Total number of candidate miRNA targets was determined by miRNet [63]. Total number of genes was based on total genes detected by RNA-seq. Genes with low reads (sum across all samples less than 10 reads) were filtered out prior to analysis.

Functional enrichment analysis for significantly dysregulated miRNA targets

To investigate which host cell response pathways are associated with our observed networks of miRNA-target regulation, we used the set of genes targeted by each candidate miRNA, independently, and performed functional enrichment analysis and miRNA association validation. Using gprofiler2 in R, we searched for Gene Ontology biological processes (GO:BP) that were significantly associated with the dysregulated target genes for each candidate miRNA. The target genes for miR-223-5p, miR-191-3p, miR-30b-5p, and miR-21-5p did not significantly associate with any particular GO functional group. However, each of the other 6 candidate miRNAs were associated with biological processes critical for defense against *Mtb* infection (**Figure 7**). Specifically, significantly dysregulated genes targeted by miR-155-5p were most associated with activation of various immune cells, primarily those in myeloid cell lineages.

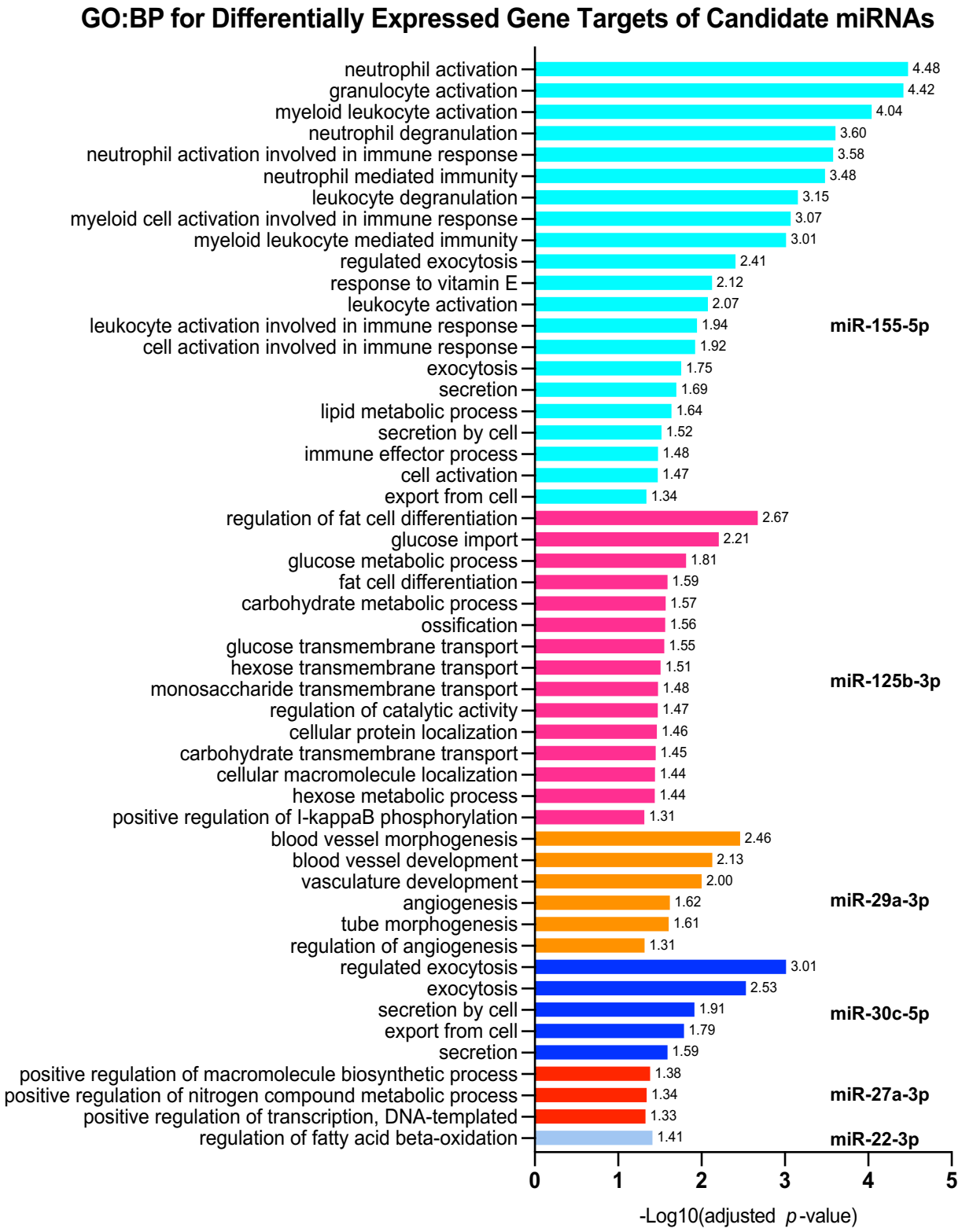
GO:BP for Differentially Expressed Gene Targets of Candidate miRNAs
neutrophil activation
granulocyte activation
myeloid leukocyte activation
neutrophil degranulation
neutrophil activation involved in immune response
neutrophil mediated immunity
leukocyte degranulation
myeloid cell activation involved in immune response
myeloid leukocyte mediated immunity
regulated exocytosis
response to vitamin E
leukocyte activation
leukocyte activation involved in immune response
cell activation involved in immune response
exocytosis
secretion
lipid metabolic process
secretion by cell
immune effector process
cell activation
export from cell
regulation of fat cell differentiation
glucose import
glucose metabolic process
fat cell differentiation
carbohydrate metabolic process
ossification
glucose transmembrane transport
hexose transmembrane transport
monosaccharide transmembrane transport
regulation of catalytic activity
cellular protein localization
carbohydrate transmembrane transport
cellular macromolecule localization
hexose metabolic process
positive regulation of I-kappaB phosphorylation
blood vessel morphogenesis
blood vessel development
vasculature development
angiogenesis
tube morphogenesis
regulation of angiogenesis
regulated exocytosis
exocytosis
secretion by cell
export from cell
secretion
positive regulation of macromolecule biosynthetic process
positive regulation of nitrogen compound metabolic process
positive regulation of transcription, DNA-templated
regulation of fatty acid beta-oxidation
4.48
4.42
4.04
3.60
3.58
3.48
3.15
3.07
3.01
2.41
2.12
2.07
1.94
1.92
1.75
1.69
1.64
1.52
1.48
1.47
1.34
2.67
2.21
1.81
1.59
1.57
1.56
1.55
1.51
1.48
1.47
1.46
1.45
1.44
1.44
1.31
2.46
2.13
2.00
1.62
1.61
1.31
3.01
2.53
1.91
1.79
1.59
1.38
1.34
1.33
1.41
miR-155-5p
miR-125b-3p
miR-29a-3p
miR-30c-5p
miR-27a-3p
miR-22-3p
0
1
2
3
4
5
-Log10(adjusted p-value)

Figure 7. Pathway analysis for significantly dysregulated targets of candidate miRNAs. Each shows gprofiler2 (g:OSt) results for a miRNA candidate. g:OSt was used to analyze the association of each miRNAs target genes with Gene Ontology biological processes functional groups (GO:BP). All significant GO:BP associations are reported. miRNAs which do not have GO:BP results listed did not have significant associations with any GO:BP functional group. g:OSt MIRNA was used to determine which miRNA is most significantly associated with each list of dysregulated targets. The top miRNA hit for each is reported.

miR-125b-5p, miR-27a-3p, and miR-22-3p targets were primarily involved in regulation of metabolism and lipid processing. Specific processes included regulation of fat cell differentiation, glucose metabolism, macromolecule biosynthesis, and fatty acid oxidation. miR-30c-5p targets were involved in regulation of exocytosis and secretion and miR-29a-3p targets were associated with regulation of blood vessel development and regulation of angiogenesis. Each list of target genes was most significantly associated with the miRNA regulator we had matched it to in our network analysis, giving further support to the relationship between each miRNA and the target list.

Though these results show that many differentially expressed targets of our 10 miRNA candidates are involved in regulation of key macrophage processes relevant to the defense against *Mtb* infection, it is likely that their expression is also controlled by other factors, such as methylation of gene regulatory regions.

Expression of immune cell pathway genes is also influenced by restructuring of methylation.

A critical mechanism for pre-transcriptional regulation of immune cell function involves epigenetic changes, which may increase or decrease transcriptional machinery access to different gene regions [64]. Evidence suggests that *Mtb* alters methylation of promoter regions, leading to changes in gene expression in host cells [65]. However, these methylation changes have not been

assessed at a genome-wide scale in *Mtb*-infected primary macrophages. Furthermore, miRNA expression may also be affected by epigenetic changes and it remains to be determined how miRNAs and methylation may work together to co-regulate important macrophage signaling pathways. Therefore, we hypothesized that *Mtb* reprograms the macrophage response by integrating pre-transcriptional regulation via methylation and post-transcriptional regulation via miRNAs of the same pathways. We also posited that changes in candidate miRNA expression may be due to differences in methylation of miRNA promoter regions. To test this, we performed whole genome next-generation bisulfite sequencing (WGBS) on the same *Mtb*-infected primary human MDMs used for RNA-seq analysis (**Figure 6**). We then analyzed our WGBS, RNA-seq and sRNA-seq datasets to identify intersecting networks between these regulatory systems.

We found that differential methylation of CG sites (DMRs, length > 50bp, target site inside DMR ≥ 3CG, $p < 1x10^{-5}$) were evenly distributed across chromosomes and that more DMRs were hypomethylated rather than hypermethylated (**Figure 8A, 8B**). We also found that differential methylation patterns were most common within introns, followed by promoter regions and exons (**Figure 8B**). Functional enrichment GO:BP analysis revealed that hypermethylated CG DMRs were most associated with pathways involved in immune cell activation, while hypomethylated DMRs were most associated with alteration of positive regulation of metabolic processes (**Figure 8C**). We then compared the set of genes we found to have differentially methylated CG regions to the differentially expressed genes identified by our RNA-seq study (**Figure 6, 8D**). Importantly, among the upregulated genes, there were more hypomethylated genes (19) compared to hypermethylated genes (8). Similarly, we found that more downregulated genes were hypermethylated (99) rather than hypomethylated (82) (**Figure 8D**).

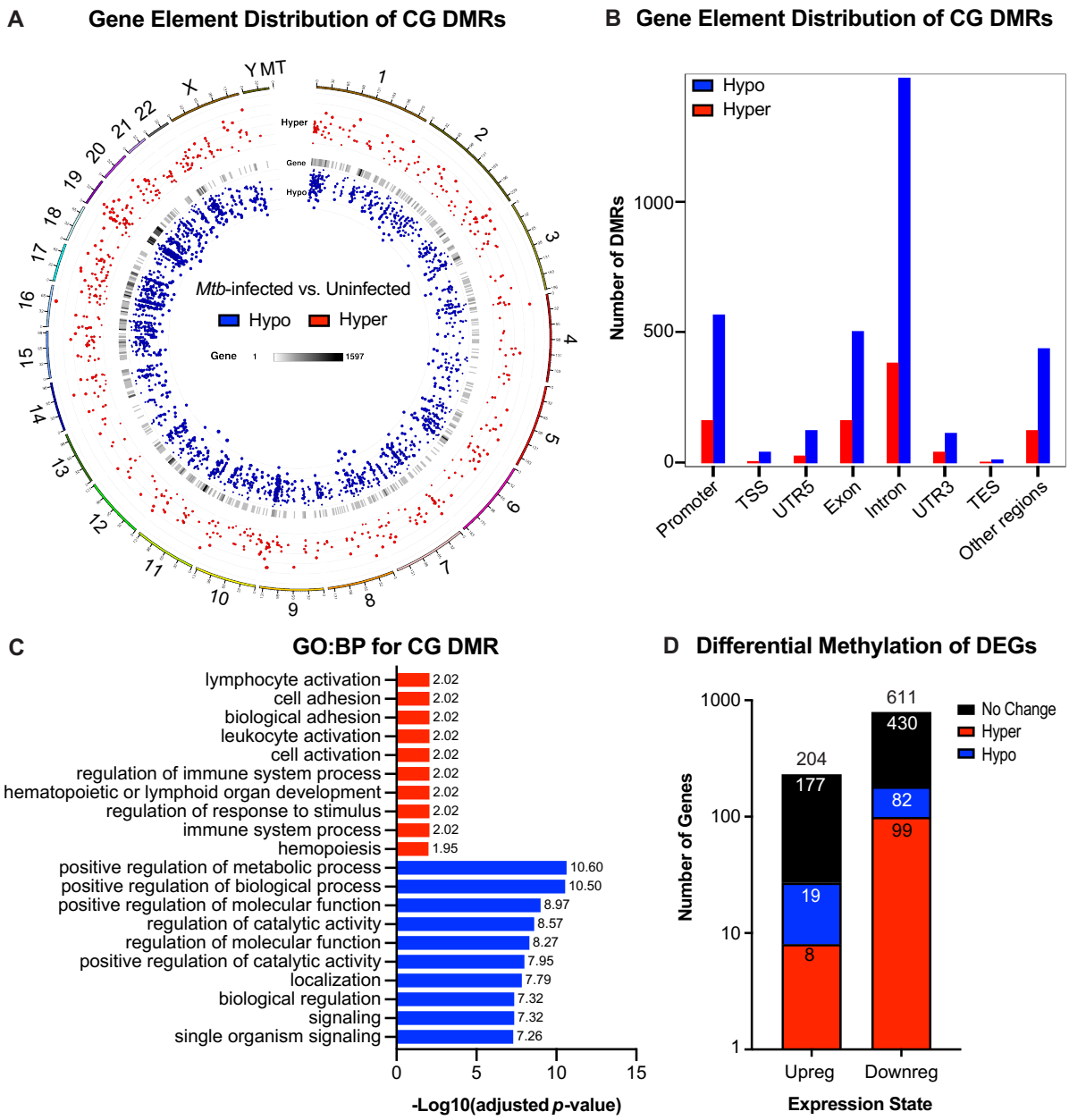

Figure 8. Genome wide differential CG methylation patterns show enrichment for genes associated with immune activation and metabolic processing.

A) Genome wide chromosomal alignment of hypo (blue) and hyper (red) methylated CG sites in *Mtb*-infected MDMs. B) Distribution of hypo and hypermethylated CGs (DMRs) over each genetic element. C) Functional enrichment gene ontology biological process (GO:BP) analysis for all differentially methylated CGs. -Log10(adjusted *p*-value) values are reported to the right of each bar. GO:BP terms associated with hypermethylated CG DMRs are highlighted in red. Terms associated with hypomethylated CG DMRs are highlighted in blue. D) Total number of up and downregulated genes from RNA sequencing results (**Figure 6**) with overlay of genes that are also hypo or hypermethylated. Number in each color coded segment represents total number of genes with a specific expression and methylation state. Number above each bar represents total up or downregulated genes. *n*=4. MDMs were infected with *Mtb* H37Rv for 48 hours at an MOI of 10.

Chi-square analysis revealed that upregulated genes were not statistically enriched for hypomethylated DMRs ($p = 0.08$) and that downregulated genes were significantly less likely to be hypermethylated compared to no methylation change ($p = 0.0002$), suggesting that differential methylation alone is not sufficient to explain differences in mRNA expression, and that other regulatory systems, such as miRNAs, are likely to contribute to overall changes in gene expression. Differential methylation of candidate miRNA-associated gene regions was found for miR-125b, though the differences in methylation were not significant, suggesting that miRNAs and methylation changes are acting largely independently in regulating mRNA expression.

To select only genes which may be directly influenced by changes in DNA methylation, we identified genes that were both differentially expressed and divergently methylated. We next sought to determine which macrophage functions may be influenced by alterations in expression of genes with differential methylation. We found that differentially methylated genes that were also differentially expressed in either direction were associated with regulation of immune cell activation and exocytosis (**Figure 9A**). We then wanted to determine if any genes that were differentially methylated and differently expressed were also targets of any of the previously identified candidate miRNAs. We found 26 genes that were differentially methylated, differentially expressed, and targeted by at least one candidate miRNA (**Figure 9B**).

In performing functional enrichment KEGG analysis on this set of 26 genes, we found that these genes were most tightly associated with the AMPK signaling pathway (**Figure 10**). Three of these 26 genes, CyclinD1 (CCND1, an important regulator of cell proliferation), TBC Domain Family Member 1 (TBC1D1, regulator of cell growth and differentiation), and cluster of differentiation 36 (CD36, involved in antigen processing, cross presentation, and low density lipoprotein binding), are central to the AMPK pathway.

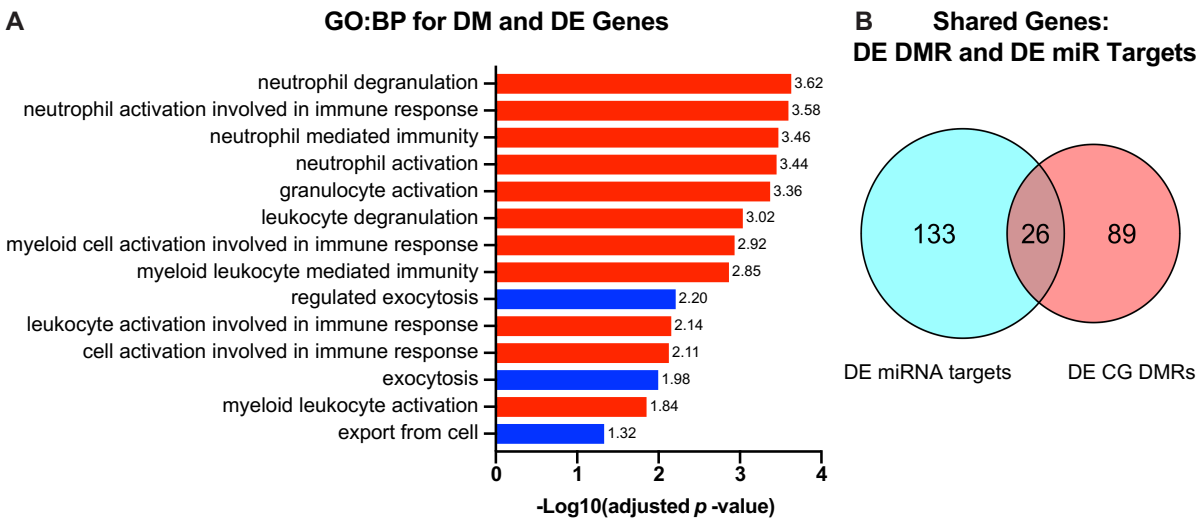

Figure 9. Genes that are both differentially methylated and differentially expressed are involved in immune cell functioning and are subject to candidate miRNA regulation.
A) Genes that were both differentially methylated and differentially expressed were selected and used for gene ontology biological process (GO:BP) functional enrichment analysis. -Log10 (adjusted *p*-value) value for each GO:BP term is reported to the right of each bar. GO:BP terms related to immune cell activation are highlighted in red. Those related to exocytosis and secretion are highlighted in blue. B) Genes that were both differentially methylated and differentially expressed were compared to genes that we found to be differentially expressed and targeted by at least one candidate miRNA. Overlap represents the number of genes that are differentially expressed by RNAseq, targets of one or more miRNA candidate, and differentially methylated.

The AMPK pathway also contains various genes that were differentially methylated alone, and one gene, C-C Motif Chemokine Ligand 22 (MCD, a chemoattractant for various immune cells), that was differentially expressed despite lack of differential methylation or targeting by any candidate miRNA. Chi-square analysis shows that the dysregulation of the AMPK pathway is statistically significant ($X^2 = 22.43$, $z = 4.74$, $p = <0.0001$) and unlikely to be due to random chance (**Table 4**). An odds ratio of 3.30 suggests that dysregulated genes are over three times more likely to be involved in the AMPK pathway than unrelated pathways.

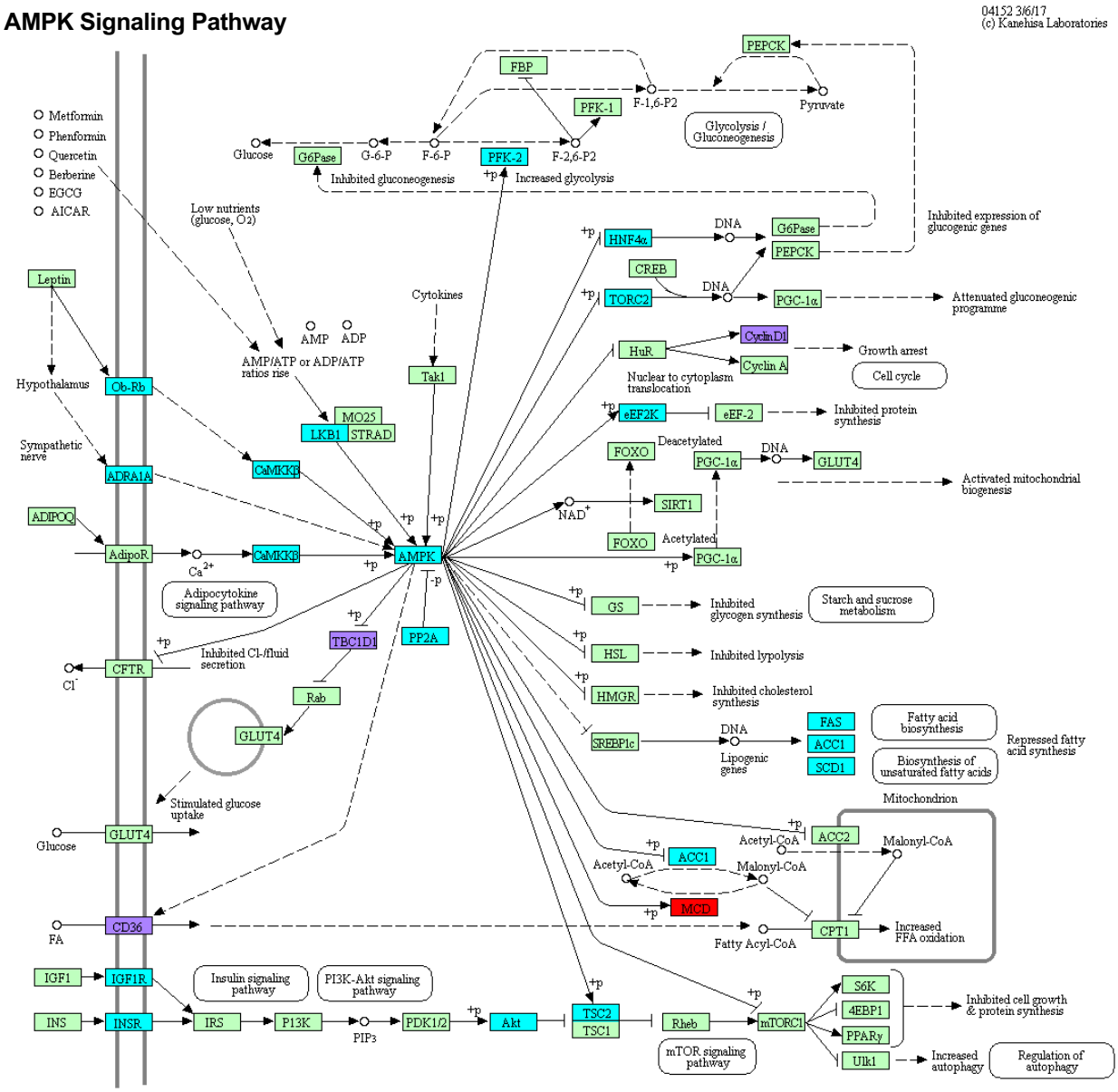

Figure 10. DMRs DEGs and DE miRNA targets intersect at the AMPK signaling pathway. Genes that were differentially methylated, differentially expressed, or targeted by candidate miRNAs were subjected to functional enrichment KEGG analysis. These genes were most significantly associated with the AMPK signaling pathway. Genes which are only differentially methylated are highlighted in cyan. Genes which are only differentially expressed are highlighted in red. Genes which are differentially methylated, differentially expressed, and regulated by one or more miRNA are highlighted in purple. Light green boxes represent other pathway genes that were not found to be significantly in our studies.

Table 4. Contingency table for enrichment of AMPK pathway dysregulation.

	Non-AMPK Genes	AMPK Pathway Genes	Total
Not dysregulated	17934	45	17979
Dysregulated	2782	23	2805
Total	20693	68	20784

Metric	X^2	z-score	*p*-value
Results	22.43	4.74	<0.0001

Chi-square analysis with Yates correction to determine if dysregulated genes (differentially methylated or expressed) are statistically enriched for AMPK pathway genes. Total number of AMPK Pathway Genes was based on KEGG pathway. Total number of genes was based on total genes detected by RNA-seq. Genes with low reads (sum across all samples less than 10 reads) were filtered out prior to analysis.

2.3 *Mycobacterium tuberculosis* infection drives mitochondria-biased dysregulation of host transfer RNA-derived fragments

* This work was published in the *Journal of Infectious Diseases* in September 2020 [49].

Because we and others have shown that *Mtb* dysregulates miRNAs, we hypothesized that *Mtb* may also significantly dysregulate the production of tRFs. We also predicted that patterns of tRF dysregulation in *Mtb* infection may differ from patterns observed during infection with other bacterial pathogens, such as *Mycobacterium bovis* (*M. bovis*), *Salmonella* typhimurium (*S.* typhimurium), *Listeria monocytogenes* (*L. monocytogenes*), and *Yersinia pseudotuberculosis* (*Y. pseudotuberculosis*). Here, we tested these hypotheses by comparing tRF dysregulation in *Mtb*-infected primary human macrophages with dysregulation in infections with other intracellular bacterial pathogens from publicly available RNA-seq datasets. In order to determine tRF abundance, we developed and validated a new tRF-finding tool, tRFcluster, which was incorporated into our miRNA alignment tool, miRge2.0 [50].

2.3.1 Methodologies

Ethics

This study was approved by the Johns Hopkins University Institutional Review Board. Usage of primary human MDMs is consistent with that detailed in section 2.2.1.

Isolating human macrophages

Isolation of human MDMs was done following the protocol laid out in section 2.2.1.

***Mycobacterium tuberculosis* infection**

Primary human MDMs from each donor were infected with H37Rv-*lux* [48], for 24 or 48 hours (multiplicity of infection (MOI) of 5 or 10) (**Figure 1**). To avoid altering cellular transcriptional responses, extracellular bacteria were not removed by washes or antibiotic treatment. Infected cells were incubated at 37°C with 5% CO_2. At each time point, matched wells were used for assessment of MDM viability and bacterial burden (described above, see section 2.2.1, **Figure 2, 3**). Cells were also harvested for RNA for small RNA-seq library preparation.

RNA extraction and sRNA-seq library preparation

RNA was extracted with the miRNeasy Mini Kit (Qiagen, Cat # 217004), following manufacturer instructions. RNA was converted into sRNA-seq libraries using the QIAseq miRNA Library Kit (Qiagen) following kit protocol. This protocol allows for preparation of small RNA libraries that include tRFs. RNA and library quantity and quality were assessed by fragment analyzer at the Johns Hopkins DNA Services Core Facility.

sRNA-sequencing of *Mtb*-infected human MDMs

Libraries were pooled to a concentration of 1 ng/µl for sRNA-seq. Sequencing was performed on an Illumina NextSeq 500 at the Transcriptomics and Deep Sequencing Core Facility at the Johns Hopkins University. Samples were sequenced with sufficient depth to achieve at least 1 million reads per sample. Sequencing run quality, including total reads, trimmed reads, and number of reads per type of small RNA, was assessed using miRge2.0. All samples were sequenced within one run to avoid batch effects.

Analyzing tRF reads through miRge2.0

FASTQ files were analyzed in miRge 2.0 for tRFs calling the –trf function. tRF-related output comprises one tRF folder showing all exact alignments and three tRF files: tRF.Counts.csv, tRF.RP100K.csv and tRFs.potential.report.tsv reporting counts.

Exclusion of unwanted variation normalization of tRF samples

The remove-unwanted-variation algorithm [66] using replicate samples (RUVSeq R/BioC package) was used to estimate twenty latent factors separately for adjustment of batch effects in the 345 samples (**data not shown**).

Analysis of differential expression of tRFs

DESeq2 was used for differential analysis of tRFs [67]. Benjamini-Hochberg correction was performed. Significantly differentially expressed tRFs were applied to hierarchical clustering, where pairwise distance was based euclidean distance. Average linkage clustering was used as agglomeration criteria.

Use of comparison tools

tDRmapper and MINTmap [68, 69] were installed locally and used to detect tRFs for the samples in (**data not shown**). The parameters were set as default.

Generating a new miRge2.0-based tRF detection method, tRFcluster

433 mature tRNA sequences were downloaded from the GtRNAdb database (Release 2.0) [34]. The 22 human mitochondrial tRNAs sequences were obtained from MINTmap [69].

sRNA-seq FASTQ files from various primary human cell types were obtained from Bioprojects PRJNA358331, PRJNA391912, and PRJNA385925 [70-72]. Samples with fewer than 10,000 tRNA-mapped reads were excluded, resulting in 711 samples for further analysis (**data not shown**).

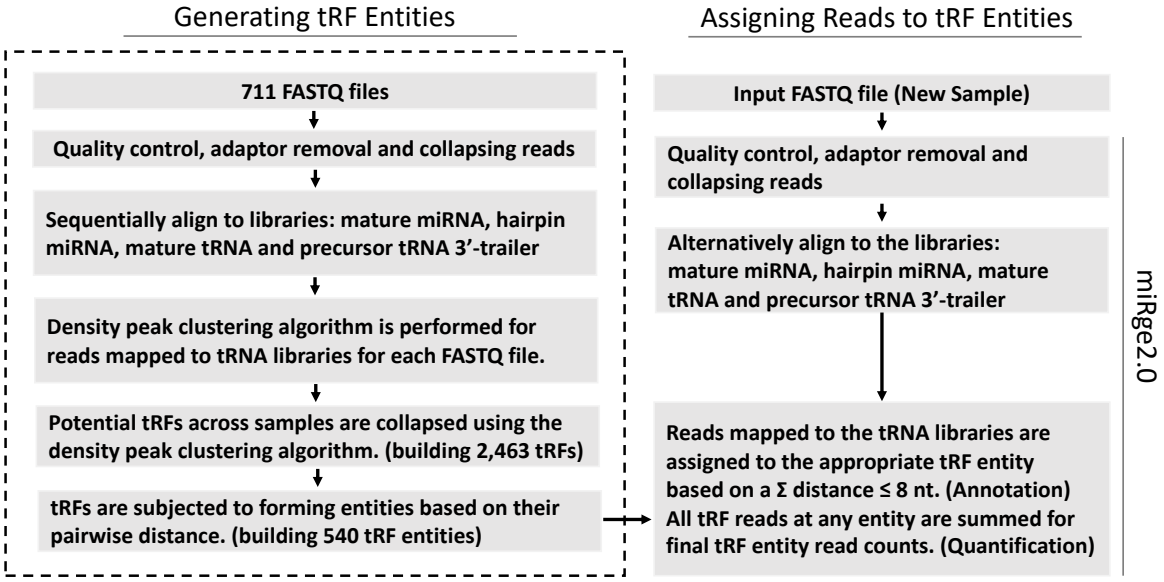

Figure 11. Workflow for creation of tRFcluster and use of the method.

Input FASTQ file(s) were analyzed using the standard miRge2.0 workflow modified only to have separate alignment to mature tRNA and precursor tRNA 3'trailer [50, 73]. Due to known RNA editing of tRNAs, the search strategy employed allowed one mismatch to mature tRNA

sequences. For tRF-1 alignments to the pre-tRNA tail, reads are required to have poly-T (≥ 3"T"s) tails and no mismatch in the read sequence region where the poly-Ts are excluded. Since some sRNA-seq reads can be mapped equally to several tRNA families, all best alignments to mature tRNA and precursor tRNA 3'-trailers were reported (**Figure 11**).

Clustering potential tRFs by means of density peak clustering

tRFcluster uses an unsupervised clustering algorithm to detect centers with local maxima in the density as a basis for assigning clusters. The cluster centers are empirically determined when local density ρ_i is ≥ *rhomin* 5.0 and ≥ *deltamin* 8.0.

The most abundant read in any given cluster is determined as the representative tRF and the tRF read count and RP100K values are the sum of the read counts and RP100K values of all reads in the cluster core.

Refining tRF entities from tRF clusters

The 711 sRNA-seq samples generated 36,901 possible tRF clusters across the tRNA libraries. These were secondarily collapsed together using the same clustering method, as described above, resulting in 2,463 tRFs. The sequence and genomic loci information of these tRF clusters is listed in (**data not shown**). Many of the tRFs had high similarity, with equal sequences but of different lengths (ex 24 vs 25 bp), or differing by a single nucleotide. Using a pairwise distance strategy, 540 tRF entities were generated. The entities and their tRFs members are listed in (**data not shown**). i-tRF, tRF-1, -3 and -5, 5' half and 3' half assignments were made on these 540 tRFs and all halves were ≥31 nt.

Biologic sRNA-seq Datasets

To validate this tRF tool, FASTQ files of nine cell types (macrophage, B lymphocyte, T lymphocyte, fibroblast, endothelial cell, retinal pigment epithelial cell, smooth muscle cell, monocyte, and neural stem cell) were chosen because they were represented in two or more of BioProjects PRJNA358331, PRJNA391912, PRJNA385925 [70-72] (N=345) (**data not shown**).

Raw data from human sRNA-seq studies in cell culture models involving bacteria or hypoxia were mined from public NCBI BioProjects PRJNA206504, PRJNA480576, PRJNA298741, PRJNA297139, PRJNA270244 (**Table 5**). FASTQ files were analyzed using tRFcluster in miRge2.0. Samples were compared across studies with DESeq2 (R).

Table 5. Details of small RNA sequencing datasets analyzed.

Type	Agent/Treatment	Cell Type	Cases	Controls	Time	MOI	BioProject #
Bacteria	*Salmonella typhimurium*	Macrophage	24	24	2 & 24 hr	10	PRJNA297139
Bacteria	*Listeria monocytogenes*	Macrophage	24	24	2 & 24 hr	5	PRJNA297139
Bacteria	*Mycobacterium tuberculosis*	Macrophage	8	16	24 & 48 hr	1	Looney, *et al.* GSE151050
Bacteria	*Yersinia pseudotuberculosis* *Salmonella typhimurium* *Mycobacterium tuberculosis* *Mycobacterium bovis*	Dendritic cells	98	18	4, 18, & 48 hr	1	PRJNA270244
--	Hypoxia	HUVEC	12	2	Multiple cycles	N/A	PRJNA480576
--	Hypoxia	MCF7	6	2	16, 32 & 48 hr	N/A	PRJNA206504

2.3.2 Results

Creation and validation of tRFcluster

Due to the complexity of tRNA structure, we currently lack a widely accepted nomenclature for cataloguing tRFs. Our new miRge2.0-based tool, tRFcluster, which uses a clustering approach optimized to account for tRF sequence complexities, was validated using 711 samples (**Table 6**). After alignment to 455 human tRNA sequences, reads were clustered together. Clusters of 2,461 unique tRFs were collapsed into 540 tRF entities comprising tRFs and tRNA halves (**Table 6**). Each entity has between 1 and 33 clusters (average 4.5) assigned to it with ~50% having only one specific sequence. Eight entities had sequences that could be aligned to more than one tRNA type. This new clustering method balances the total number of tRFs to be counted with appropriate alignment that accounts for sequences mapping to more than one genetic locus.

Table 6. Comparison of tRFcluster, MINTmap, tDRmapper, tRFfinder, and tRFdb.

	tRFcluster	MINTmap	tDRmapper	tRFfinder	tRFdb
Runs locally	Yes	Yes	Yes	No	No
Catalogs tRFs and miRNAs	Yes	No	No	No	No
Number of human tRFs	2,461*/540**	594,972	NA	NA	552
tRF-5	Yes	Yes	Yes	Yes	Yes
tRF-3	Yes	Yes	Yes	Yes	Yes
i-tRF	Yes	Yes	Yes	No	Yes
tRF-1	Yes	No	Yes	Yes	Yes

Table 7. Comparison of tRFcluster, MINTmap, tDRmapper, tRFfinder, and tRFdb.

Tool	Alignment strategy	Total read counts of tRFs	Total read counts of tRFs after filter	Proportion of tRF reads after filter	Total tRF counts	Total tRF counts after filter
tRFcluster	1 mismatch	176,584,695	175,683,293	0.99	540	324
MINTmap	0 mismatch	143,792,494	133,141,746	0.93	79,404	858
tDRmapper	2 mismatches & 3 deletions	193,952,012	187,599,715	0.97	1469	374

We then validated tRFcluster against MINTmap and tDRmapper to test our ability to generate robust and meaningful analyses of sRNA-seq data. We determined the distributions of tRFs in 345 human primary cell samples, comprising nine cell types, across tRFcluster, MINTmap and tDRmapper (**Table 7**). We found that the most abundant tRF subtype was 5' tRNA halves (31%) (**Figure 12A**). The most abundant tRFs came from valine, glycine, glutamine, and lysine tRNAs (**Figure 12B**). These data suggest that our goal of developing a robust new tRF analysis tool that captures a high number of tRF reads in a reasonable number of entities was achieved.

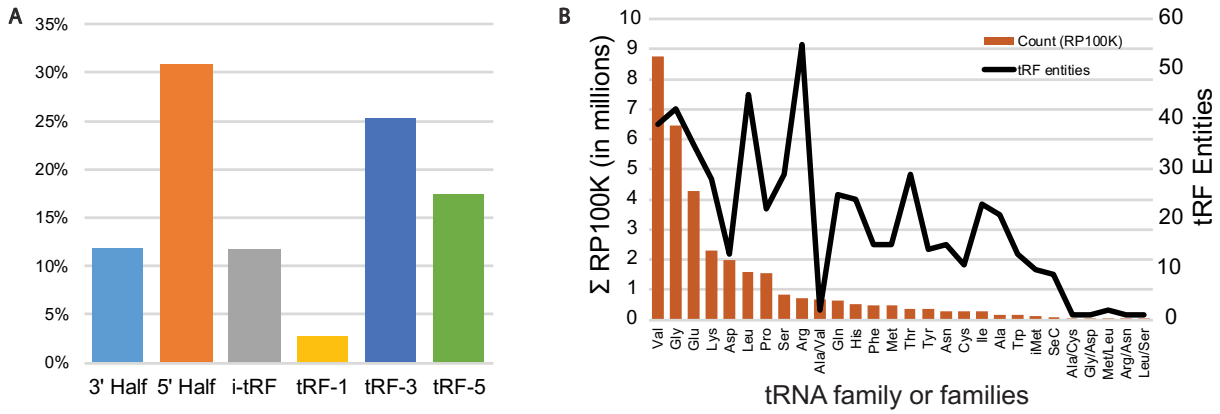

Figure 12. Features of tRFs from 345 cell samples.
A) Distribution of tRNA fragments (tRFs and tRNA halves) showing that 5' halves and tRF-3 segments are the most abundant. B) Distribution of tRF entities by tRNA family. Abundance of tRF reads does not fully correlate with number of tRF entities by tRNA family.

tRFs show pathogen-specific patterns of alteration during infection

Using tRF cluster, we examined how tRFs differed in infection with *Mtb* compared to other intracellular bacterial pathogens. We infected primary human MDMs *ex vivo* with virulent *Mtb* strain H37Rv-*lux* [48]. Small RNAs from uninfected MDMs and MDMs infected at MOIs of 5 or 10 were sequenced and analyzed at 24 and 48 hours post-infection. We found that tRFs were significantly dysregulated by infection with *Mtb* at all MOIs and time points (**Figure 13A**).

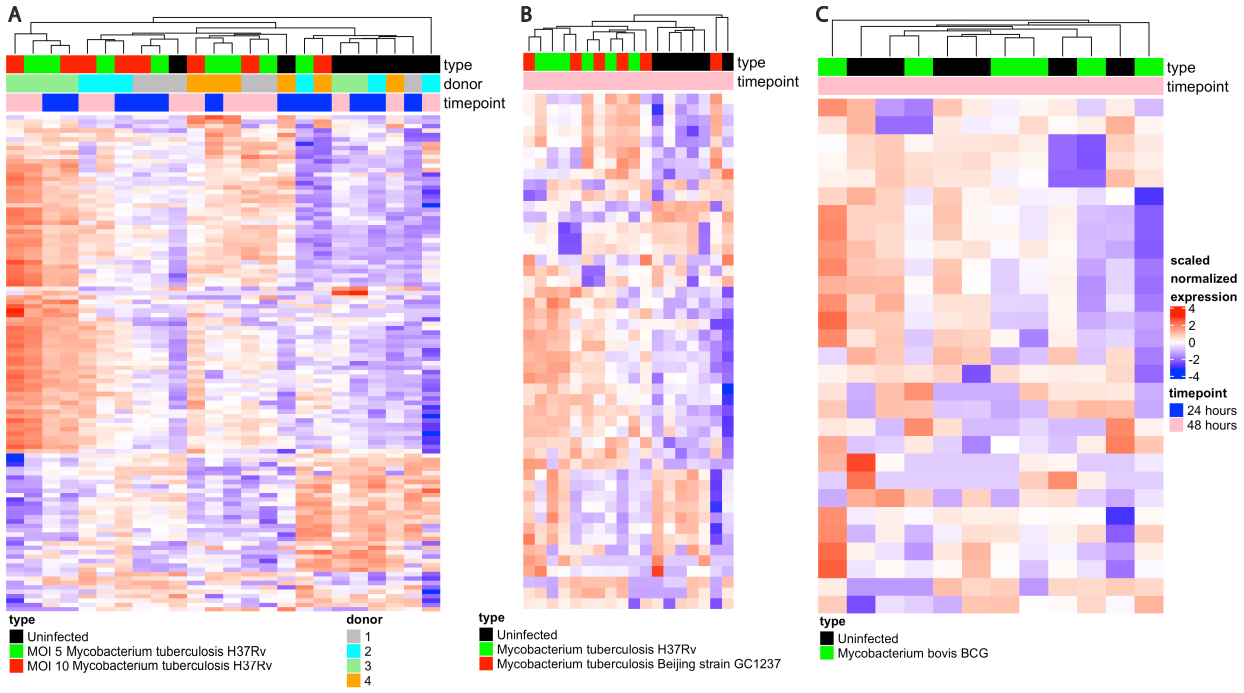

Figure 13. Virulent strains of *Mtb*, but not *Mycobacterium bovis*, significantly dysregulate tRF production.
A) tRF changes between uninfected and primary human MDMs. Top bar indicates infection type. Uninfected (*black*), infected with *Mtb* strain H37Rv-*lux* at an MOI of 5 (*green*) or 10 (*red*). Identity of each of the four biological replicates (donors) are color coded by the second horizontal bar to show inter-donor variability. B) Assessment of tRFs in infection with virulent *Mtb* strains from publicly available dataset (SRP051119). tRFs were assessed in uninfected DCs (*black*) vs. DCs infected with *Mtb* strain H37Rv (*green*) or Beijing GC1237 (*red*) for 48 hours. C) Assessment of tRFs in infection with non-tuberculous mycobacteria (NTM) *Mycobacterium bovis* strain BCG from publicly available dataset (SRP051119). tRFs were compared between uninfected DCs and DCs infected with BCG for 48 hours.

To validate these findings, we performed the same tRF analysis using a publicly available sRNA-seq dataset of dendritic cells (DCs) that had been infected with virulent *Mtb* strain H37Rv (lineage 4) or *Mtb* Beijing strain GC1237 (lineage 2) [74]. We found strikingly similar patterns of tRF dysregulation between our own dataset and the publicly available *Mtb* dataset (**Figure 13B**). Additionally, H37Rv and Beijing strains did not cluster separately, suggesting that *Mtb* infection drives significant lineage-independent changes in tRF production. Unlike other intracellular pathogens, *Mtb* possessed unique mechanisms of immune evasion, allowing it to survive within host cells [75-77]. Therefore, we hypothesized that *Mtb*-induced patterns of tRF dysregulation may be distinct from those of other, less virulent intracellular bacterial pathogens. To test this, we analyzed publicly available datasets containing sRNA-seq data of cells infected with *M. bovis, S. typhimurium, L. monocytogenes, and Y. pseudotuberculosis* [74, 78]. We then used tRFcluster to examine tRF dysregulation during each of these infection conditions.

Interestingly, compared to virulent strains of *Mtb*, *M. bovis* strain BCG, a live attenuated strain of *M. bovis* used as a vaccine for TB [79, 80], did not cluster based on infection status (**Figure 13C**). This suggests that tRFs are not significantly dysregulated by infection with BCG and implies that there may be a connection between degree of virulence and tRF dysregulation. We next examined tRF dysregulation in non-mycobacterial infections. We found that *L. monocytogenes* drove the strongest changes in tRF dysregulation. In contrast, neither *S. typhimurium* nor *Y. pseudotuberculosis* showed significant tRF dysregulation (**Figure 14**). Interestingly, all species examined here are known to alter miRNA expression [74, 78]. However, our data show that only some dysregulate tRFs. This suggests that tRF dysregulation may be species-specific and independent of miRNA dysregulation.

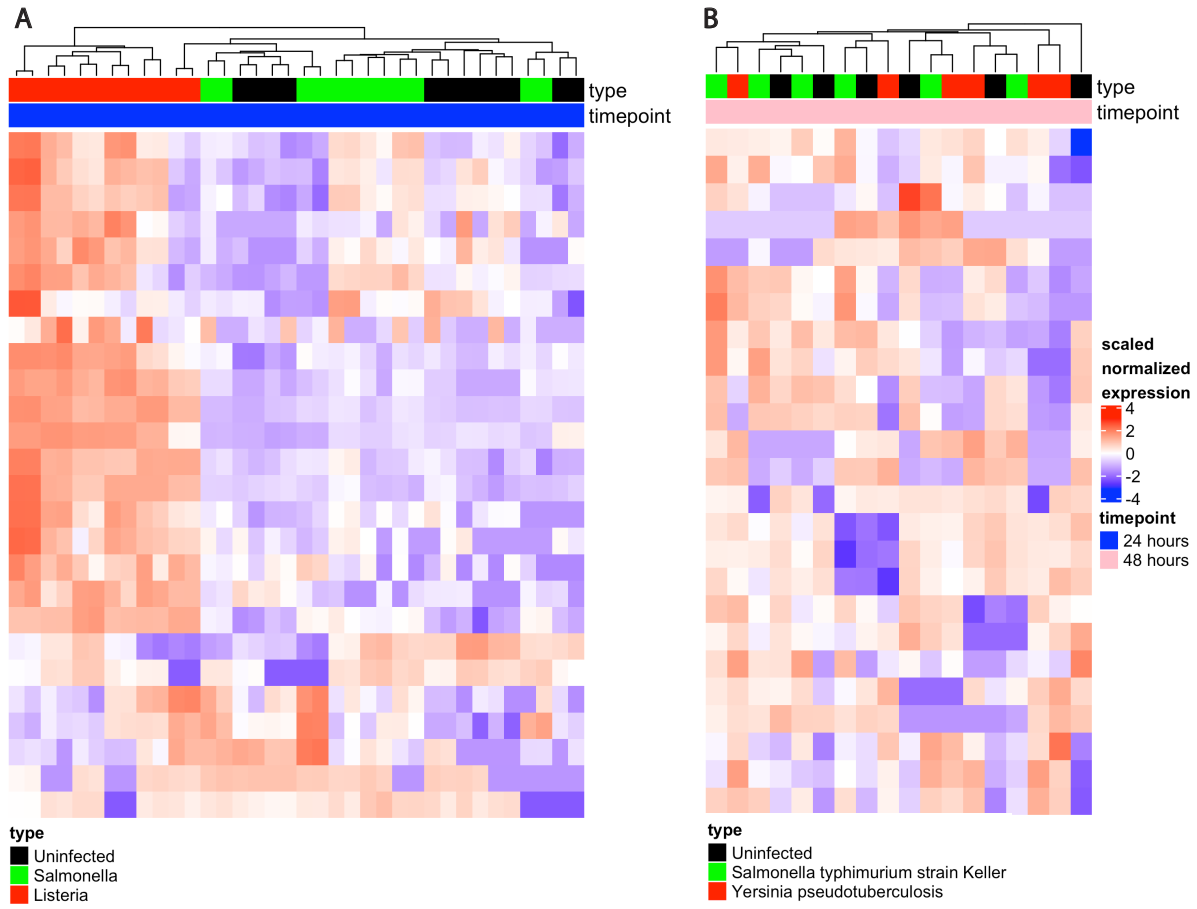

Figure 14. *Listeria monocytogenes* shows stark tRF dysregulation compared to other non-mycobacterial intracellular bacterial pathogens.
A) tRF production was compared for uninfected macrophages (*black*) vs. macrophages infected with *Salmonella* typhimurium (*green*) or *Listeria monocytogenes* (*red*) for 24 hours. Raw data from publicly available dataset (SRP064235). B) tRFs were compared between uninfected macrophages (*black*) and macrophages infected with *Salmonella* typhimurium (*green*) or *Yersinia pseudotuberculosis* (red) for 48 hours. Raw data from publicly available dataset (SRP051119).

Finally, we sought to compare *Mtb* infection-mediated tRF dysregulation with that of other TB pathology-related cell stresses. As hypoxia is known to be an important stress encountered by *Mtb* within necrotic lung granulomas and is known to drive tRF dysregulation [81, 82], we selected this as our non-infectious comparison. We found that hypoxic stress led to alterations in tRF

production that increased with degree of hypoxia (**Figures 15, 16**). While this is unlikely to be relevant to the tRF dysregulation observed during *ex vivo Mtb* infection of primary human MDMs, it may be important to understand in the context of how cells respond to disease within a human host.

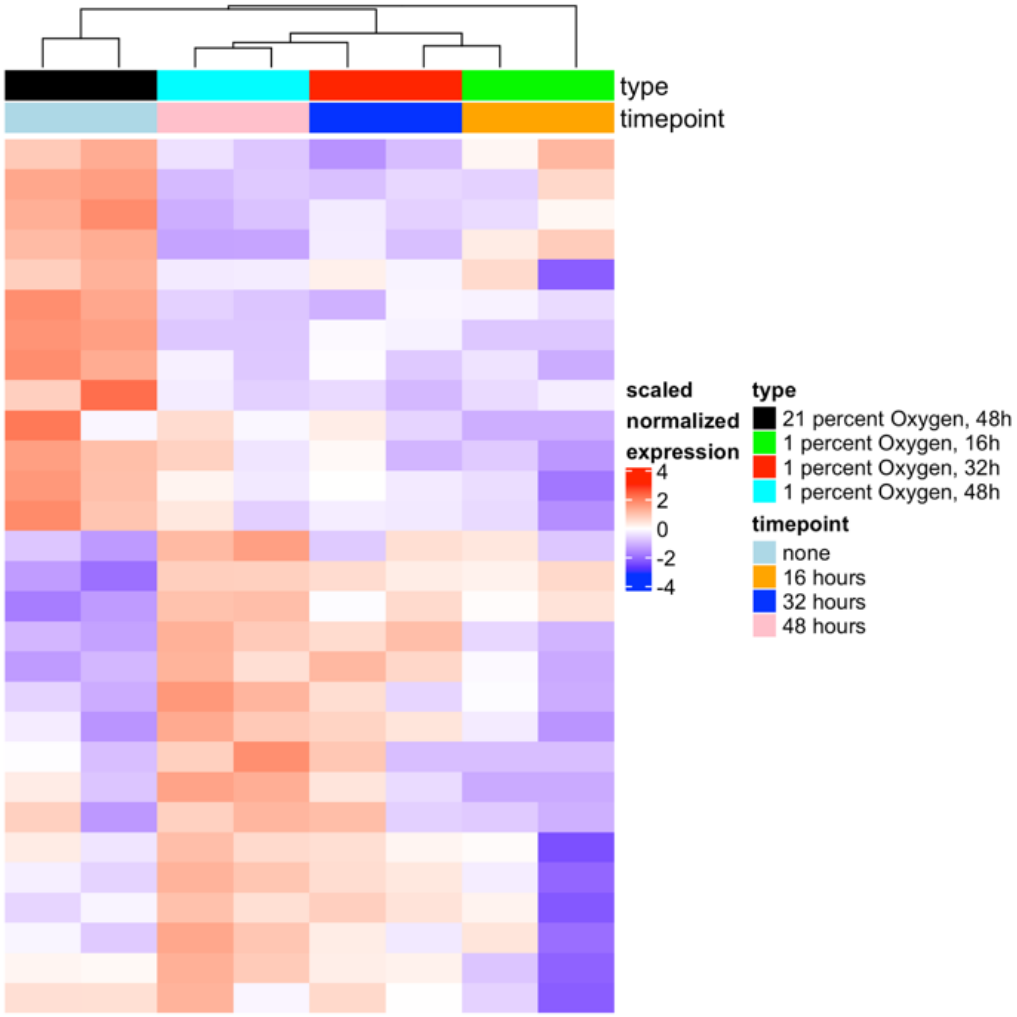

Figure 15. Heat map of tRF abundance during hypoxic stress.
MCF7 cells were exposed to hypoxic conditions (1.0% oxygen) for increasing intervals up to 48 hours. 21% oxygen for 48 hours was used as a negative control and represents normoxia (*black*). Raw data obtained from publicly available dataset (SRP023533).

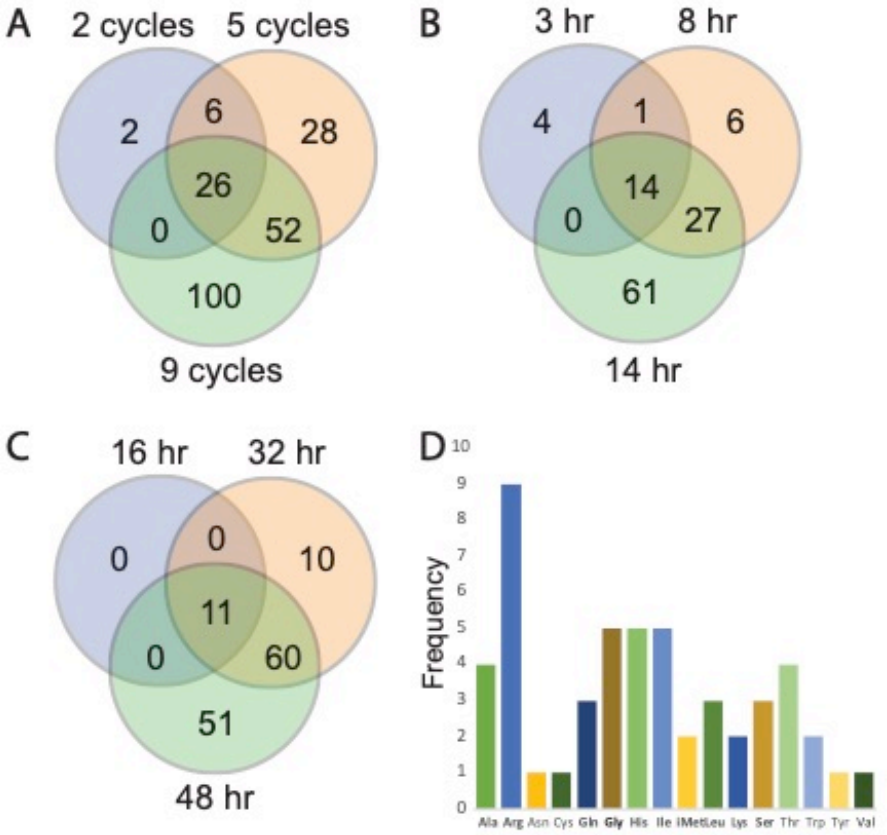

Figure 16. Venn diagram of tRFs in three hypoxia studies over 3 time points.
In all three studies the number of tRFs increased with increasing hypoxia and most tRFs at the earliest time point remained significant at the later time points. A) Two, five, or nine cycles of 1 hour of hypoxia (0.9% O_2) followed by 36 minutes of normoxia in pooled HUVECs. B) 3, 8, or 14 hours of hypoxia (0.9% O_2) in pooled HUVECs. C) 16, 32, or 48 hours of hypoxia (1% O_2) in MCF7 cells. D) The distribution of 51 tRFs that were present at all three time points across each study. tRFs in bold indicate those that had specific tRF entities found across two studies. Only one tRF, His_Comb_5, was identified at all 9 time points evaluated in the three studies. Raw data were obtained from publicly available datasets (SRP153017, SRP023533).

tRF dysregulation increases with severity of *Mtb* infection

Next, we sought to determine whether there was a relationship between tRF production and intracellular bacillary burden and/or duration of *Mtb* infection. To test this, we assessed tRF production for all *Mtb*-infected samples, and for each individual condition, and compared them to

matched uninfected controls. When considering all samples without distinguishing between MOI or time post-infection, we found 66 tRFs which met our thresholds for significant dysregulation (|log2(fold change)| > 1 ; adjusted p-value < 0.01) (**Figure 17A**).

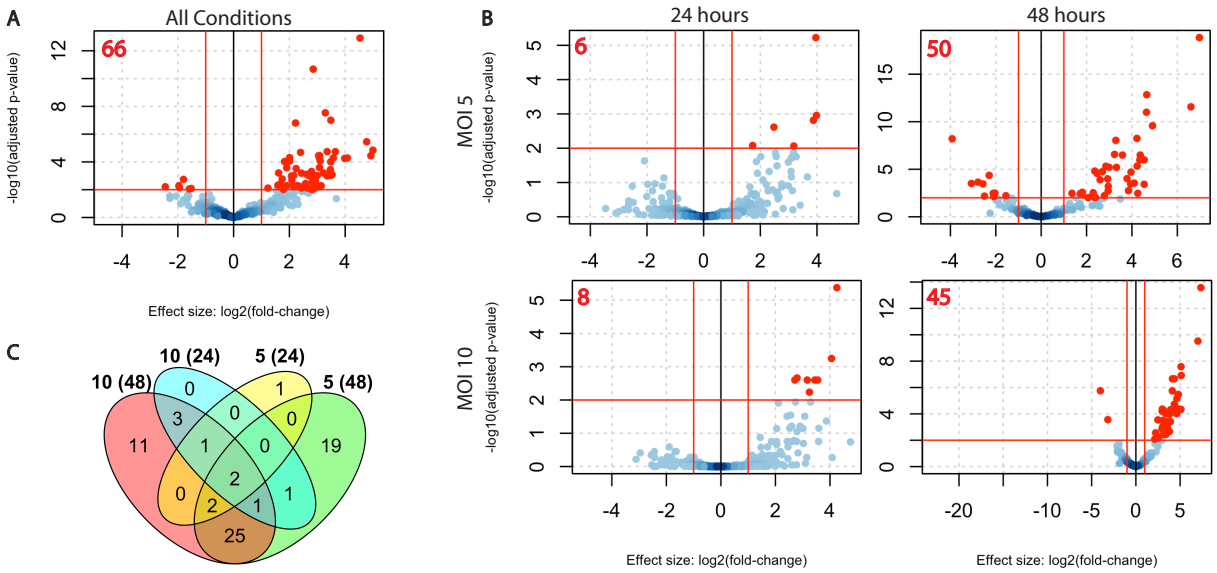

Figure 17. tRF dysregulation increases with severity of *Mtb* infection.
A) Volcano plot showing differentially produced tRFs in *Mtb*-infected primary human MDMs. tRFs from four infection conditions (MOI of 5 - 24 hours, MOI of 5 - 48 hours, MOI of 10 - 24 hours, and MOI of 10 - 48 hours) are compared to tRFs from uninfected cells at matched time points. Red lines indicate significance cutoffs (|log2(fold change)| > 1 ; adjusted p-value < 0.01), adjusted p-value < 0.01). Red points indicate tRFs which are significantly dysregulated between infected and uninfected conditions. Red points indicate tRFs which are significantly dysregulated between infected and uninfected conditions. Red points indicate tRFs which are significantly dysregulated between infected and uninfected conditions (66 total). B) Volcano plots showing differential production of tRFs in each independent infection condition separated by MOI and time post-infection. Significance indicators are the same as in (A) Red bolded numbers in upper left corner of each volcano plot represent the total number of significantly dysregulated tRFs. C) Venn diagram showing the number of significantly dysregulated tRFs shared in each infection condition. Bolded numbers outside each oval represent the MOI and time point (in parentheses).

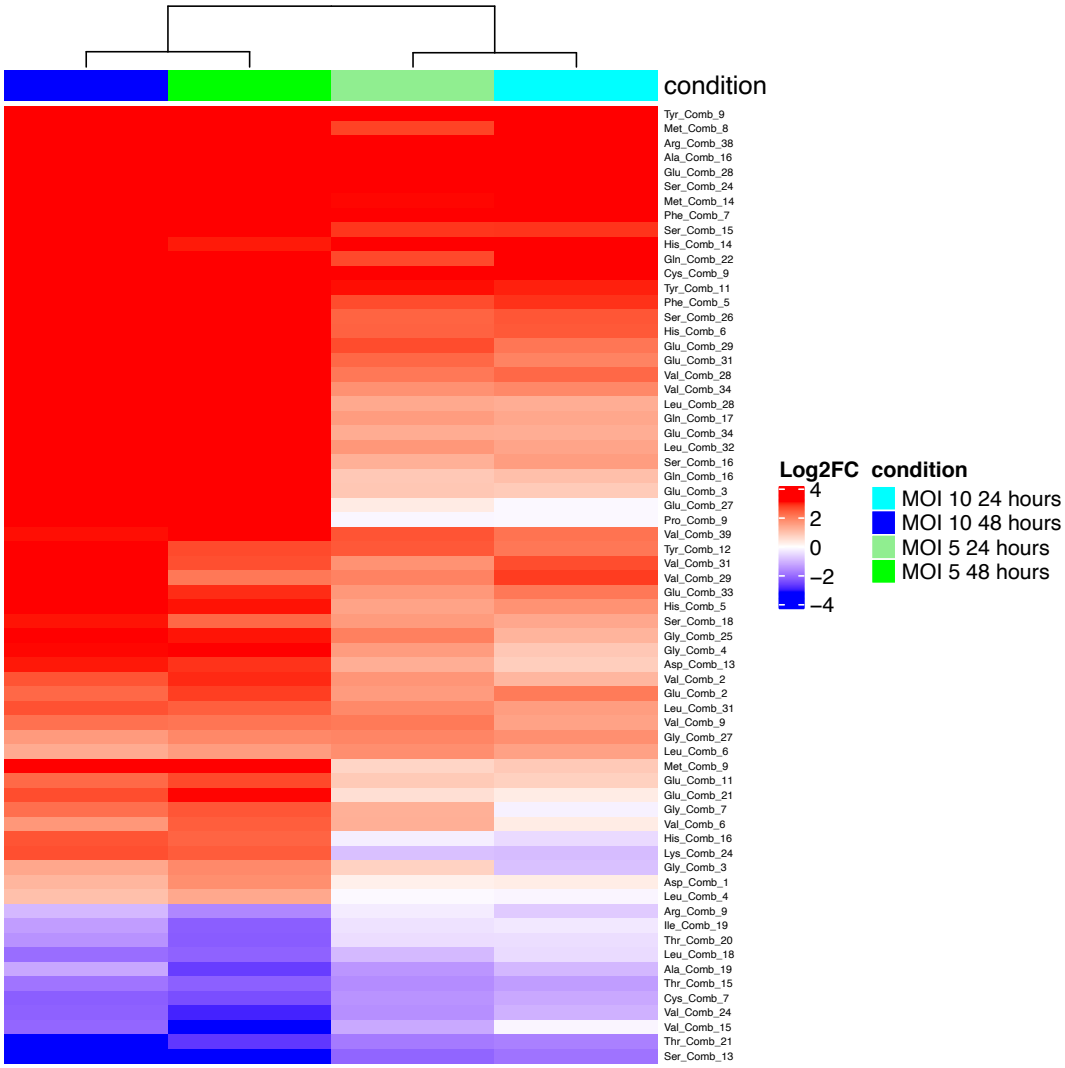

Figure 18. Log$_2$(fold-change) of each significantly dysregulated tRF across Mtb infection conditions.
All 66 tRFs which were significantly dysregulated in more than one *Mtb* infection condition are reported to show consistency in direction of dysregulation between infection conditions.

The number of dysregulated tRFs for each MOI increased between 24 and 48 hours post-infection. A similar increase was observed at each time point with increasing MOI (**Figure 17B**). Importantly, many of the tRFs dysregulated by less severe infection conditions were also significantly dysregulated in the more severe conditions. Five of six tRFs that were significantly

differentially abundant at MOI of 5/24 hours were also observed at 48 hours. All of the tRFs that were significantly dsyregulated at an MOI of 10 at 24 hours were also significantly dysregulated at 48 hours. Cells infected at MOIs of 5 and 10 shared approximately 50% of their significantly different tRFs at 48 hours (**Figure 17C**). Importantly, all tRFs that were significantly dysregulated in more than one condition were dysregulated in the same direction (**Figure 18**). The consistent dysregulation of these tRFs suggests that their altered abundance likely reflects a true biological phenomenon.

Mtb infection is associated with a bias towards dysregulation of mitochondria-derived tRFs

Given the stark differences in tRF dysregulation among various bacterial species, and the propensity for *Mtb* to induce mitochondrial distress, we next sought to assess the origin of significantly dysregulated tRFs by determining whether the sequence originated from the host nuclear or mitochondrial genome. We then compared the percent of significantly dysregulated mitochondrial-derived tRFs (mtRFs) from our own dataset to that from publicly available datasets generated for host cells infected by *Mtb, L. monocytogenes, Y. pseudotuberculosis,* and *S. typhimurium.* Hypoxia in MCF7 cells was again used as a non-infectious control. In addition to its relevance to TB disease, hypoxia also alters mitochondrial function [83], allowing us to determine whether mtRF dysregulation is specific to *Mtb* infection or simply due to general stress-induced mitochondrial dysfunction. Interestingly, we found that *Mtb* infections were associated with a strong bias toward mtRFs, whereas other intracellular bacterial pathogens and hypoxia were not. Of the significantly dysregulated tRFs in *Mtb* infections, 59-76% originated from mitochondria. For datasets that showed clear clustering of tRFs based on infection status (*Mtb and L. monocytogenes*), we examined mtRF dysregulation among all time points, as well as at the last

Table 8. tRFs dysregulated in mycobacterial infections are primarily of mitochondrial origin.

	Time (hrs)	mtRF	non-mtRF	% mtRF	X^2	*p*-value
Mtb	all	57	18	76.0%	1.04E+02	2.20E-16
Mtb	48	54	24	69.2%	8.09E+01	2.20E-16
Mtb (Looney, *et al.*)	all	44	22	66.7%	5.72E+01	3.94E-14
Mtb (Looney, *et al.*)	48	27	19	58.7%	2.42E+01	8.60E-07
L. monocytogenes	24	45	72	38.5%	9.51E+00	2.05E-03
Hypoxia MCF7 cells	all	29	66	30.5%	5.80E-01	4.46E-01
L. monocytogenes	all	17	44	27.9%	1.40E-03	9.70E-01
Y. pseudotuberculosis	all	3	21	12.5%	1.92E+00	1.65E-01
*S. typhimurium**	all	1	11	0.1%	N/A	N/A
BCG*	all	0	1	0%	N/A	N/A

Genomic origins of significantly dysregulated tRFs for each dataset were analyzed using miRge2.0. Percent of significantly dysregulated tRFs for each dataset that originated from the mitochondrial genome (% mtRF) are reported along with X^2 test results, with p-values. * X^2 analysis was excluded due to insufficient data points.

time point only. The last time points were analyzed independently, as tRF dysregulation increases with time post-infection. For datasets that did not show clustering, we included all time points, as time post-infection did not significantly alter tRF dysregulation. Analysis of our independently generated dataset showed that mtRFs accounted for 66.7% of all dysregulated tRFs (X^2 = 57.20; p= 3.94×10^{-14}) across all time points and 59% at 48 hours post-infection (X^2 =24.20, p=8.60×10^{-07}). Similarly, the analysis of the publicly available *Mtb* dataset showed that mtRFs accounted for 76% of all dysregulated tRFs (X^2=104.00, p=2.20×10^{-16}) across all time points and 69% at 48 hours post-infection (X^2=80.86, p=2.20×10^{-16}). In contrast, mtRFs comprised a smaller proportion of dysregulated tRFs following macrophage infection with other intracellular bacteria or exposure to hypoxia. *L. monocytogenes* was the only other organism which achieved statistical significance, though a smaller proportion of dysregulated tRFs were mitochondria-derived compared to *Mtb* infections (39%, p=2.05×10^{-3}, **Table 8**). This suggests that *Mtb* infections bias towards tRF production from mitochondrial tRNAs.

2.4 *Mycobacterium tuberculosis* disrupts mitochondrial responses to evade host macrophage mediated killing

*This study was done in collaboration with Grant Butschek and Anna Saorin of the Anne Hamacher-Brady Laboratory

Given our finding that the large majority of dysregulated tRFs in *Mtb* infection derive from the host mitochondrial genome, we hypothesized that *Mtb* may shift the balance towards necrosis by altering expression and recruitment of protein factors associated with mitochondrial distress and cell death. We also suspected that the mtRF bias observed in *Mtb* infection may be related to an aberrant mitochondrial response to infection. To examine this, we performed a series of widefield imaging-based and mechanistic studies to determine if *Mtb* infection is associated with perturbation of various markers of mitochondrial function and/or angiogenin (ANG), the RNase responsible for cleavage of tRNAs into tRFs. Mitochondrial markers of interest were selected based on their known roles in regulating the mitochondrial response and include Tom20, an OMM translocase used as a broad mitochondrial marker, Bax, an OMM associated pore-forming protein that facilitates release of cytochrome c to initiate apopotosis, cytochrome c, typically sequestered to the mitochondrial intermembrane space but released during apoptosis initiation to activate caspases 9, 3, and 7, Rab5, an early endosome marker and intracellular trafficking-associated GTPase, Rab7, a late endosomal marker and endocytosis-associated GTPase, and XIAP, a TRAF 1 and TRAF 2 binding apoptotic suppressor known to inhibit activation of caspase 3 and 7 [84-86]. Though it is known that *Mtb* pushes macrophages towards necrosis to promote its own growth and survival, little is known about how *Mtb* inhibits apoptosis to shift the balance towards necrosis. To test this, we examined the aforementioned markers in combination with ANG for their

subcellular localization in *Mtb*-infected primary human MDMs to determine their roles in regulating the mitochondrial response to *Mtb* infection.

2.4.1 Methodologies

Ethics

This study was approved by the Johns Hopkins University Institutional Review Board and does not classify as human subjects research. Blood samples used for MDM isolation were deidentified prior to use.

Macrophage culture

Primary human MDMs were isolated from platelet-depleted whole blood from healthy human donors at the Anne Arundel Medical Center, Maryland. MDM isolation was done as described above (section 2.2.1, **Figure 1**) using Ficoll-paque density centrifugation and passive plastic adherence. Isolated MDMs were plated in Ibidi-treat 8 well μ-slides (Ibidi, Cat # 80826) in 250μl of RPMI-1640 + 4mM L-glutamine + 10% regular FBS for one week to allow differentiation into macrophages. Media was changed every 2-3 days.

Bacterial culture

Mtb strain H37Rv-lux was cultured and maintained as described above (section 2.2.1). *Mtb* strain H37Rv-GFP was provided as a gift from Alvaro Ordoñez and originally generated by Jeff Cirillo. H37Rv-GFP constitutively expresses GFP from a kanamycin-resistant cassette. H37Rv-GFP was grown in 7H9 broth media or on 7H10 agar containing 50mg/ml kanamycin. P1 glycerol stocks for all strains were frozen from single colonies.

MDM viability and bacterial load

MDM viability and bacterial load were assessed by MTS assay and luminescence assay, respectively, described in detail above in section 2.2.1.

Bacterial infections for imaging

For imaging experiments, MDMs plated in Ibidi chambers were washed once with 1X PBS to remove residual complete culture media. Cells were then infected with H37Rv-*lux* or H37Rv-GFP at an MOI of 10 for 4 hours in RPMI-1640 + 4mM L-glutamine + 2.5% regular FBS low-serum infection media. After 4 hour incubation, cells were washed 3X with 1X PBS to remove extracellular bacteria and media was replaced with fresh bacteria-free low-serum infection media and allowed to incubate for an additional 24-48 hours. After 24 or 48 hours of infection, cells were washed once in 1X PBS and fixed in 4% paraformaldehyde (PFA) at room temperature for 20 minutes. After fixation cells were washed once with 1X PBS to remove residual PFA and stored at 4°C until staining and imaging.

Antibodies and stains

The following primary antibodies and stains were used for widefield imaging studies. Mouse anti-Tom20 (Santa Cruz, Cat # 17764, 1:200 dilution), rabbit anti-Bax (AB clonal, Cat # A12009, 1:800 dilution), mouse anti-cytochrome c (BD biosciences 556432, 1:500 dilution), mouse anti-Rab5 (Cell Signaling, Cat # 46449S, 1:300 dilution), rabbit anti-Tom20 (AB Clonal, Cat # A6774, 1:500 dilution), mouse anti-XIAP (Santa Cruz, Cat # 55551, 1:200 dilution), rabbit anti-Rab7 (Cell Signaling 9367, 1:100 dilution), and mouse anti-ANG (AB Cam, Cat # 10600, 1:800 dilution). Secondary fluorophore-conjugated antibodies were interchanged based on imaging needs and included Alexa Flour 546 and Alexa Fluor 647 (ThermoFisher) and were exchanged depending on primary antibody combinations.

Fluorescent staining and imaging

Fixed cells were washed once with 1X PBS and permeabilized using Triton X-100 (ThermoFisher, Cat # 85111) for 10 minutes and blocked with 3% w/v bovine serum albumen (ThermoFisher, Cat # B14) in 1X PBS for 1 hour at room temperature. Following permeabilization, cells were incubated with primary antibodies at room temperature for 1 hour or at 4°C overnight (based on optimizations). Cells were then stained with fluorophore-conjugated secondary antibodies for 1 hour at room temperature and with Hoechst stain for 15 minutes at room temperature. Stained cells were imaged in 1X PBS on a DeltaVision widefield microscope (GE Health Care) equipped with a Scientific CMOS camera (Chip size: 2560 32160 pixels, an Ultra Fast solid-state illumination, oil emersion objective, Ultimate Focus module, and 488 nm and 568 nm laser modules. Images were taken at 40X or 60X magnification with oil emersion. Z stacks were taken with 0.3 μm step size Raw images were processed and analyzed using Fiji (Image J). 3D colocalization analysis was generated using Colocalization Colormap [87].

Bacterial infections for ANG knock downs and knock ins

Cells were infected as detailed above for 72 hours with or without siRNAs or recombinant ANG. During infection, cells were incubated with either a scrambled non-targeting negative control Accell siRNA (Dharmacon, Cat# D-001950-01-50, sequence UGGUUUACAUGUCGACUAA), an ANG-targeting experimental Accell siRNA SMARTpool (Dharmacon, Cat# E-011206-00-0050, sequences CUUGGAUCAGUCAAUUUUC, UCAGAAACGUUGUUGUUGC, CCCUCACAGAGAAAACCUA, and UGACCCAGC-ACUAUGAUGC) in primary cell optimized Accell siRNA delivery media (Dharmacon, Cat# B-005000-500) and siRNA buffer (Dharmacon, Cat# B-002000-UB-100) for knockdown, or incubated with complete cell culture media supplemented with 500ng/ml recombinant human

ANG (abcam, Cat# ab151351). After infection, cells were washed once with 1X PBS and lysed in Trizol. Following infection, supernatant was collected and cells were lysed in RIPA buffer. All supernatants and lysates were stores at -80°C until use in RNA extraction and ELISA.

ELISA

ELISA was performed using the Human Angiogenin ELISA Kit following manufacturer instructions (abcam, Cat # ab219629). Starting samples were cell culture supernatant and RIPA buffer cell lysates.

RNA extraction

RNA was extracted from samples homogenized in TRIzol and frozen at -80°C. RNA extractions were performed using the Qiagen RNeasy Mini Kit (Qiagen, Cat # 74104) following manufacturer instruction. RNA quality was assessed via Nanodrop prior to qRT-PCR.

qRT-PCR

cDNA conversion was performed using the High-Capacity RNA-to-cDNA reverse transcriptase kit (Applied Biosystems, Cat# 4387406) following manufacturer instructions and using 10ng of total RNA input per reaction. qPCR to quantify expression of ANG compared to cyclophilin D housekeeping gene was performed following manufacturer instructions for the Power SYBR Green PCR Master Mix (Applied Biosystems, Cat# 4368577) and primers designed with NCBI Primer Blast and ordered from IDT (sequences for ANG: forward TTGTTCTGAGGCCGAGGAGC, reverse GGCATCATAGTGCTGGGTCA; sequences for cyclophilin D: forward CTTCCGGCCTCAGCTGTC, reverse AGGTCAAAATACACCTTGACGG). qPCR reactions were run on a StepOnePlus Real-Time PCR system (ThermoFisher).

Data and statistical analysis

ELISA and qRT-PCR data was analyzed in GraphPad Prism v8.0. Significance was calculated by two-way ANOVA using the Holm-Sidak correction for multiple comparisons.

2.4.2 Results

Mtb infection of macrophages drives cytochrome C retention in mitochondria despite BAX recruitment to the outer mitochondrial membrane

Healthy uninfected MDMs and MDMs infected with *Mtb* strain H37Rv were stained with the broad mitochondrial marker, Tom20, the OMM transporter, Bax, and cytochrome c, which is released into the cytoplasm during the initial phase of apoptosis. In uninfected controls, we did not observe any Bax upregulation of mitochondrial colocalization, suggesting that the uninfected cells were not stressed or initiating apoptosis (**Figure 19A, top row**). In contrast, we found Bax is strongly upregulated and recruited to mitochondria during infection with *Mtb*, suggesting initiation of the apoptotic pathway (**Figure 19A, bottom rows**). In conditions which stimulate apoptosis, Bax recruitment to the OMM is normally accompanied by robust release of cytochrome c from the mitochondria to the cytoplasm, resulting in the activation of downstream apoptotic signaling cascades, such as the activation of caspase 9, 3, and 7. Interestingly, we found that in *Mtb*-infected cells, despite the robust upregulation and recruitment of Bax to the OMM, cytochrome c was retained in mitochondria (**Figure 19B**).

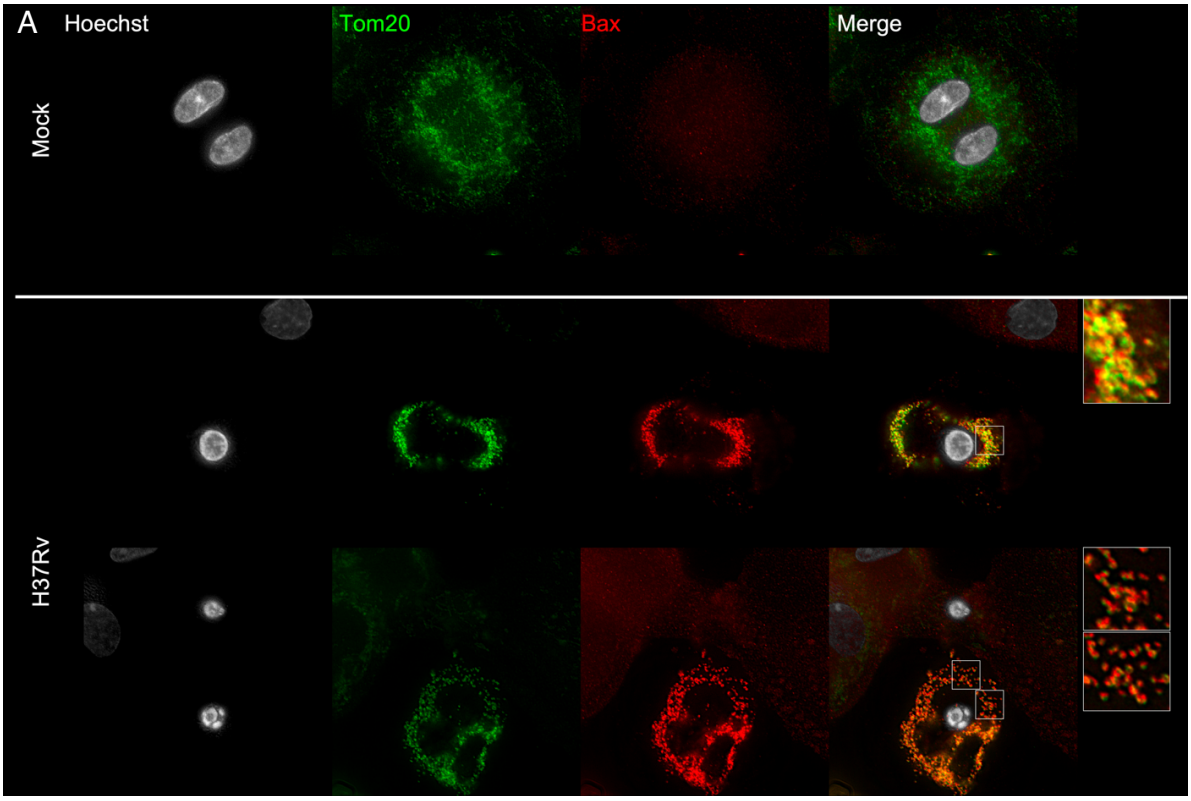
A
Hoechst
Tom20
Bax
Merge
Mock
H37Rv

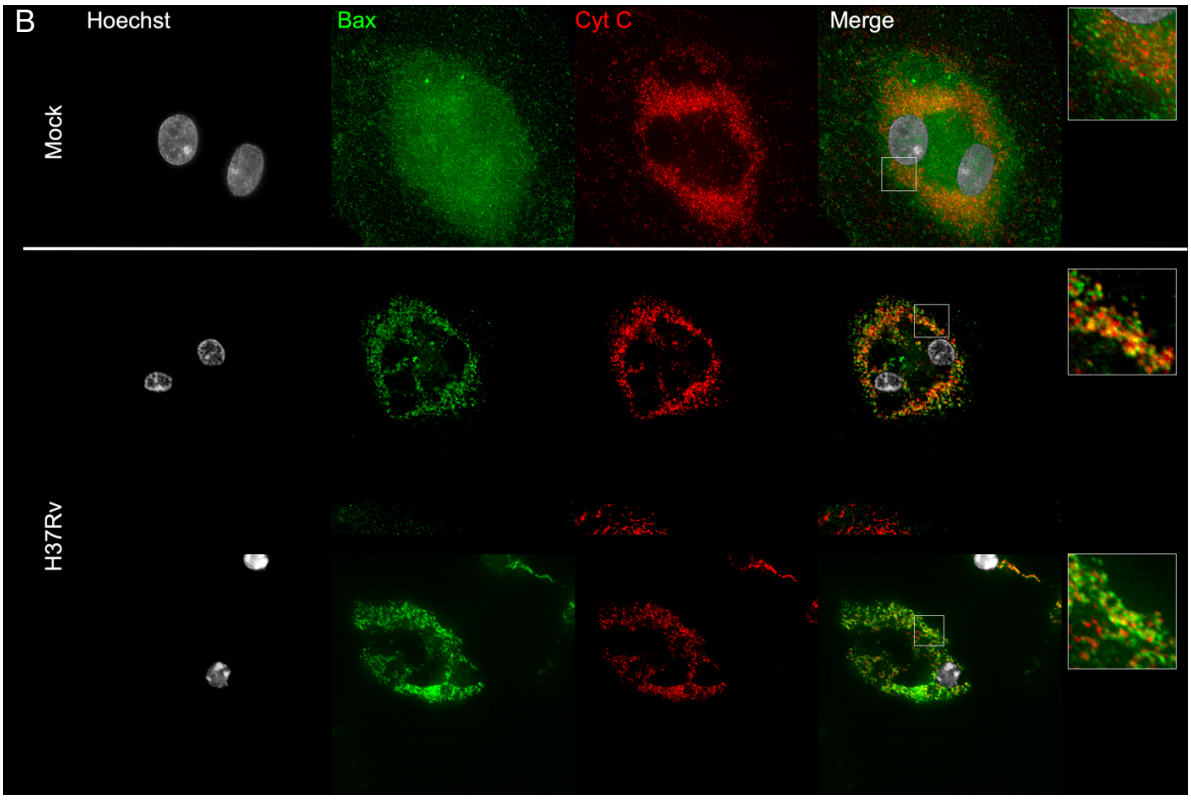
B
Hoechst
Bax
Cyt C
Merge
Mock
H37Rv

Figure 19. *Mtb* infection is associated with uncoupling of Bax recruitment to OMM and Cytochrome C release.
A) Representative images of uninfected (top row) vs. MDMs infected with *Mtb* at an MOI of 10 for 48 hours (two bottom rows) stained with Hoechst (gray, far right), anti-Tom20 (green, second right), anti-Bax (red, second left), and merge image (far left). B) Shows uninfected and *Mtb* infected cells stained with Hoechst (gray, far right), anti-Bax (green, second right), anti-cytochrome c (red, second left), and merge images (far left). Images taken on widefield fluorescent microscope at 60X resolution under oil emersion.

Upregulation and mitochondrial localization of early, but not late, endosomal markers during *Mtb* infection

Mtb is known to disrupt progression of endosomal maturation and endosome-lysosome fusion in infected macrophages [88]. To study the relationship of early and late endosomes with the mitochondria in *Mtb* infection, and to determine if any differences were unique to *Mtb*-infected cells or if disruptions could be seen in neighboring, uninfected cells, we infected MDMs with a GFP-expressing strain of *Mtb*, H37Rv-GFP, at an MOI of 10 for 48 hours and examined recruitment of Rab5, an early endosomal marker, and Rab7, a late endosomal marker, to mitochondria. We found that Rab5, but not Rab7, showed mitochondrial localization in *Mtb*-infected cells (**Figure 20**). Rab5 appeared to be expressed and diffusely present throughout the cytoplasm in uninfected cells, however, in cells infected with *Mtb*, Rab5 was more tightly colocalized with mitochondria. Conversely, Rab7, which was not detectable in uninfected cells, was highly abundant in the cytoplasm of *Mtb*-infected macrophages, but did not colocalize with mitochondria. Given these findings, it appears that Rab5 may be more likely to influence mitochondrial responses in *Mtb*-infected macrophages compared to Rab7.

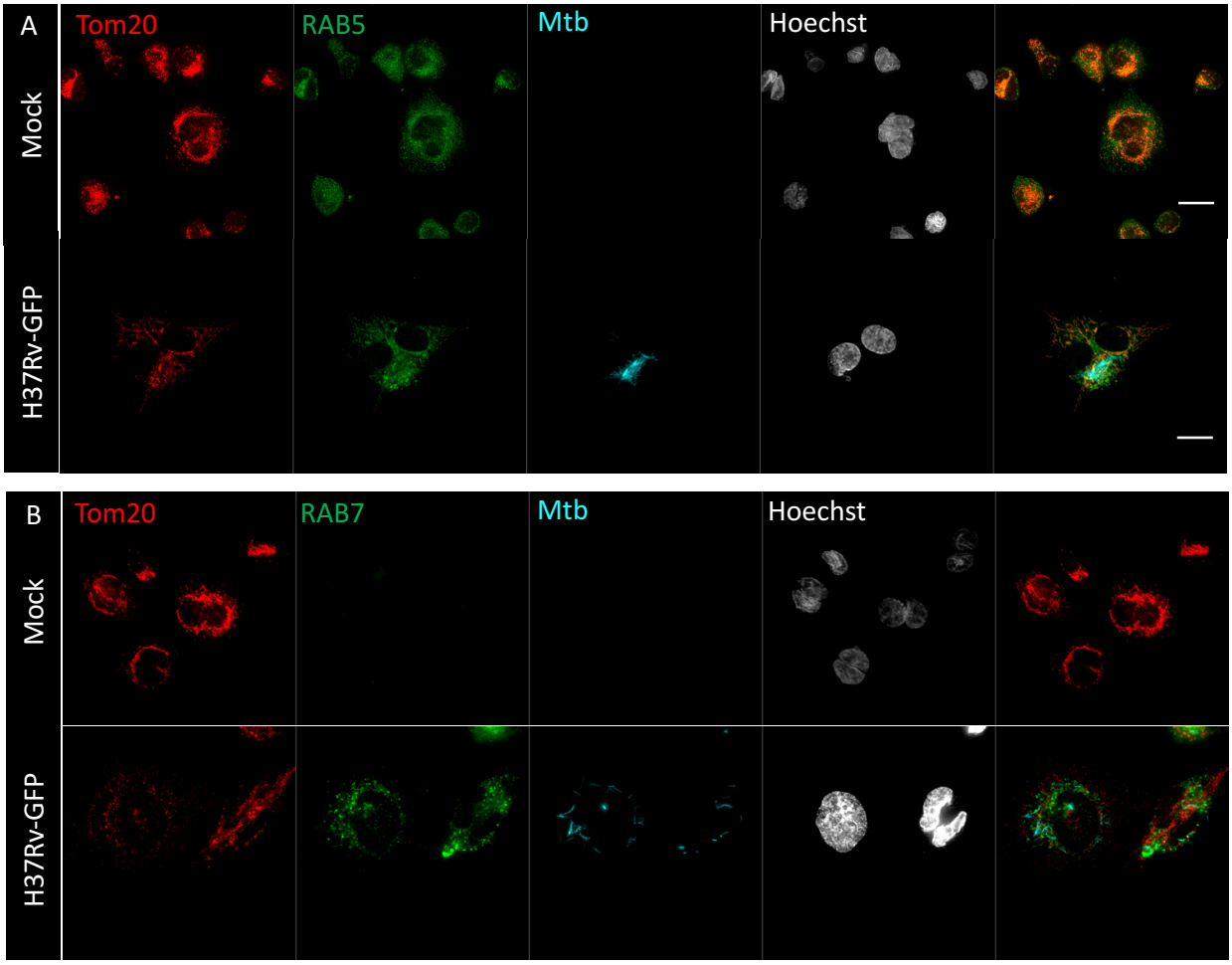

Figure 20. Early, but not late, endosomal markers localize to the mitochondria during *Mtb* infection of macrophages.
Representative images of MDMs infected with *Mtb* strain H37Rv-GFP (cyan, middle) at an MOI of 10 for 48 hours. anti-Tom20 (red, far right), anti-Rab5 (A) or anti-Rab7 (B) (green, second right), and Hoechst (gray, second left). Merge images are shown far right. Images were taken on a widefield microscope at 60X with oil emersion.

Recruitment of the apoptosis inhibitor, XIAP, is seen in some infected cells and may increase with intracellular bacterial burden.

As *Mtb* inhibits apoptosis to promote necrosis, it is likely that the expression and/or activity of certain anti-apoptotic factors are increased in *Mtb* infection. Additionally, since apoptosis is initiated by mitochondria, it is possible that those anti-apoptotic factors may be recruited to

mitochondria during *Mtb* infection. We observed that X-linked inhibitor of apoptosis protein (XIAP), a member of a family of apoptotic suppressors that binds TNF receptor-associated factors 1 and 2 (TRAF1 and TRAF2, respectively) and inhibits caspases 3 and 7, is upregulated and localized to the mitochondria in some, but not all *Mtb*-infected and neighboring cells. As not all cells are infected with *Mtb* and some may have higher bacterial burdens than others, we examined the association between XIAP expression/localization and intracellular *Mtb* burden. We found that XIAP expression and mitochondrial localization in cells was positively correlated with higher intrabacillary content, suggesting that XIAP may be recruited to the mitochondria to inhibit apoptotic processes in macrophages with high infection burdens (**Figure 21**). Images show a representative field containing two cells, one with many *Mtb* bacilli and one with comparatively few. Only the cell with a high *Mtb* burden shows XIAP recruitment to mitochondria.

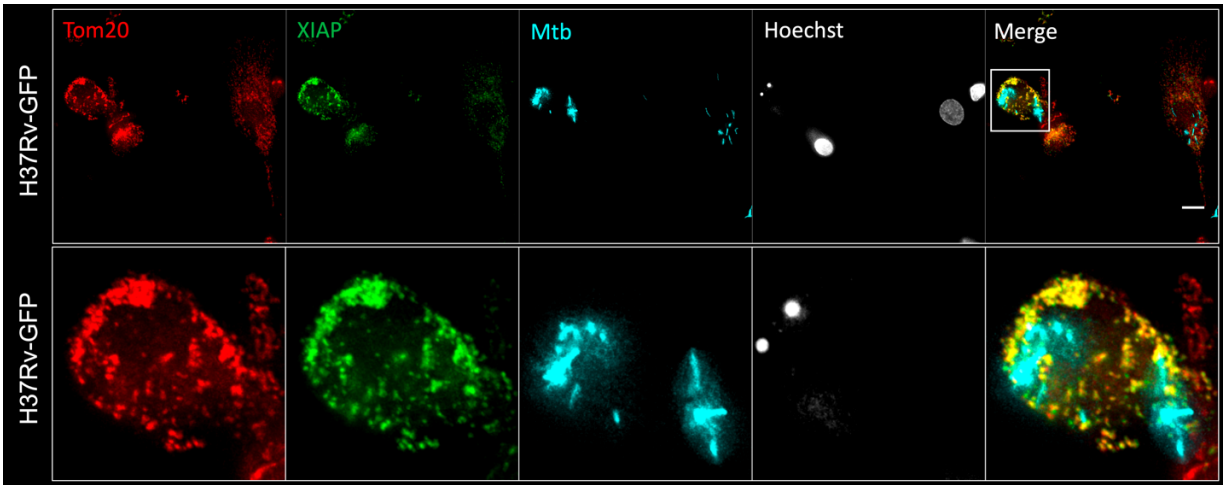

Figure 21. XIAP recruitment to mitochondria is robust in some cells with high bacillary burden.
Representative images of MDMs infected with *Mtb* H37Rv-GFP (cyan, middle) at an MOI of 10 for 48 hours. Cells were stained with anti-Tom20 (red, far right), anti-XIAP (green, second right), and Hoechst (gray, second left). Merge images are shown far right. Top row shows two cells, one with high bacillary burden (left) and one with lower bacillary burden (right). The cell with high bacillary burden that shows robust XIAP upregulation and mitochondrial localization is shown in a zoomed-in version in the bottom row. Images were taken on a widefield microscope at 60X with oil emersion. Scale bar = 10μm.

ANG upregulation and recruitment to mitochondria is robust and specific to cells with high intracellular *Mtb* burden.

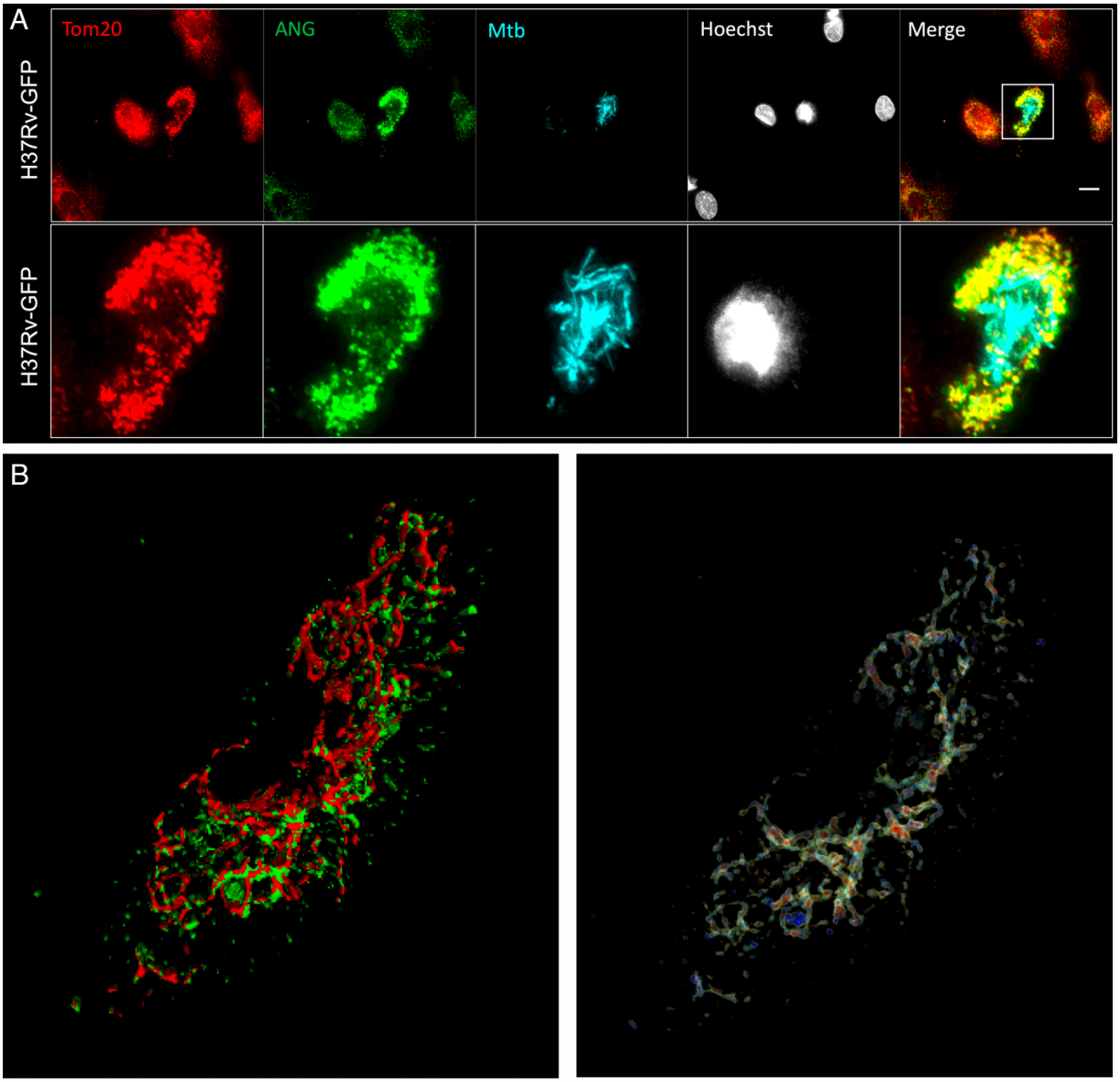

Figure 22. ANG is recruited to the mitochondria in *Mtb*-infected MDMs.
A) Top row shows an image field showing 5 cells, including four low-burden or uninfected cells and a central highly infected cell. Cells are stained with anti-Tom20 (red, far right), ANG (green, second right), and Hoechst (gray, second left). Merge images are shown far left. Bottom row shows a zoomed-in image of the central cell with high infection burden. B) 3D modeling of Tom20 (red) and ANG (green) marker localization (right). 3D heatmap showing degree of marker colocalization. Scale bar = 10μm.

We found previously that tRFs produced in *Mtb* infection derive primarily from tRNAs encoded by the mitochondrial genome (**Table 8**) [49]. Therefore, we hypothesized that ANG, the enzyme responsible for cleaving most tRFs, may be trafficked to mitochondria during *Mtb* infection where it may gain access to otherwise inaccessible mitochondrial tRNAs and cleave them into mtRFs.

We found that ANG is, in fact, recruited to mitochondria in *Mtb*-infected MDMs and that ANG is most robustly upregulated and mitochondria-localized in cells that have high *Mtb* burden. Neighboring uninfected cells show relatively low expression of ANG or mitochondrial colocalization, suggesting that these processes are *Mtb* infection-dependent (**Figure 22A**). 3D modeling of ANG and Tom20 colocalization shows that ANG is very tightly colocalized with mitochondria during *Mtb* infection (**Figure 22B**).

ANG production is not associated with altered overall infection outcome *in vitro*

Given the specificity of the ANG response seen in *Mtb*-infected MDMs, we suspected that ANG levels within the cell may alter outcome of infection. To test this hypothesis, we used ANG siRNA or exogenous recombinant human ANG (rhANG) to silence or knock in, respectively, expression of ANG in *Mtb*-infected MDMs. We found that neither intervention resulted in significant differences in MDM viability or bacterial burden over 3 days post-infection (**Figure 23**). Despite this finding, it is possible that ANG upregulation and recruitment to mitochondria may still play a role in a more complex system, such as *in vivo*.

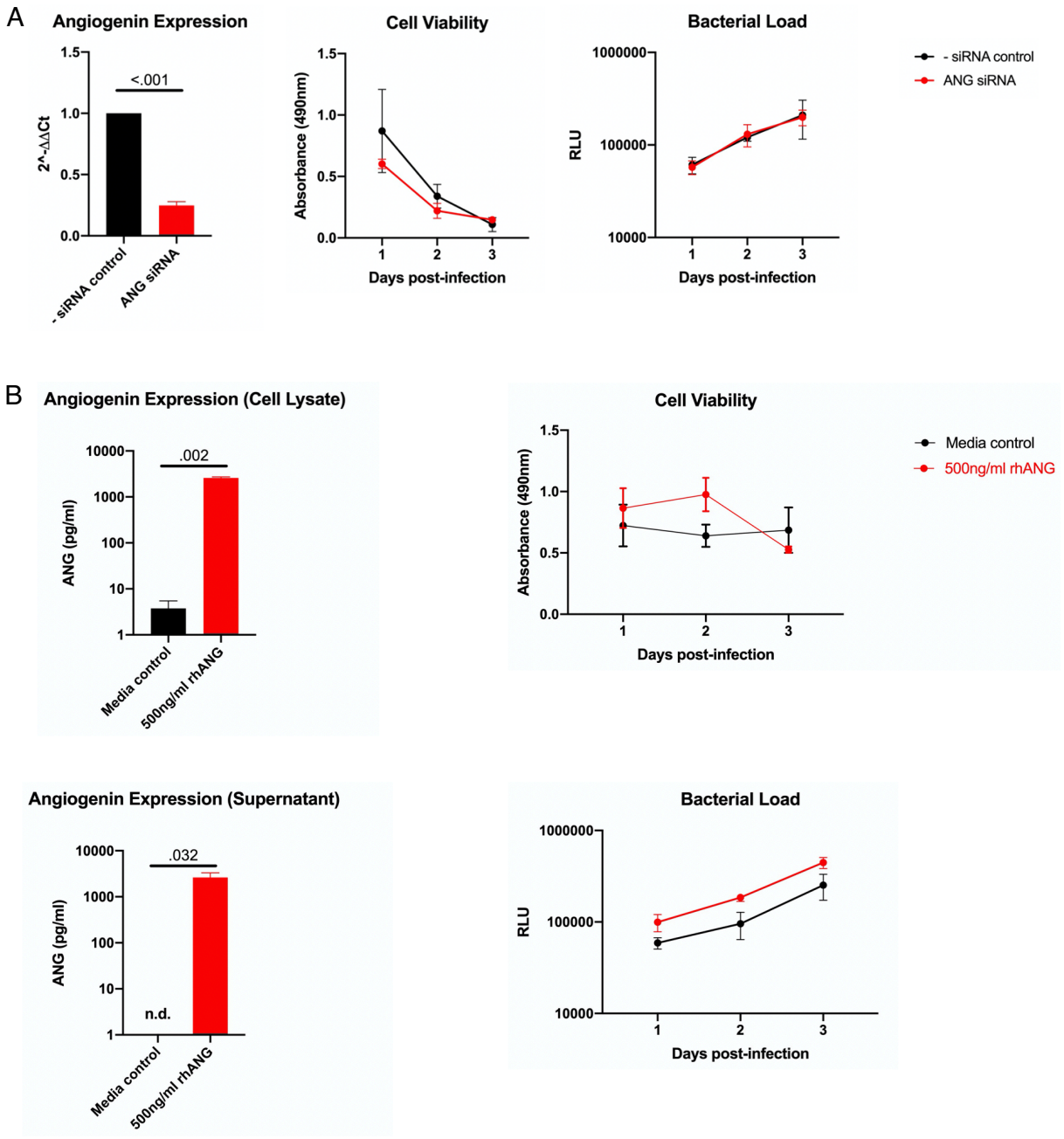

Figure 23. ANG does not affect MDM viability or bacterial burden *in vitro*.
A) ANG was knocked down in MDMs using an anti-ANG siRNA pool and infected with *Mtb*. ANG expression was assessed by qRT-PCR on day 3 post infection. Cell viability was assessed by MTS assay at days 1, 2, and 3 post-infection. Bacterial load was assessed by luminescence assay at days 1, 2, and 3 post infection. B) MDMs were cultured in regular complete media or in media supplemented with 500ng/ml rhANG. ANG protein in cell lysates and supernatant was assessed by ELISA on day 3 post-infection. MDM viability and bacterial load were assessed as in A.

2.5 Conclusions

2.5.1 Integrated transcriptomic and epigenetic analyses reveal network of pre- and post-transcriptional regulation of macrophage responses in *Mtb* infection

Taken together, our results show that critical innate immune processes and signaling are influenced by both pre-transcriptional regulation via changes in DNA methylation and post-transcriptional regulation via altered miRNA expression. Application of next generation sRNA-seq allowed us to identify a small profile of candidate miRNAs that are likely to serve a biological function during *Mtb* infection. By integrating our sRNA-seq data with total RNA-seq, we found that all of our candidate miRNAs had mRNA targets that were also differentially expressed in *Mtb*-infected cells. These miRNA-targeted differentially expressed genes were involved in various biological processes that are critical for the host defense against *Mtb* infection. The pathways that were most significantly represented amongst these miRNA-targeted differentially expressed mRNAs included innate immune cell activation, regulation of metabolic and lipid synthesis processes, vasculature development, and intracellular transport, exocytosis, and secretion.

More specifically, dysregulated targets of miR-155-5p are associated with activation of various immune cell types. Macrophages are responsible for initiating many of the signaling cascades to drive activation of different immune cells. Defense against *Mtb* requires a complex, but coordinated, cascade of immune cell activation. Disruption of these pathways may impede the host's ability to recognize and respond to *Mtb* infection [21, 22]. Additionally, *Mtb* may disrupt host metabolic pathways to induce lipid accumulation and synthesis in host macrophages to increase access to nutrients and facilitate persistence [89-91]. miR-30c-5p targets were involved in regulation of exocytosis and secretion which is important for cell-to-cell signaling, and miR-

29a-3p targets were associated with regulation of blood vessel development, which is a critical process involved in the formation of granulomas and nutrient acquisition in *Mtb* infection [92-94].

Though this study is the first to integrate multiple next-generation sequencing-based analyses of miRNAs, mRNAs, and methylation in primary human monocyte-derived macrophages infected with *Mtb*, previous studies have investigated each of these components individually and in different models. Consistent with the published literature, we found that miR-155-5p was robustly upregulated. miR-155-5p is one of the most studied miRNAs in TB disease and known to be dysregulated by infection in different systems [95]. In dendritic cells, upregulation of miR-155-5p in *Mtb* infection is associated with suppression of autophagy, suggesting a host-detrimental effect [96]. However, miR-155-5p knock out mice display increased susceptibility to *Mtb* infection and higher bacterial burden in the lung. This is also associated with altered immune cell infiltrates in the lung, such that miR-155-5p knock out mice lungs have fewer T cells and more monocytes and neutrophils [97]. miR-155-5p has also been associated with increased survival of *Mtb*-infected bone marrow-derived macrophages (BMDMs), which is thought to provide a more stable niche environment that promotes survival of intracellular bacteria. However, this increased macrophage survival is balanced by increased survival of *Mtb*-specific T cells, which is critical for elimination of infection [98]. Taken together, these studies show that miR-155-5p is involved in regulating cellular immune responses to *Mtb*, but that it may have both host-beneficial and host-detrimental effects depending on when it is expressed and what genes are targeted. This is in line with our study which shows many of the miRNA-155-5p targets that are dysregulated are involved in immune cell activation and coordination of cellular immune responses, but also that some targets are upregulated while others are downregulated.

While miR-125b-5p was not statistically different in our study, it has been shown to be upregulated by qRT-PCR in previous studies. Previously, miR-125b-5p was found to be upregulated in *Mtb* infection and upregulation was associated with lower levels of TNF, suggesting suppression of an inflammatory response [28]. Despite lack of significantly different expression of miR-125b-5p by sRNA-seq in our study, we found significantly altered expression of miR-125b-5p targets, which are involved in regulation of metabolism, lipid processing, and small molecular transport and subcellular localization. This may suggest that even small changes in miRNA expression that failed to meet our stringent statistical thresholds may still have biological impact. Also, given that gene targets within any pathway can be targeted by multiple miRNAs, there may be redundancies in which more than one miRNA may target different genes within the same pathway such that the expression change in each individual miRNA may be small, but the combined effects are sufficient to alter the activation of the downstream pathway. This is represented by functional enrichment pathways for miR-125b-5p, miR-27a-3p, and miR-22-3p. These three miRNAs all targeted pathways involved in regulation of metabolism and lipid processing, which is important for shaping the intracellular environment in *Mtb*-infected macrophages.

In line with the likely additive or complimentary effects of multiple non-significantly dysregulated miRNAs that target the same pathways, miR-27a-3p was also not significantly dysregulated, though its dysregulated targets were involved in biosynthetic and metabolic processes as described above. This miRNA was included in our studies due to its representation in relevant literature, which has shown its involvement in the cellular response to mycobacterial infections. miR-27a-3p was shown to be downregulated and to target IRAK4 in THP1 cells. Downregulation of miR-27a-3p resulted in less repression of IRAK4 and subsequent increases in

production of IFNγ, IL-1β, IL-6, and TNFα, which are key cytokines associated with a successful anti-TB response [99]. miR-27a was also shown to inhibit intracellular survival of non-tuberculous mycobacteria by targeting IL-10 and TAB2 in RAW264.7 cells and murine BMDMs [100]. Differences between studies could be due to differences in model systems, experimental conditions, and detection methods.

While miR-22-3p is less well characterized in TB models, we found it to be significantly downregulated in *Mtb*-infected primary MDMs by sRNA-seq. Though this is the first time it has been described in macrophages, miR-22-3p has been found to be differentially abundant in the plasma of TB patients vs. healthy controls and has been considered for inclusion as a potential blood-based TB biomarker [101]. More work should be done to investigate the role of miR-22-3p in *Mtb* infection.

Both miR-30b-5p and miR-30c-5p were significantly downregulated in our study. Like miR-155-5p, the miR-30 family has been implicated in host immunity to TB, given its known role in targeting genes involved in important anti-TB responses, such as autophagy [102]. Earlier studies have shown dysregulation of miR-30a and miR-30e in THP1 cells, whereas miR-30c and miR-30d were not differentially expressed as measured by qRT-PCR [103]. While the GO:BP enrichment analysis of differentially expressed miR-30c-5p targets showed significant involvement in exocytosis and secretion, the miR-30b-5p and miR-30c-5p target, IL-1α, was significantly upregulated and is known to induce autophagy in macrophages [104, 105]. Taken together, these findings suggest that downregulation of miR-30c-5p and miR-30b-5p in *Mtb* infection may reflect the macrophage's effort to induce autophagy and cell-to-cell communication via exocytosis.

miR-29a-3p was included in our studies, as it has been found previously to be dysregulated in human MDMs infected with *Mycobacterium avium* by qPCR, and was shown to target caspase 7, which is involved in apoptosis [106]. While we did not observe significant dysregulation of miR-29a-3p in *Mtb*-infected primary human MDMs by sRNA-seq, targets of miR-29a-3p, including those involved in angiogenesis and blood vessel development, were significantly differentially regulated. The variability in miRNA expression between studies may be a result of differences in detection method but may also indicate that miR-29a-3p is more dysregulated following infection by non-tuberculous mycobacterial infections relative to *Mtb*. Additionally, the lack of dysregulation of miR-29a-3p expression in our study may suggest that dysregulation of angiogenesis may be mediated via altered macrophage responses, but occur independently of miR-29a-3p. This association has not yet been described in the context of TB and may be an important relationship to pursue for further investigation in more complex animal models, in which blood vessel formation may influence granuloma formation and dissemination of disease.

We found dysregulation of miR-191-3p, which has not yet been well-characterized in TB disease, though there were only two differentially expressed target genes, which did not associate with a specific biological process. Nonetheless, miR-191-3p has been implicated in other disease states and may warrant further study [107].

Unlike previous studies, we found that miR-21-5p was significantly downregulated in *Mtb*-infected MDMs. Earlier studies have shown upregulation of miR-21-5p in *Mtb*-infected murine RAW264.7 cells and human THP1 cells, which are both cancer-derived macrophage cell lines. Induction of miR-21-5p expression was associated with increased *Mtb* survival and reduced production of inflammatory cytokines, such as IL-1β, IL-6, and TNFα [108]. Conversely, we found that miR-21-5p was downregulated while its target, IL-1β, was significantly upregulated.

This suggests that compared to the cancerous cell lines, primary MDMs may generate more pro-inflammatory cytokines through downregulation of miR-21-5p.

We included miR-223-5p in our analyses based on previous literature, which has shown increased susceptibility of miR-223-5p knock out mice to TB [26]. In our study, we did not find miR-223-5p to be significantly dysregulated and we did not find a significant pathway association for the differentially expressed miR-223-5p target genes. This could indicate differences in the roles of this miRNA between model systems, such that changes in miR-223-5p expression are more important in non-macrophage cell types that are present *in vivo*. For instance, increased susceptibility of miR-223-5p knock out mice to TB disease is associated with robust neutrophil-mediated lung inflammation, which suggests that neutrophils may be critical for mediating the effects of miR-223-5p expression changes [26]. It may also indicate that changes in miR-223-5p expression must be quite large in order to have a biological effect.

Analysis of genome wide methylation changes in *Mtb*-infected cells by WGBS showed no significant methylation of promoter or gene regions of candidate miRNAs, suggesting that changes in the expression of miRNAs is likely to occur in a methylation-independent manner. On the other hand, various differentially expressed genes were also found to be differentially methylated by WGBS following *Mtb* infection in macrophages. Like differentially expressed genes targeted by the 10 miRNA candidates, macrophage genes that were both differentially expressed and divergenty methylated following *Mtb* infection were involved in various pathways important for anti-*Mtb* responses. Importantly, hypermethylated genes appeared to be involved in driving activation of innate and adaptive immune cells. This suggests that one mechanism by which *Mtb* may suppress immune activation is by increasing methylation of genes involved in related pathways in infected macrophages. Conversely, hypomethylated genes were most significantly

associated with the positive regulation of metabolic processes, which may underlie the ability of *Mtb* to alter macrophage metabolic processes to increase access to nutrient sources and promote bacterial growth and survival.

Finally, integration of sRNA-seq and RNA-seq data with WGBS showed that processes affected by changes in miRNA and mRNA expression are also divergently methylated. Most DMRs were hypomethylated, which may indicate the macrophage's effort to open chromatin to allow for rapid changes in transcriptional reprogramming during infection. Interestingly, in line with our miRNA and mRNA data, hypermethylation was associated with suppression of immune cell activation, while hypomethylation was associated with enhanced macrophage metabolism. Together, these opposing effects may reflect the generation of an environment in which intracellular bacilli are shielded from immune-mediated killing and able to access metabolic resources required for growth and survival within the host.

Genes that were differentially expressed, divergently methylated and targeted by at least one miRNA of interest were significantly associated with the AMPK signaling pathway, which is central to various cellular processes that shape the response to *Mtb* infection, including regulation of autophagy, fatty acid biosynthesis, glucose metabolism, and cell proliferation [109]. This pathway is of particular importance given that AMPK-targeting host-directed therapies, such as metformin, have been shown to promote *Mtb* killing in macrophages and in lungs of *Mtb*-infected mice [110] and to improve mortality when included in treatment regimens for TB patients with diabetes mellitus [111].

Overall, our data, combined with findings from previous literature, suggest that miRNAs are multifunctional in that they may target multiple genes from redundant and complimentary pathways. Additionally, multiple miRNAs may co-regulate the same targets or pathways, which

indicates that even small changes in a group of miRNAs may be biologically relevant. Additionally, alternate forms of gene regulation, including DNA methylation changes, also control miRNA-targeted pathways during *Mtb* infection of macrophages. This emphasizes the complexity of regulation of host responses and shows that the overall response of the macrophage is shaped by multiple contributing factors that must coordinate with one another in order to generate the appropriate response required to eliminate infection. While reductionist evaluations of these regulatory elements is powerful for determining specific targets, to understand how they shape disease outcome, they must also be examined in a broader context that provides insight into how they fit into broader regulatory networks.

These large scale transcriptomic and methylomic studies are descriptive by nature. Limitations include absence of non-tuberculous mycobacterial controls and individual validation of each differentially expressed miRNA, gene, or DMR. However, this study is not intended to investigate the impact of specific dysregulated elements on overall outcome of *Mtb* infection, but rather to provide an unbiased, global analysis of the complex network of macrophage transcriptional regulation. As such, these studies are valuable for providing novel insights into how multiple forms of regulation integrate to shape the overall macrophage response to *Mtb* infection. These findings are intended to serve as a roadmap for future studies exploring the relationship between pre-transcriptional DNA methylation and post-transcriptional miRNA regulatory mechanisms. Additional work should focus on targeted analysis of candidate miRNA-differentially expressed gene target pairs and genes which are both differentially methylated and differentially expressed. Overall, these studies show that dysregulation of methylation and miRNA candidate target genes centers on suppression of immune activation. Understanding how to restore balance of these elements may have implications for altering outcome of *Mtb* infection in

macrophages, particularly in the context of developing host-directed therapies which target AMPK signaling and other key regulatory pathways.

2.5.2 *Mtb* infection drives over-production of mitochondria-derived tRFs

Until now, tRFs had not been assessed in the context of bacterial infections. We found that *Mtb* drives significant dysregulation of tRFs and that tRF dysregulation increased with severity of infection. *L. monocytogenes* induced a pattern of tRF dysregulation that was similar to that seen in *Mtb* infection. However, other bacteria tested here did not significantly alter tRF abundance.

Only *Mtb* infection drove strongly biased dysregulation of mtRFs. This may reflect the severity of mitochondrial distress during *Mtb* infection, manifested by disruption of membrane potential and a shift towards necrosis, which is associated with mitochondrial swelling, mitochondrial outer membrane permeabilization, and bacterial release and survival [112-116]. These changes to mitochondrial membrane architecture can allow movement of certain protein and nucleic acid factors across the membrane [117, 118]. We predict that ANG, one of the RNAses that cleaves tRFs, and/or mtRNAs may be among these factors. Under normal conditions, ANG is sequestered to the nucleus. However, during cell stress, ANG is translocated to the cytoplasm [119]. *Mtb* infection induces cell stress and may drive translocation of ANG out of the nucleus. Given this, we have developed two hypotheses that may help explain the overabundance of mtRFs produced in *Mtb* infection: 1) Mitochondrial tRNAs are cleaved within the mitochondria after ANG (or other tRF-cleaving RNAses) is translocated into the mitochondria, or 2) Intact mitochondrial tRNAs are released from mitochondria into the cytoplasm, allowing them to be cleaved by ANG. These two hypotheses are represented diagrammatically below (**Figure 24**).

Reasons for the lack of mtRF-biased dysregulation in other infections remain unclear. Host cells infected with *Mtb* exhibit robust, stable signs of mitochondrial distress at least through 24 hours [113, 114]. This may allow for sustained interaction between mtRNAs and ANG and could result in increased producion of mtRFs. In contrast, though *L. monocytogenes* and *S. typhimurium* induce mitochondrial fragmentation, this effect is transient and mitochondria recover within 24

hours [120, 121]. There is no clearly defined link between *Y. pseudotuberculosis* infection and mitochondrial distress. It is, therefore, possible that the degree of mtRF dysregulation is proportional to the duration and extent of mitochondrial distress. However, additional research is required to elucidate this mechanism.

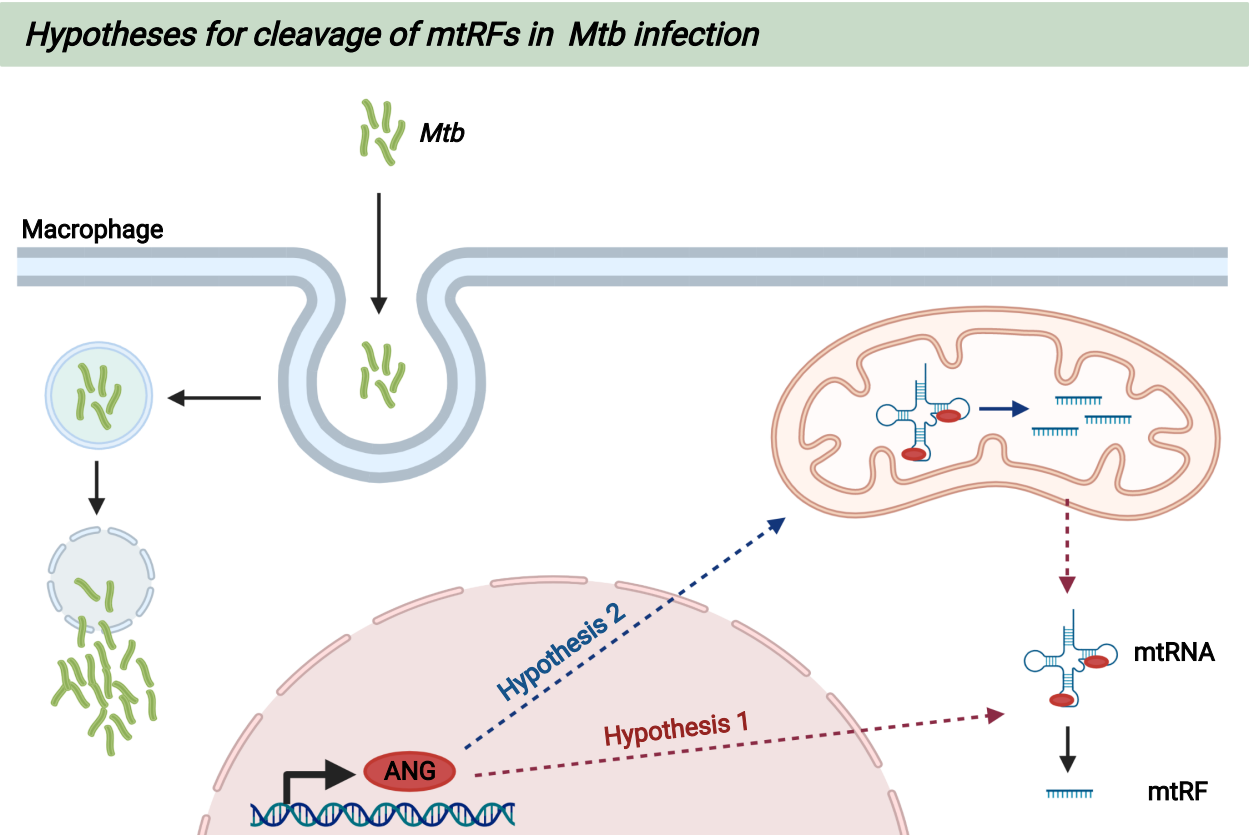

Figure 24. Hypotheses for cleavage of mtRFs in *Mtb* infection.
In hypothesis 1, during *Mtb* infection, angiogenin is upregulated and transported to the cytoplasm. Intact mtRNAs are exported or released from the mitochondria where they may encounter ANG in the cytoplasm. ANG binds mtRNA cleavage sites and cleaves mtRNAs into mtRFs. In hypothesis 2, ANG is upregulated and trafficked to the mitochondria so that it may bind mtRNAs and cleave mtRFs within the mitochondria.

In this study, we also designed tRFcluster as a module to miRge2.0. This tool allows for simultaneous identification of miRNAs and tRFs for downstream analyses. Herein, we validated our clustering approach for these complicated reads, successfully identified tRF clusters, and had performance at least equivalent to stand-alone tRF tools. Our approach is intermediate between MINTmap/MINTbase v2.0, which take a maximalist approach in uniquely identifying and naming

each sequence aligning to tRNA, resulting in 23,413 human tRFs, and the minimalist approach of tRFdb which lists only 552 human tRF sequences [69, 122, 123]. Despite our bacterial focus, this tool should have generalizable utility for analysis of tRF production and regulation in virtually any biological condition or disease state.

Limitations of this study include the inherent variability in experimental conditions between datasets. Factors that may have impacted comparisons are different cell types, library preparation protocols, and equipment for sRNA-seq. However, despite these methodological differences, we observed good consistency between our *Mtb* dataset and the publicly available *Mtb* dataset, suggesting that our results are reproducible and biologically relevant.

Overall, our results suggest that host cell tRFs are dysregulated by infection with certain bacterial pathogens, but the particular pattern is dependent on the infecting bacterial species. Additionally, our tRF data suggest that *Mtb* infection may alter mitochondrial physiology in such a way that creates a unique opportunity for interaction between mitochondrial tRNAs and tRF-cleaving enzymes.

2.5.3 *Mtb* infection is associated with disruption of classic apoptotic cascades and recruitment of ANG to host mitochondria

The unique overproduction of mtRFs led us to hypothesize that either ANG is being actively trafficked to mitochondria or intact mitochondrial tRNAs are being released to the cytoplasm during *Mtb* infection. As technology to adequately study the subcellular localization of tRFs does not yet exist, we aimed to investigate the first possibility by examining ANG localization in *Mtb*-infected primary human MDMs. We found that, not only is ANG upregulated and recruited to mitochondria during infection, but also that the ANG response is highly specific and appears to occur mostly in cells with high intracellular *Mtb* burden.

Our investigations also showed perturbations of some additional mitochondria-associated markers, including cytochrome c and XIAP. The retention of cytochrome c in the mitochondria

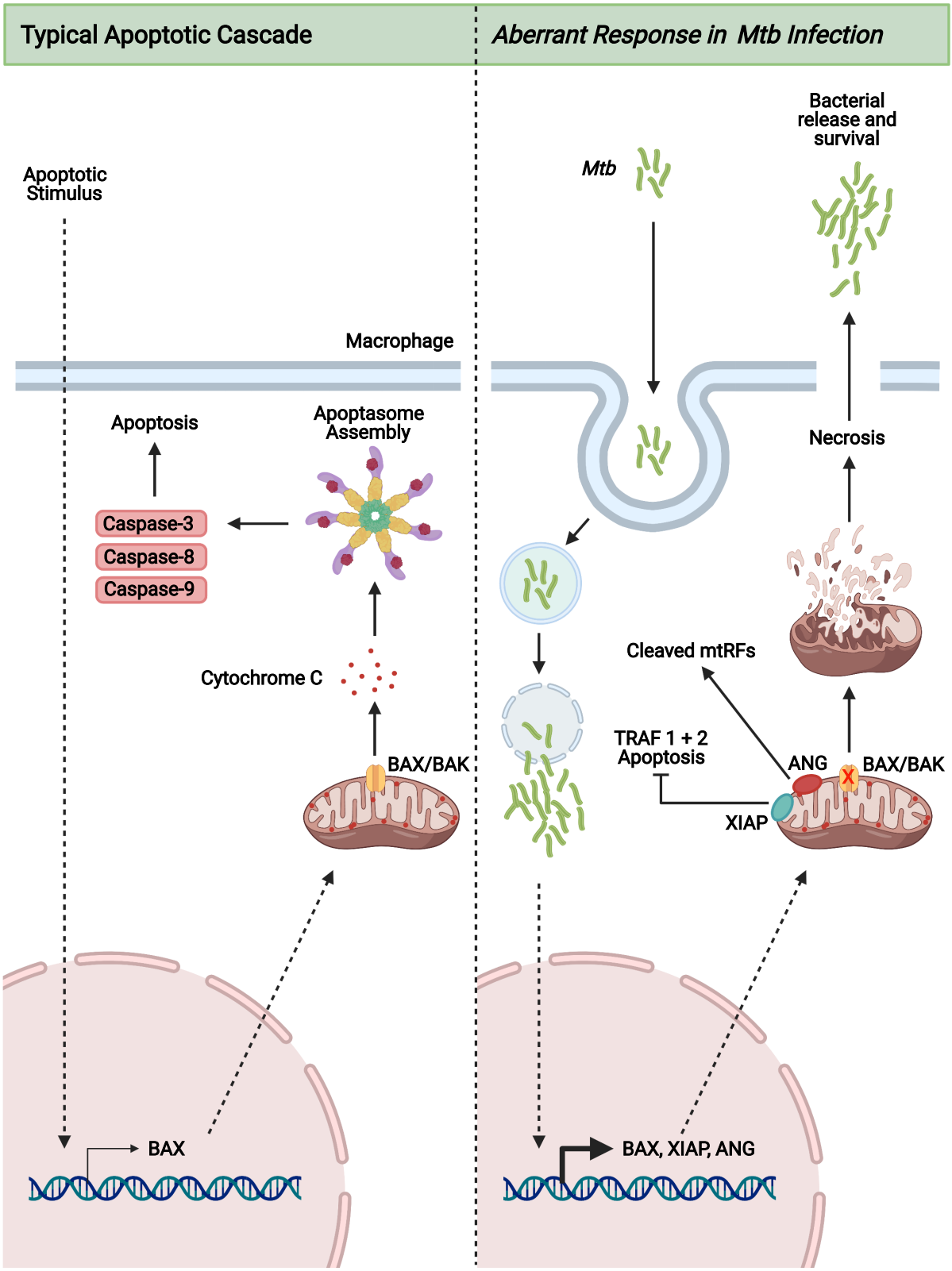

Figure 25. *Mtb* infection is associated with aberrant recruitment of Bax, XIAP, and ANG to mitochondria.

During a typical apoptotic cascade, an apoptotic stimulus triggers expression of Bax and translocation of Bax to the OMM. Formation of Bax/Bak pores allow the release of cytochrome c, formation of the apoptosome, activation of caspases, and cell death by apoptosis. In *Mtb* infection, we observe internalization of *Mtb*, cytoplasmic replication of *Mtb*, upregulation of Bax, XIAP, and ANG and translocation of all three proteins to the OMM. Recruitment of ANG may allow for the cleavage of mtRNAs into mtRFs while XIAP may suppress apoptosis. Despite Bax recruitment, cytochrome c remains retained within the mitochondria which may lead to mitochondrial rupture and necrosis.

despite normal Bax recruitment to the OMM suggests that in *Mtb* infection, one of the mechanisms of suppressing apoptosis may involve preventing the formation of functional Bax pores [114]. In this scenario, even if apoptotic cascade is initiated through recruitment of Bax to the OMM, Bax may not complex properly to allow the release of cytochrome c to the cytoplasm. As a result of cytochrome sequestering, mitochondria may undergo swelling, followed by activation of the necrotic programmed cell death pathway. Additionally, upregulation and mitochondrial localization of XIAP in cells with higher *Mtb* burden suggests that XIAP may also play a role in inhibiting apoptosis. Understanding the pivot point between apoptosis and necrosis is critical given that necrosis allows for release and survival of *Mtb* [112, 115, 116, 124]. A graphical summary of these changes is included above (**Figure 25**).

Our study investigated only the effects of *Mtb* infection vs. uninfected controls. Future work expanding on the difference between *Mtb* infection and infection with various non-tuberculous mycobacteria, such as BCG or *Mycobacterium avium*, would provide additional value and rigor to these findings. Additionally, thus far, these analyses are qualitative in nature and relatively low resolution, future work should focus on supplementing these findings with quantitative measurement of each observed phenotype and higher resolution analyses of subcellular localization, including electron microscopy.

Some of the major technical limitations of this study include our inabilities to perform live cell imaging of *Mtb*-infected cells and single molecule detection of tRFs within cells. As *Mtb* is a biosafety level 3 (BSL3) pathogen and we do not have access to a fluorescent widefield or confocal microscope inside our BSL3 facilities, all *Mtb*-infected samples must be fixed prior to removal

from BSL3 facilities and imaging. As fixation kills both the macrophages and bacteria, it is not possible to perform live capture imaging on infected samples [125, 126]. Live capture imaging would allow us to examine the change in these markers in real time as opposed to only at several discrete time points post-infection. Though technology for single molecule detection, including optimizations for single molecule fluorescence *in situ* hybridization (smFISH), has improved significantly over the last decade, lower size limits for target molecules remain a major challenge [65]. Often RNA targets of less than 0.5-1kb are not recommended for smFISH as the technique requires binding of multiple 20-100 base long probes, ligation of adaptors and detectors, which is simply not feasible for a tRF target, which may only be 18-24 nucleotides in length [65, 127].

Despite these limitations, we believe our studies have uncovered a novel association between ANG and dysregulation of mitochondrial responses in *Mtb* infection. The process of ANG recruitment to host mitochondria in *Mtb* infected cells may drive the overproduction of mtRFs and affect the balance between apoptosis and necrosis.

Chapter 3: Host Response to SARS-CoV-2

3.1 Background

3.1.1 Inflammasome activation in viral infections

Like *Mtb*, SARS-COV-2 pathogenesis is driven by various host responses. One hallmark of severe disease appears to be immune dysregulation in the later stages of illness that is characterized by elevated proinflammatory markers (such as C-reactive protein) and inflammatory cytokines, such as IL-6 [128-132]. Early investigation into the innate immunological programs induced by SARS-CoV-2 demonstrated that type I and type III interferon stimulation appears to be decreased by SARS-CoV-2 infection compared to infection with influenza [133], suggesting an alternative immune pathway may be responsible for the robust inflammation seen in COVID-19. Inflammasomes are another innate immune antiviral pathway known to be critical in both the control of and pathogenesis of other viral infections [134-136]. Activation of this intracellular signaling cascade by infection or tissue damage leads to an inflammatory type of cell death called pyroptosis and release of the proinflammatory cytokines, including IL-1β and IL-18 [137]. Lactate dehydrogenase (LDH), which is released by cells undergoing pyroptosis [138, 139] is elevated in plasma of COVID-19 patients, [131, 140] IL-1β transcripts are elevated in bronchoalveolar lavage fluid (BALF), and inflammasome cytokines, IL-1β and IL-18, are elevated in patients with severe COVID-19 [132, 141] suggesting that inflammasome activation is occurring *in vivo*. Whether cellular sensing of SARS-CoV-2 directly activates the inflammasome or whether viral replication in cells and associated tissue damage caused by the immune response triggers this pathway remains unknown.

A number of RNA viruses, including SARS-CoV-1, are known to directly activate inflammasome signaling [135, 138, 142-145]. This process typically starts with recognition of pathogen-associated molecular patterns (PAMPs), including viral RNA, by a pattern recognition receptor (PRR), such as one of the Toll-Like receptors (TLR) or retinoic acid-inducible gene I (RIG-I)-like receptors [146, 147]. This primes the cell by inducing the nuclear factor κB (NF-κB) pathway, which leads to upregulation and synthesis of inflammasome components, particularly pro-caspase-1 and pro-IL-1β. The second signal occurs when one of multiple inflammasome adaptor proteins senses a viral structure or cellular stress signal (such as potassium flux or mitochondrial damage). Many of these adapter proteins come from the nucleotide-binding domain and leucine-rich repeat-containing receptors (NLR) family of proteins, which are capable of sensing a diverse array of danger or stress signals [148, 149]. Once activated, these adapter proteins lead to assembly and oligomerization of the inflammasome complex via apoptosis-associated speck-like molecule containing a caspase recruitment domain (ASC). In turn, pro-caspase-1 is recruited to the complex, and through autocatalysis becomes active caspase-1. Caspase-1 then cleaves pro-IL-1β, pro-IL-18, and gasdermin-D (GSDMD) leading to GSDMD-based pores in the cellular membrane and release of active IL-1β and IL-18 [137, 150, 151]. NLRP3 is an inflammasome adapter that is central to inflammasome signaling in many viral infections, including SARS-CoV-1 [135, 138, 152]. Specifically, several SARS-CoV-1 gene products, including ORF3a, ORF8b, and viral protein E have been shown to trigger NLRP3 inflammasome signaling through multiple mechanisms [138, 142, 144]. However, danger-associated molecular patterns (DAMPs), such as mitochondrial DNA, ATP, and heat shock proteins, released by dying or damaged cells are also capable of activating inflammasomes [153]. It is unclear if inflammasome activation in response to SARS-CoV-2 is directly dependent on viral PAMPs,

release of DAMPs during infection, and/or sensing of these molecules by bystander cells, including macrophages. Moreover, it is not known whether nasal and respiratory epithelial cells (the primary targets of SARS-CoV-2 infection) activate inflammasomes in response to infection [154].

3.2 Macrophage sensing of SARS-CoV-2 induces NLRP3-dependent inflammasome activation via MyD88 signaling

*This study was done in collaboration with Andrew Karaba, Lee-Yang Hsieh, and Alexis Figueroa of the Andrea Cox Laboratory

We sought to determine in what cell types inflammasome activation occurs in response to SARS-CoV-2 and whether it is due to direct sensing of SARS-CoV-2. Our study demonstrates that SARS-CoV-2 directly activates inflammasomes through an NLRP3-, caspase-1-, and ASC-dependent process in human macrophages, but not in respiratory epithelial cells.

3.2.1 Methodologies

Ethics

For experiments involving primary human macrophages, deidentified human blood Leuko Paks were obtained from the Anne Arundel Medical Blood Donor Center (Anne Arundel, Maryland, USA). The researchers had no interaction with the donors and did not have any knowledge about them beyond their status as volunteer blood donors. This is considered non-human subjects research by the institutions where the research was conducted and US Department of Health and Human Services guidelines.

Cells and Viruses

Cells were incubated at 37°C and 5% CO_2 unless otherwise stated. The generation of the THP-1 cell was described previously [155]. VeroE6 cells were maintained in low-glucose Dulbecco's modification of Eagle medium plus GlutaMAX supplement and sodium pyruvate (ThermoFisher Scientific, Cat # 10567022) with 10% heat-inactivated fetal bovine serum (Corning Cellgro, Cat # 35-011-CV) and penicillin/streptomycin (100 U/mL, ThermoFisher Scientific, Cat # 15140122) (DMEM). THP-1 cells were maintained in RPMI 1640 media, 10% heat-inactivated fetal bovine serum, MEM nonessential amino acids (1:100, Corning, cat# 25–025), Penicillin/Streptomycin, sodium pyruvate, and L-glutamine (2mM) at a density of $5x10^5$ – $2x10^6$ cells/mL. To differentiate into macrophages, THP-1 cells were plated at a density of $2x10^5$ cells/well in a sterile U-bottom 96-well plate and stimulated overnight in RPMI 1640 media, 2% heat-inactivated fetal bovine serum, Penicillin/Streptomycin, L-glutamine (2mM), and phorbol 12-myristate 13-acetate (PMA) 5 ng/mL.

PBMCs were isolated by Ficoll-Hypaque gradient centrifugation. Primary monocytes were magnetically sorted by negative isolation per the manufacturer's specifications (Miltenyi Biotec, Somerville, Massachusetts) and cultured in RPMI 1640 (Invitrogen, Waltham, Massachusetts) with 10% heat-inactivated fetal bovine serum, Penicillin/Streptomycin, L-glutamine (2mM) and 50 ng/mL of recombinant human M-CSF (R&D Systems, Minneapolis, Minnesota) for 6 to 7 days to differentiate them to macrophages. Adherent macrophages were washed with sterile PBS and then incubated with the non-enzymatic cell disassociation media, CellStripper (Corning, Tewksbury, Massachusetts), for 30-60 minutes at 37°C and 5% CO_2 followed by counting, centrifugation at 400g for 5 min, and plating at a density of $2x10^5$ cells/well in a sterile U-bottom 96-well plate. For differentiation, macrophages were cultured overnight in RPMI 1640 with 10%

heat-inactivated fetal bovine serum, Penicillin/Streptomycin, L-glutamine (2mM), 100ng/mL LPS (Cell Signaling Technologies), and IFNγ (50ng/mL) (Peprotech, Rocky Hill, New Jersey). M0 macrophages were cultured in the same base media, but without IFNγ or LPS.

VeroE6 cells for propagation of SARS-CoV-2 (see below) were obtained from the National Institute of Infectious Diseases (Tokyo, Japan) and the Japanese Collection of Research Bioresources and Sekisui XenoTech, LLC (JCRB1819 Takeda, Makoto).

Cytokine measurement

Supernatants from THP-1, hNEC, HBE, and MDM cultures were collected and human IL-18 was measured with the human IL-18 ELISA Kit (MBL, Woburn, Massachusetts) according to the manufacturer's instructions using cell culture supernatant at a 1:5 dilution and data were acquired on a SpectraMax M2 with a lower limit of detection of 12 pg/mL. Additionally, cytokines from cell culture supernatants (IFN, IL-18, IL-1β, and IL-6) were measured using the meso scale discovery system described above. Data were analyzed using R version 3.6.3.

Influenza A Virus (IAV) was the generous gift of Richard Longnecker (Northwestern University). Virus was propagated in Vero cells (also a gift from R. Longnecker) cultured in Dulbecco's modification of Eagle medium with 1% fetal bovine serum as previously described [156]. Standard plaque titrations to determine viral titers were performed on confluent monolayers of Vero cells.

SARS-CoV-2/Wuhan-1/2020 virus was obtained through the US Center for Disease Control and Prevention (CDC). The virus was propagated in a Biosafety Level 3 (BSL3) laboratory in VeroE6 cells using methods described previously [157, 158]. Briefly, VeroE6 cells were infected at an MOI 0.01 for 1 hour, rocking every 10 minutes, at 37°C. After one-hour incubation, supernatant was removed and replaced with fresh serum-free infection media and incubated for

24-72 hours (whenever cultures showed ~50% cytopathic effect (CPE)). After incubation, cell-free supernatants were collected and stored at -80°C. Frozen stocks were used immediately upon thawing and were not subjected to multiple rounds of freeze-thaw. Original virus stocks were only passaged once before use in the described experiments. SARS-CoV-2/Wuhan-1/2020 virus stocks were thawed once and titered in VeroE6 cells using a standard Median Tissue Culture Infectious Dose (TCID50) assay using methods described previously [157, 158].

***In vitro* experiments with macrophages**

Unless otherwise stated, all infections in THP-1 cells were carried out at an MOI of 0.2 for SARS-CoV-2. Inoculations of primary MDMs were carried out at an MOI of 5. For SARS-CoV-2 infection and nigericin stimulation, media were gently aspirated from the cell culture wells containing the indicated cells and replaced with RPMI 1640 media containing 2% heat-inactivated fetal bovine serum (R2) and either SARS-CoV-2 or nigericin (5μM) (MilliporeSigma, Burlington, Massachusetts) and LPS (1 μg/mL), or no additional reagents (mock/media control). Twenty-four hours later, supernatant was removed and used for downstream assays. To deactivate any virus in the cell culture supernatant, all samples were incubated in 1% TX-100 for 30 minutes at room temperature prior to removal from BSL-3.

***In vitro* experiments with epithelial cells**

Human nasal epithelial (hNEC), human bronchial epithelial (HBE), and ACE2-overexpressing human lung epithelial (A549-ACE2) cells were grown in standard cell culture conditions. hNEC and HBE cells were infected with SARS-CoV-2 or IAV at an MOI of 2 for 24 hours after which supernatants were harvested, inactivated in 1% TX-100 for 30 minutes at room temperature, removed from the BSL-3, and used for assessment of IL-18 and IL-1β levels by ELISA (described above). Viral titers from apical surfaces of infected hNEC cultures were

measured by $TCID_{50}$. Infected and mock-infected control cultures were imaged by confocal microscopy. Microtubules in epithelial cells were stained with goat anti-mouse 555 anti-beta tubulin IV antibody and SARS-CoV-2 was detected with goat anti-rabbit 488 anti-nucleocapsid antibody. A549-ACE2 cells were exposed to SARS-CoV-2 at an MOI of 2 and physiological levels of exogenous human IFN, IL-18, IL-1β, or IL-6 for up to 72 hours. At each 24 hour time interval, supernatants were collected for measurement of viral burden by both qRT-PCR and $TCID_{50}$.

Measurement of LDH Activity

LDH activity was measured in cell culture supernatants using the Cytotoxicity Detection Kit (LDH) (Roche, Cat # 11644793001) according the manufactures instructions.

3.2.2 Results

SARS-CoV-2 activates inflammasomes *in vitro*

Although data from our group and many others [132, 159-161] strongly support a role for inflammasome activation in SARS-CoV-2 infection, inflammasomes can be activated by cellular stress and damage independent of direct sensing of a pathogen [162, 163]. Macrophages are one of the primary producers of inflammasome cytokines in many viral infections, [136, 164-166] therefore we inoculated phorbol-12-myristate-13-acetate (PMA) stimulated THP-1 cells (a human monocyte/macrophage cell) with SARS-CoV-2, nigericin and LPS (Ng+LPS, a potent activator of the NLRP3 inflammasome [167], or media alone, collected cell culture supernatants at 24 hours post-inoculation (PI), inactivated virus, and measured IL-18 and IL-1β. SARS-CoV-2 exposure led to significantly increased amounts of both IL-18 and IL-1β compared to media control (**Figure 26A**). To determine whether THP-1 cells are capable of supporting SARS-CoV-2 replication we collected supernatants at 24, 48, and 72 hours post-infection and found that viral titers decreased

by a full log within 24 hours and then were undetectable after that indicating that THP-1 cells are not capable of supporting SARS-CoV-2 replication (**Figure 26B**).

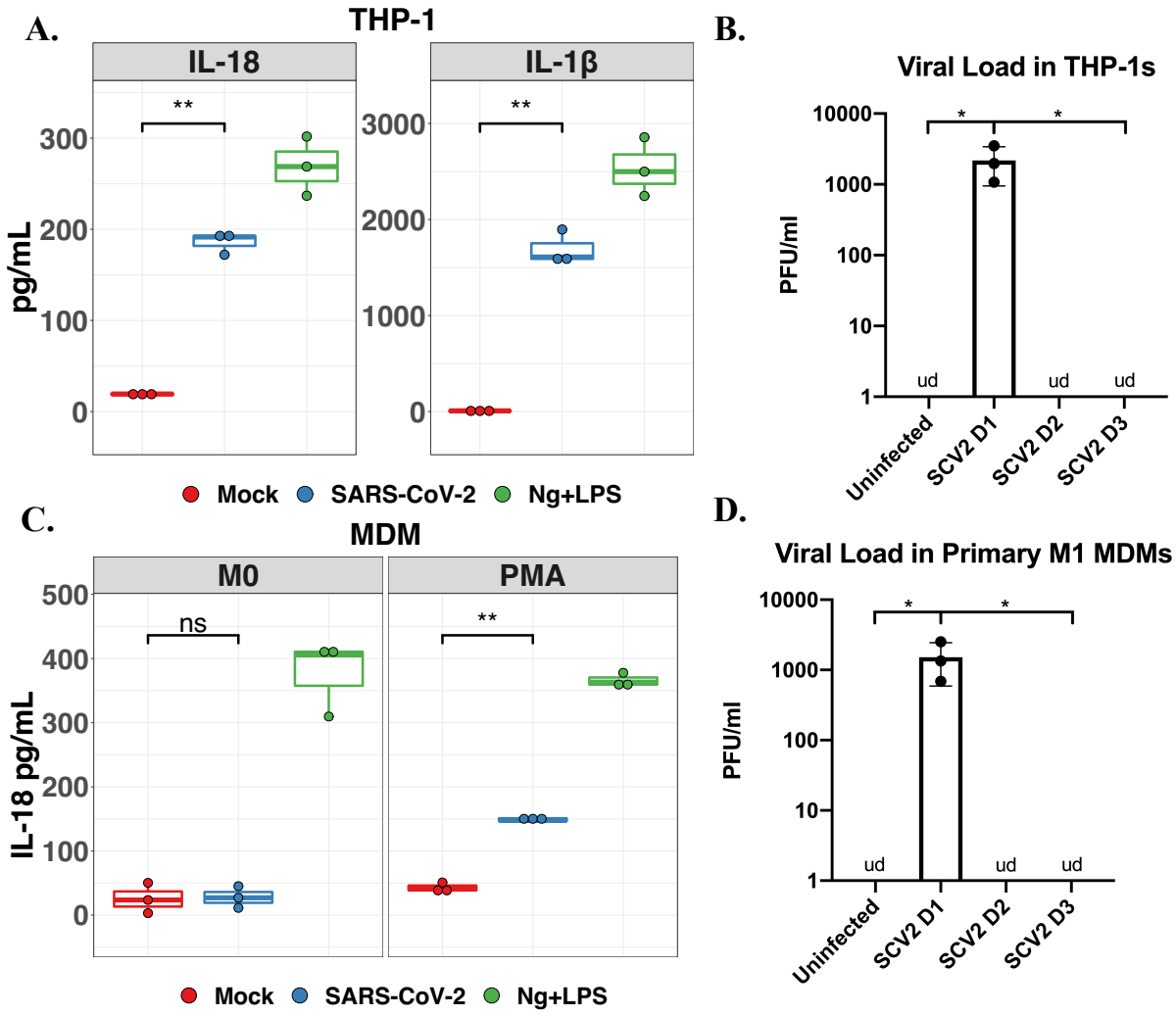

Figure 26. Macrophages inoculated with SARS-CoV-2 produce IL-18 and IL-1β.
PMA stimulated THP-1 cells were inoculated with SARS-CoV-2 (blue), Ng+LPS (green), or media alone (red). 24hrs later, supernatants were collected and IL-18 (A left panel), IL-1β (A right panel), and viral titers (B) were measured. Primary human monocytes were differentiated into macrophages with M-CSF. Resting (C, left panel) or PMA stimulated (C, right panel) were inoculated with SARS-CoV-2 (blue), Ng+LPS (green), or media alone (red). Supernatants were collected 24 hours later and IL-18, IL-1β and viral titers were measured. Differences between groups indicated by brackets were determined by a Student's *t*-test. NS, *,** indicate p-values >0.05, <0.05, <0.01, respectively.

Taken together these results suggest SARS-CoV-2 is capable of inducing inflammasome activation directly in THP-1 cells. Next, we investigated whether SARS-CoV-2 also induced inflammasome activation in primary MDMs. We inoculated both resting MDMs and PMA stimulated MDMs with media, SARS-CoV-2, or Ng+LPS and measured IL-18 and IL-1β in supernatants 24 hours post-infection. While SARS-CoV-2 inoculation did not result in significant amounts of IL-18, the PMA-stimulated MDMs did produce IL-18 in response to the virus indicating that SARS-CoV-2 is capable of activating the inflammasome in primary human cells under certain conditions (**Figure 26C**). Primary MDMs also do not support SARS-CoV-2 replication, as supernatants from inoculated MDM cultures showed a decline in viable viral particles nearly identical to that seen in THP-1 cells (**Figure 26D**).

SARS-CoV-2 Inflammasome Activation in Macrophages Requires NLRP3, Caspase-1, and ASC

Studies in SARS-CoV-1 indicate that the inflammasome adapter, NLRP3, is predominantly responsible for inflammasome formation in SARS [142, 144, 145]. Given the genetic similarity to SARS-CoV-1, it has been hypothesized that SARS-CoV-2 also activates the NLRP3 inflammasome [138, 168]. To test whether SARS-CoV-2 inflammasome activation requires NLRP3, we inoculated a panel of THP-1 cells deficient in various inflammasome-related genes with SARS-CoV-2 and collected cell culture supernatants at 24 hours post-infection. These cells were constructed using the CRISPR-Cas9 system and previously used to determine the requirements for human cytomegalovirus (HCMV) and herpes simplex virus type 1 (HSV-1) inflammasome activation in macrophages [155, 165]. The ΔHUMCYC cell-line (WT) was derived

from the same THP-1 cells, but targeting a human pseudogene (HUMCYCPS3) and was used to control for any off-target effects of the CRISPR-cas9 system.

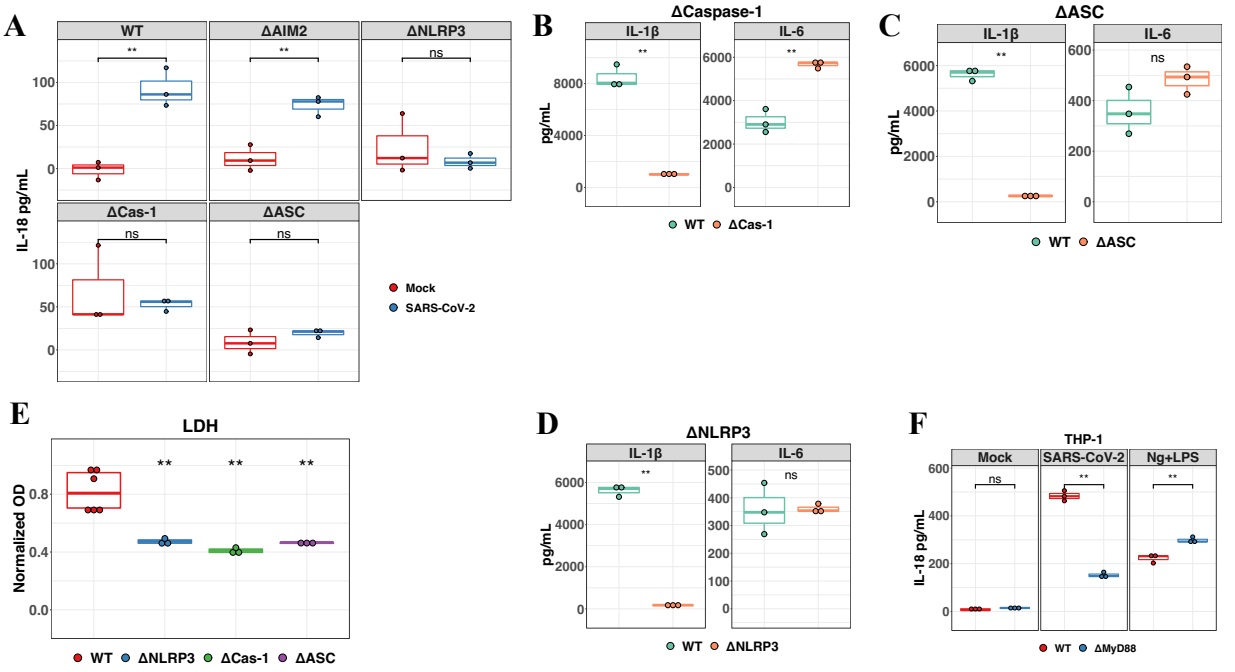

Figure 27. SARS-CoV-2 inflammasome activation is primed through MyD88 and is activated through NLRP3, Caspase-1, and ASC.
A) THP-1 cells with the indicated gene disrupted via CRISPR-cas9 (Δ) were stimulated overnight with PMA, inoculated with SARS-CoV-2 (blue) or media (red) alone for 24 hours before IL-18 was measured by ELISA. B, C, D) WT (light green) or KO (orange) THP-1 cells were stimulated overnight with PMA and inoculated with SARS-CoV-2 prior to measurement of IL-1β (left panels) and IL-6 (right panels) by ELISA. E. LDH activity was measured in cell culture supernatants from A and normalized to mock inoculation. F. WT (red) or ΔMyD88 THP-1 cells from Invivogen were stimulated overnight with PMA, inoculated with media alone (left panel), SARS-CoV-2 (middle panel), or Ng+LPS (right panel) and supernatants were collected 24 hours later and IL-18 was measured. ΔHUMCYC cells are labeled as "WT" in A-E. Differences between groups were determined by a Student's *t*-test. NS, *,** indicate p-values >0.05, <0.05, <0.01, respectively.

We measured IL-18 in cell culture supernatants from these THP-1 cells inoculated with SARS-CoV-2, media control, or nigericin and lipopolysaccharide (Ng+LPS). Inoculation of cells lacking NLRP3, ASC, and caspase-1 with SARS-CoV-2 did not produce amounts of IL-18 significantly different from media control (**Figure 27**). However, WT and ΔAIM2 cells produce

significant amounts of IL-18 in response to SARS-CoV-2. AIM2 is a dsDNA sensor and therefore would not be expected to be involved in the inflammasome response to the RNA virus SARS-CoV-2. These results are consistent with the hypothesis that SARS-CoV-2 activates canonical caspase-1-dependent inflammasomes through NLRP3. As expected, cells lacking NLRP3, ASC, and caspase-1 did not produce significant amounts of IL-18 in response to Ng+LPS either (**Figure 28**).

Disruption of NLPR3, ASC, or caspase-1 also led to reduced amounts of IL-1β in response to SARS-CoV-2, but did not decrease IL-6 production (**Figure 27 B,C,D**). These data support the idea that inflammasome signaling in SARS-CoV-2 is dependent on the NLRP3 inflammasome, but disruption of this pathway leaves additional innate sensing pathways intact.

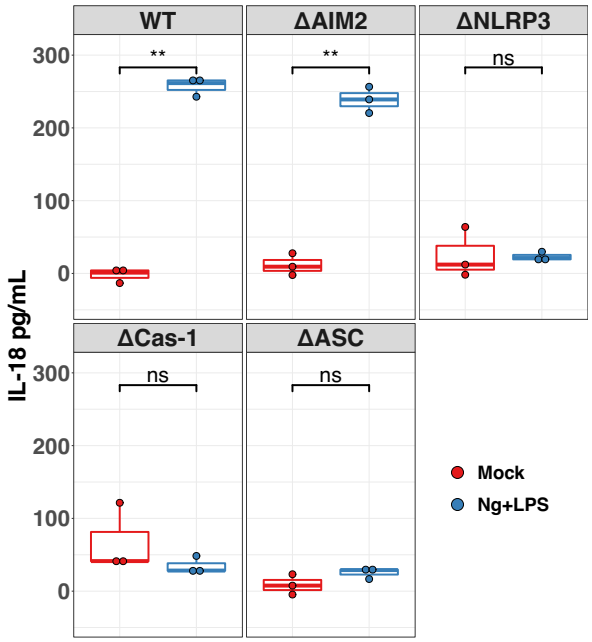

Figure 28. Cells with NLRP3 inflammasome pathway knockouts do not show IL-18 production in response to positive control agents.
WT, ΔAIM2, ΔNLRP3, ΔCaspase-1, and ΔASC knockout THP-1 cells were exposed to Ng+LPS for 24 hours and then supernatants were used for quantification of IL-18 by ELISA. Differences between groups were determined by a Student's *t*-test. NS, *,** indicate p-values >0.05, <0.05, <0.01, respectively.

LDH activity was also measured in the THP-1 cells after inoculation with SARS-CoV-2 to assess for cell death. While knock-out of NLRP3, ASC, and caspase-1 reduced LDH activity compared to WT THP-1 cells, disruption of these inflammasome genes did not reduce LDH levels to those of media control (**Figure 27E**). These findings suggest that while inflammasome activation/pyroptosis is responsible for some cell death in response to SARS-CoV-2, there are additional cell death pathways activated. Recently, a study on mouse hepatitis virus (another Betacoronavirus), demonstrated that coronaviruses can induce necroptosis when the NLRP3 inflammasome is inhibited which likely explain our findings of reduced, but not absent LDH activity [169].

Macrophage Priming for Inflammasome Signaling In Response to SARS-CoV-2 is MyD88-dependent

As described above, the NLRP3 inflammasome is thought to require a priming step through activation of the NF-κB pathway [152]. It is not known exactly how SARS-CoV-2 is initially sensed, but it is possible that multiple TLRs or intra-cellular PRRs could act as sensors [138]. Most known TLRs (aside from TLR3 and TLR4) depend on the adapter molecule, MyD88, for signaling [146]. Therefore, we inoculated MyD88 KO THP-1 cells with SARS-CoV-2 or Ng+LPS and measured IL-18 24 hours post-infection. While deletion of MyD88 had no effect on IL-18 produced in response to Ng+LPS, it significantly reduced IL-18 released in the SARS-CoV-2 inoculated cells (**Fig 27F**). However, MyD88KO did not reduce the IL-18 to background levels implying that while a MyD88-dependent TLR is primarily responsible for SARS-CoV-2 sensing, there are potentially other innate sensing pathways capable of sensing the virus and priming for inflammasome activation.

Inflammasome Activation Does Not Occur in SARS-COV-2-infected Respiratory Epithelial Cells

Respiratory epithelia are the primary targets of SARS-CoV-2 [170]. Consistent with this, SARS-CoV-2 replicates well in primary human nasal epithelial cultures (hNEC), as shown by viral titer and by immunofluorescence in (**Fig 29A,B**). To determine if infection of primary hNEC

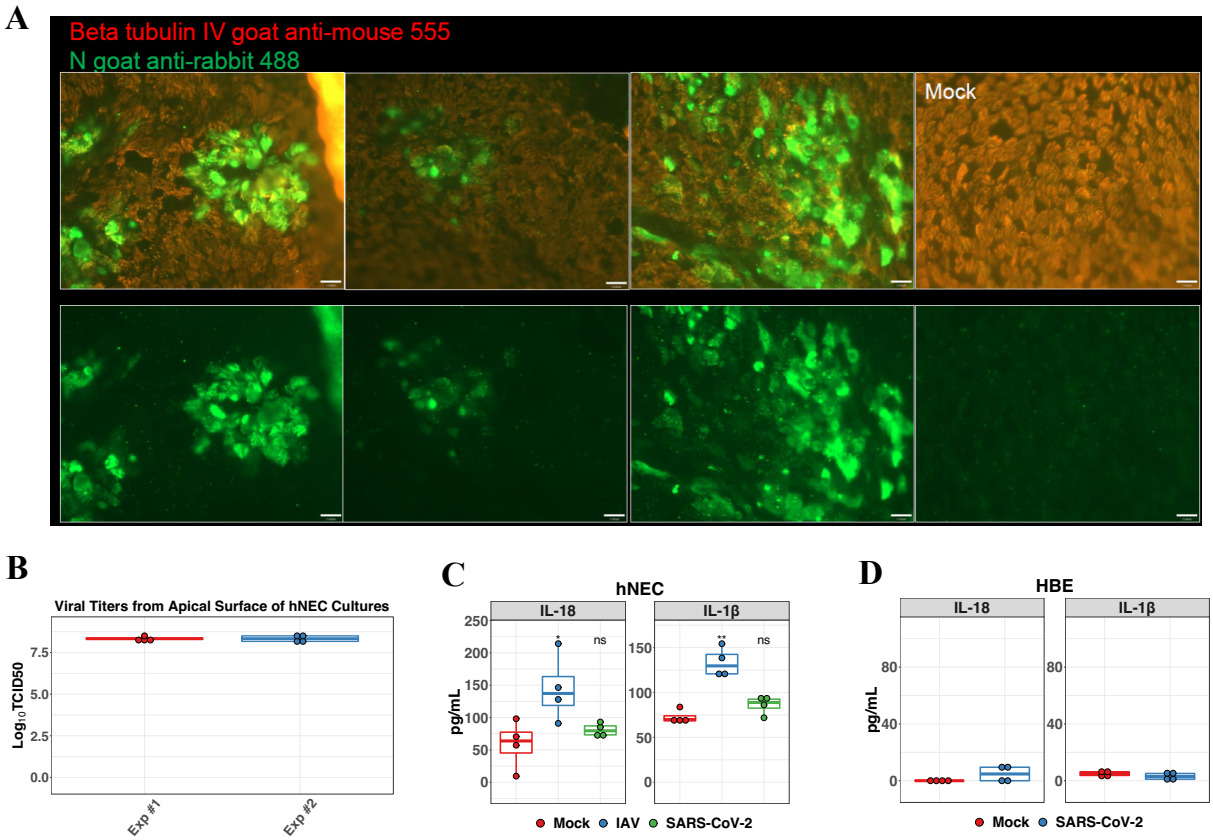

Figure 29. Respiratory Epithelial Cells Support SARS-CoV-2 Replication, But Do Not Activate Inflammasomes.
A) Confocal images showing 3 examples of SARS-CoV-2-infected hNEC cells and one mock-infected culture (right). Cells are stained with anti-S antibody to viral antigen (green) and beta tubulin IV epithelial cell marker (red). The top row shows both markers, and the bottom row shows green fluorescent channel only. B) TCID50 of two hNEC infections to show consistently high viral burden. C and D) IL-18 and IL-1β measured by ELISA from supernatants of hNEC (C) and HBE cells (D) infected with SARS-CoV-2. Differences between conditions containing virus and mock infection were determined by a Student's *t*-test. NS, *,** indicate p-values >0.05, <0.05, <0.01, respectively.

results in elevations of inflammasome cytokines we measured these cytokines in basolateral cell culture supernatants from SARS-CoV-2 infected hNEC and compared to influenza or mock infected hNEC. Unlike macrophages exposed to SARS-CoV-2, we did not observe elevations in IL-18 or IL-1β in SARS-CoV-2 infected primary hNEC, but IL-18 and IL-1β were produced in response to influenza (**Fig. 28C**). These data indicate that hNEC are capable of activating inflammasomes in response to an RNA virus, but that these responses are not unique to SARS-CoV-2. We also measured these cytokines in cell culture supernatants from human bronchial epithelial (HBE) cells infected with SARS-CoV-2. Similarly, the inflammasome cytokines IL-18 and IL-1β were not elevated in supernatants from SARS-CoV-2-infected HBEs (**Fig. 29D**). These data illustrate that inflammasome activation is a result of interactions between SARS-CoV-2 and macrophages rather than infection of epithelial cells.

IL-1β, but not IL-18, increases SARS-CoV-2 viral burden

Given the finding that macrophages activate the NLRP3 inflammasome when exposed to SARS-CoV-2 and, in contrast, that epithelial cells support viral replication in absence of inflammasome activation, we sought to understand how inflammasome activation in macrophages may alter overall outcome of SARS-CoV-2 infection. To test this, we exposed ACE2 overexpressing A548 lung epithelial cells (A549-ACE2) to SARS-CoV-2 at an MOI of 2 with or without addition of exogenous human IFN, IL-18, IL-1β, or IL-6. We found that viral genome copies and viable viral particles were higher in infected cells exposed to exogenous IL-1β (**Figure 30**). Both viral copies and viral titer increased over controls that were not exposed to any exogenous cytokines and cells exposed to IFN, IL-18, or IL-6 starting at 48 hours and continuing through 72 hours post infection. This suggests that IL-1β produced by macrophages following

viral sensing of SARS-CoV-2 may stimulate viral replication in epithelial cells and drive higher viral burdens and worse disease.

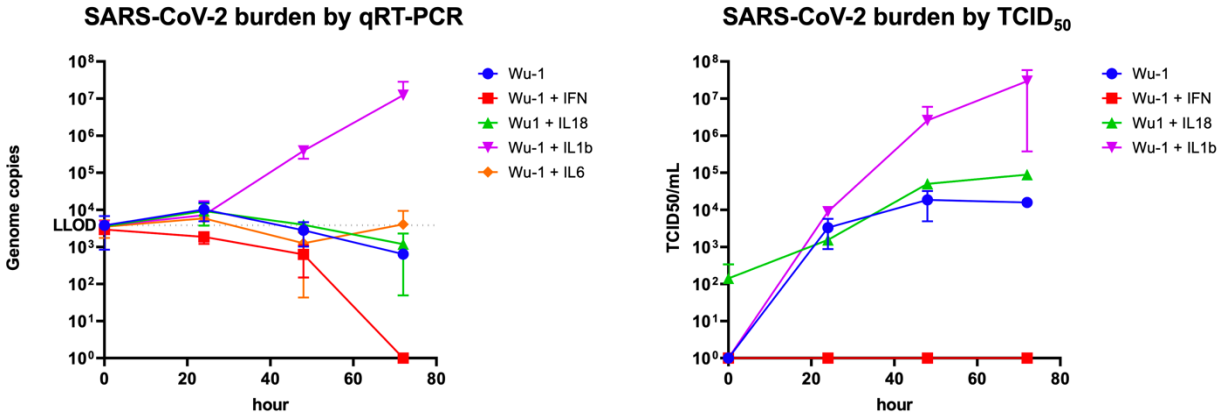

Figure 30. Exogenous IL-1β drives viral replication in SARS-CoV-2-infected lung epithelial cells.
Human lung epithelial A549-ACE2 cells were exposed to physiological levels of exogenous IFN, IL-18, IL-1β, and IL-6 and SARS-CoV-2 at an MOI of 2 for various time points up through 72 h.p.i. For all time points, viral burdens were measured by qRT-PCR and $TCID_{50}$.

3.3 Conclusions

We provide evidence that inflammasome activation by SARS-CoV-2 in macrophages takes place through direct sensing via a MyD88 dependent TLR and activation though the NLRP3- and caspase-1- dependent canonical inflammasome. Furthermore, this activation is not the result of productive replication in these cells. In contrast, robust infection of replication-permissive respiratory epithelial cells does not result in production of inflammasome cytokines. Therefore, it is likely that the elevated IL-18 and IL-1β detected in patients with COVID-19 is a result of sensing by myeloid-derived cells rather than infection of the respiratory epithelium.

This is the first direct evidence that NLRP3 is required for SARS-CoV-2-induced inflammasome activation. This is important as numerous potential therapeutics targeting NLRP3 and/or IL-1β and IL-18 are in preclinical and clinical trials [168]. While our data provide rational mechanistic evidence for their use, what remains unclear is whether IL-1β or IL-18 exert any specific anti-viral effect in SARS-CoV-2. IL-1β can have both direct and indirect antiviral effects in other viruses, but is also associated with a variety of pathological inflammatory disorders including autoimmunity, cardiovascular disease, and cancer [164, 171-173]. It remains unclear in COVID-19 if this is primarily driving pathology, or if the elevations in IL-1β and IL-18 are appropriate in response to uncontrolled viral replication. There is evidence that severe COVID-19 cases are associate with both elevations in these (and other) proinflammatory cytokines and higher viral loads (as measured by qRT-PCR) [132]. So, it is possible that the excess inflammasome activation is an appropriate response to uncontrolled viral replication. Clinical studies demonstrating that non-specific immunosuppression with dexamethasone or specific inhibition of IL-1β and IL-1α with Anakinra provide therapeutic benefit argue for a predominantly pathological role for these cytokines [174-176]. Furthermore, it is possible that pyroptosis itself is also pathological. If this is the case, then inhibition of inflammasome formation with either a caspase-1 or NLRP3 inhibitor may be a logical therapeutic strategy and potentially more beneficial than blocking the cytokines alone.

Our results clearly identify NLRP3 as the inflammasome adapter responsible for SARS-CoV-2-mediated inflammasome activation by using both knock-out cell lines and pharmacological inhibitors with whole replication competent SARS-CoV-2. However, in this study we do not identify the specific viral PAMP responsible for this interaction. While multiple ORFs of SARS-CoV-1 are postulated to activate the inflammasome [144, 157, 177], early evidence in SARS-CoV-

2 suggests that the SARS-CoV-2 viroporin (ORF3a) leads to NLRP3 activation likely through potassium efflux [178]. These authors also posulate that ORF3a primes cells for inflammasome activation through stimulation of the NF-κB pathway. However, we did not find evidence that macrophages support a productive replication cycle and the protein encoded by ORF3a is not part of the viral particle [179]. Therefore, there are either multiple mechanisms of inflammasome activation, or a small amount of ORF3a is transcribed and translated before the infectious cycle is aborted. It is possible that other viral proteins found in the viral particle might serve as PAMPs for NLRP3 recognition or the viral genome itself as in the case of HCV [136, 180]. On the contrary, in epithelial cells where the virus does complete a replication cycle, we did not find evidence of inflammasome activation as measured by IL-1β and IL-18 in cell culture supernatants. Therefore, the role of ORF3a (and other non-structural proteins) in the innate response to SARS-CoV-2 remains unclear.

With regard to the priming step, we provide evidence that this is at least partially mediated through a MyD88-dependent process. While multiple TLRs signal through MyD88, TLR7 is a reasonable candidate for the PRR sensing of SARS-CoV-2 as it recognizes ssRNA such as the viral genome [146], and is encoded on the X chromosome, potentially contributing to the male bias in severe disease and death due to COVID-19 [181]. Remarkably, a recent study identified mutations in the *TLR7* gene associated with severe cases of COVID-19 in young men lending credence to the possibility that the sensing is predominantly through TLR7 [182]. The potential mechanism of SARS-CoV-2 mediated NLRP3 inflammasome activation is depicted below (**Figure 31**).

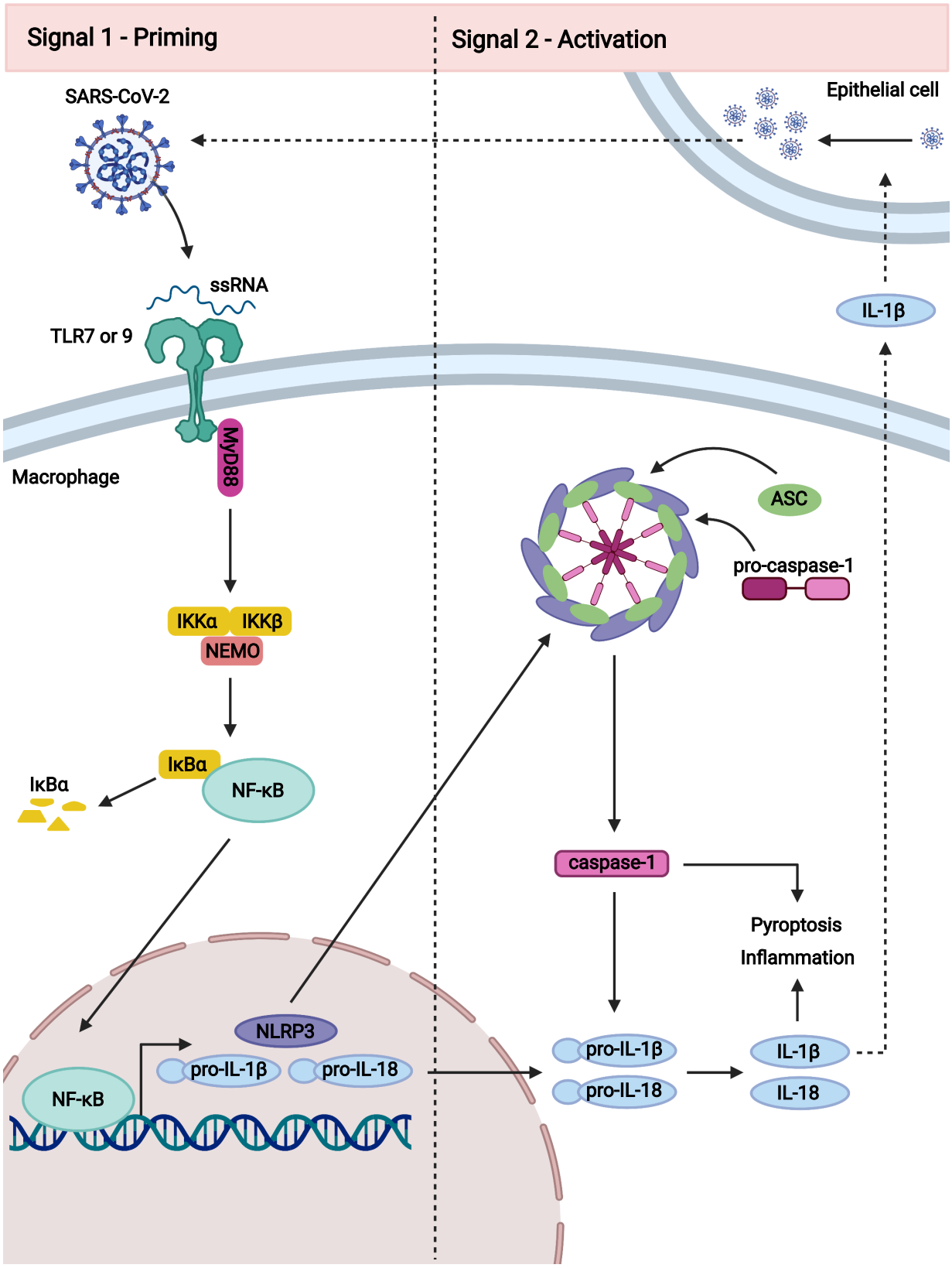
Signal 1 - Priming
Signal 2 - Activation
SARS-CoV-2
Epithelial cell
ssRNA
TLR7 or 9
IL-1β
Macrophage
MyD88
ASC
pro-caspase-1
IKKα
IKKβ
NEMO
IκBα
IκBα
NF-κB
caspase-1
Pyroptosis
Inflammation
NLRP3
pro-IL-1β
pro-IL-18
NF-κB
pro-IL-1β
pro-IL-18
IL-1β
IL-18

Figure 31. SARS-CoV-2 infection drives MyD88-dependent activation of the host NLRP3 inflammasome via direct macrophage sensing.
Viral PAMPs (likely viral RNA) bind MyD88 dependent TLRs (likely TLR7 or 9) on the surface of macrophages. This acts as signal one priming that triggers activation of the NLRP3 inflammasome. Here the MyD88-NFkB signaling signal cascade drives the expression of NLRP3, pro-IL-1β, and pro-Il-18. Complexing of NLRP3 with ASC and pro-caspase-1 activates the NLRP3 inflammasome which drives cleavage and activation of caspase-1 which then cleaves pro-IL-1β and pro-Il-18 into their active forms. Increases in these cytokines drives the pro-inflammatory programmed cell death pathway of pyroptosis.

Aside from challenges identifying the specific TLR responsible for sensing, other limitations of this study include reliance on cancer-derived macrophage cell lines in absence of validation in primary human MDMs. In our optimization studies, we found MDMs to require a much higher MOI to generate inflammasome activation when unstimulated. We were able to observe inflammasome activation in MDMs pre-treated with PMA, as is done for the THP-1 cells. This may suggest that inflammasome activation occurs primarily in M1-stimulated MDMs and that PMA facilitates inflammasome activation during SARS-CoV-2 exposure by skewing a larger proportion of the MDMs towards an M1 phenotype. While validation data in PMA-stimulated MDMs is currently being generated, further optimizations are required.

In summary, we present compelling evidence that NLRP3 inflammasome activation occurs in by macrophages sensing of SARS-CoV-2, but not epithelial cells. These findings significantly advance our understanding of the pathogenesis of this infection and highlight areas for potential pharmacological intervention.

Chapter 4: Discussion and Future Directions

Overall, this collective work has provided insight into the host response to two important pathogens, *Mtb* and SARS-COV-2. Together, the unbiased descriptive and targeted mechanistic work detailed here show that a complex network of factors including miRNAs, tRFs, mRNAs, and methylation regulates the macrophage response to infection with *Mtb*. These studies represent the first description of tRF dysregulation in bacterial infections and uncover a novel relationship between ANG and mitochondrial function during *Mtb* infection. Further, this work has shown that inflammasome activation in SARS-COV-2 infection is mediated by direct macrophage sensing of extracellular virus and occurs through the MyD88-dependent NLRP3 pathway. Though they are very different pathogens, it is clear that host macrophages play major roles in controlling infection with both *Mtb* and SARS-COV-2.

This research has also laid the foundation for a significant amount of continuing and future work. Future studies should be aimed at targeted manipulation of miRNA candidates, differentially expressed mRNA targets, and differently methylated genes discovered by our next generation sequencing studies. These unbiased analyses of transcriptomic and epigenetic changes may serve as a guide for identifying candidates for mechanistic studies designed to uncover the function of each small RNA or gene in regulating specific pathways central to the macrophage response to *Mtb*.

Additionally, further investigations of the biological mechanisms underlying the biased production of mtRFs could improve our understanding of this novel phenomenon. These studies may include technical tool development to allow for the detection of fluorescently labeled intracellular tRFs and protein studies designed to elucidate how ANG interacts with other mitochondria-associated markers, such as XIAP and Bax. As the key mechanism by which *Mtb*

suppresses apoptosis to shift cells towards necrosis remains unknown, expanding knowledge of critical pivot points such as functional Bax pore formation may provide important answers for a longstanding question in TB research. Future imaging studies should include investigations complexing between Bax and Bak, the second component of OMM pores involved in cytochrome c release. High resolution imaging including electron microscopy should be performed to determine how the structure of Bax/Bak pores are altered and whether or not ANG is binding to mitochondrial membranes or fully internalized.

In silico and *in vitro* assays for tRF-target binding may also provide a more concrete understanding of if and how specific tRFs interact with their cognate mRNA targets, similarly to miRNAs. *In vivo* experiments that investigate the importance of ANG in the overall outcome of *Mtb* infection will also be important for determining the essentiality of ANG and the tRFs it cleaves in acute and chronic TB.

Our studies on inflammasome signaling in SARS-COV-2 infection also provide opportunities for more in depth research. Importantly, future work should focus on identifying the specific TLRs that are responsible for sensing extracellular virus. Technical challenges with finding specific inhibitors for TLRs 7 and 9 have complicated the identification of a single essential TLR, however, these obstacles can be overcome through generation and use of stable single TLR knockout THP-1 cell lines created via CRISPR-Cas9-targeted genome editing. Additionally, further functional analysis of the role of the inflammasome in altering the outcome of infection *in vivo* will be critical. Given that elevated levels of IL-18 have been associated with worse prognosis in patients with COVID-19 patients, more research should be done on developing NLRP3-inhibitors as potential host-directed therapies for COVID-19 [159].

In addition to continuing bench research built on these studies, there is a desperate need for additional focus on all areas of research related to TB and COVID-19. The WHO and Global Fund estimate that there is a gap in funding of approximately $1.6 billion annually [1]. This constitutes a small fraction of the $2.59 trillion budget allocated for COVID-19 in the US in 2020 alone [183]. While neither amount of funding has resulted in eradication of each respective disease, undeniable progress has been made. The rapid development of the COVID-19 vaccines exemplifies the power of global attention and dedicated funding. Especially given the setbacks in global TB management that will follow the COVID-19 pandemic, the fight to end TB will depend on our ability to bring TB back to the forefront of discussion and secure increased funding. As for COVID-19, though the development of effective vaccines is reassuring, continuing research is required to achieve a complete understanding of this devastating disease and the virus that causes it, improve vaccines, and expand on effective treatment options.

The research detailed in this dissertation expands our understanding of basic biological mechanisms that underlie TB and COVID-19 disease. With continued focus, this work could serve as a foundation for future translational work.

Bibliography

1. WHO. Global Tuberculosis Report. 2020 ed, **2020**.

2. WHO. WHO Coronavirus Disease (COVID-19) Dashboard. Available at: https://covid19.who.int/?gclid=Cj0KCQiAvP6ABhCjARIsAH37rbSPIPZ-TIcFO3arhNT1za4IJ2wlGbWLvq17Zid6OB77BOsPEhb8XBAaAmimEALw_wcB.

3. Oren E. Health Disparities in Respiratory Medicine: Health Disparities and Tuberculosis. Humana Press, **2016**.

4. WHO. Global Tuberculosis Report. 2016 ed, **2016**.

5. Rozenfeld Y, Beam J, Maier H, et al. A model of disparities: risk factors associated with COVID-19 infection. Int J Equity Health **2020**; 19:126.

6. CDC. COVID-19 Hospitalization and Death by Race/Ethnicity. Available at: https://www.cdc.gov/coronavirus/2019-ncov/covid-data/investigations-discovery/hospitalization-death-by-race-ethnicity.html.

7. Barberis I, Bragazzi NL, Galluzzo L, Martini M. The history of tuberculosis: from the first historical records to the isolation of Koch's bacillus. J Prev Med Hyg **2017**; 58:E9-E12.

8. Luca S, Mihaescu T. History of BCG Vaccine. Maedica (Bucur) **2013**; 8:53-8.

9. WHO. Immunization, vaccines and biologicals: Tuberculosis vaccine development, **2020**.

10. Darrah PA, Zeppa JJ, Maiello P, et al. Prevention of tuberculosis in macaques after intravenous BCG immunization. Nature **2020**; 577:95-102.

11. Hatherill M, White RG, Hawn TR. Clinical Development of New TB Vaccines: Recent Advances and Next Steps. Front Microbiol **2019**; 10:3154.

12. Rabahi MF, Silva Junior J, Ferreira ACG, Tannus-Silva DGS, Conde MB. Tuberculosis treatment. J Bras Pneumol **2017**; 43:472-86.

13. Heemskerk DC, M.; Marais, B.; and Farrar, J. Tuberculosis in Adults and Children. **2015**.

14. Yang H, Lu S. COVID-19 and Tuberculosis. J Transl Int Med **2020**; 8:59-65.

15. Tapela K, Ochieng' Olwal C, Quaye O. Parallels in the pathogenesis of SARS-CoV-2 and M. tuberculosis: a synergistic or antagonistic alliance? Future Microbiol **2020**; 15:1691-5.

16. Hossain MF, Hasana S, Mamun AA, et al. COVID-19 Outbreak: Pathogenesis, Current Therapies, and Potentials for Future Management. Front Pharmacol **2020**; 11:563478.

17. Shah VK, Firmal P, Alam A, Ganguly D, Chattopadhyay S. Overview of Immune Response During SARS-CoV-2 Infection: Lessons From the Past. Front Immunol **2020**; 11:1949.

18. Pahari S, Kaur G, Negi S, et al. Reinforcing the Functionality of Mononuclear Phagocyte System to Control Tuberculosis. Front Immunol **2018**; 9:193.

19. Chai Q, Wang L, Liu CH, Ge B. New insights into the evasion of host innate immunity by Mycobacterium tuberculosis. Cell Mol Immunol **2020**; 17:901-13.

20. de Martino M, Lodi L, Galli L, Chiappini E. Immune Response to Mycobacterium tuberculosis: A Narrative Review. Front Pediatr **2019**; 7:350.

21. Kumar R, Singh P, Kolloli A, et al. Immunometabolism of Phagocytes During Mycobacterium tuberculosis Infection. Front Mol Biosci **2019**; 6:105.

22. Goldberg MF, Saini NK, Porcelli SA. Evasion of Innate and Adaptive Immunity by Mycobacterium tuberculosis. Microbiol Spectr **2014**; 2.

23. Harapan H, Fitra F, Ichsan I, et al. The roles of microRNAs on tuberculosis infection: meaning or myth? Tuberculosis (Edinb) **2013**; 93:596-605.

24. Zheng L, Leung ET, Wong HK, et al. Unraveling methylation changes of host macrophages in Mycobacterium tuberculosis infection. Tuberculosis (Edinb) **2016**; 98:139-48.

25. Das K, Garnica O, Dhandayuthapani S. Modulation of Host miRNAs by Intracellular Bacterial Pathogens. Front Cell Infect Microbiol **2016**; 6:79.

26. Dorhoi A, Iannaccone M, Farinacci M, et al. MicroRNA-223 controls susceptibility to tuberculosis by regulating lung neutrophil recruitment. J Clin Invest **2013**; 123:4836-48.

27. Sharbati S, Sharbati J, Hoeke L, Bohmer M, Einspanier R. Quantification and accurate normalisation of small RNAs through new custom RT-qPCR arrays demonstrates Salmonella-induced microRNAs in human monocytes. BMC Genomics **2012**; 13:23.

28. Rajaram MV, Ni B, Morris JD, et al. Mycobacterium tuberculosis lipomannan blocks TNF biosynthesis by regulating macrophage MAPK-activated protein kinase 2 (MK2) and microRNA miR-125b. Proc Natl Acad Sci U S A **2011**; 108:17408-13.

29. Tarashi S, Badi SA, Moshiri A, et al. The inter-talk between Mycobacterium tuberculosis and the epigenetic mechanisms. Epigenomics **2020**; 12:455-69.

30. Das K, Saikolappan S, Dhandayuthapani S. Differential expression of miRNAs by macrophages infected with virulent and avirulent Mycobacterium tuberculosis. Tuberculosis (Edinb) **2013**; 93 Suppl:S47-50.

31. Mesitov MV, Soldatov RA, Zaichenko DM, et al. Differential processing of small RNAs during endoplasmic reticulum stress. Sci Rep **2017**; 7:46080.

32. Fu H, Feng J, Liu Q, et al. Stress induces tRNA cleavage by angiogenin in mammalian cells. FEBS Lett **2009**; 583:437-42.

33. Anderson P, Ivanov P. tRNA fragments in human health and disease. FEBS Lett **2014**; 588:4297-304.

34. Lab TL. GtRNAdb tRNAscan-SE analysis of complete genomes. Vol. 18.1, **2019**.

35. Yamasaki S, Ivanov P, Hu GF, Anderson P. Angiogenin cleaves tRNA and promotes stress-induced translational repression. J Cell Biol **2009**; 185:35-42.

36. Sobala A, Hutvagner G. Small RNAs derived from the 5' end of tRNA can inhibit protein translation in human cells. RNA Biol **2013**; 10:553-63.

37. Haussecker D, Huang Y, Lau A, Parameswaran P, Fire AZ, Kay MA. Human tRNA-derived small RNAs in the global regulation of RNA silencing. RNA **2010**; 16:673-95.

38. Li Z, Ender C, Meister G, Moore PS, Chang Y, John B. Extensive terminal and asymmetric processing of small RNAs from rRNAs, snoRNAs, snRNAs, and tRNAs. Nucleic Acids Res **2012**; 40:6787-99.

39. Kuscu C, Kumar P, Kiran M, Su Z, Malik A, Dutta A. tRNA fragments (tRFs) guide Ago to regulate gene expression post-transcriptionally in a Dicer-independent manner. RNA **2018**; 24:1093-105.

40. Martinez G, Choudury SG, Slotkin RK. tRNA-derived small RNAs target transposable element transcripts. Nucleic Acids Res **2017**; 45:5142-52.

41. Goodarzi H, Nguyen HCB, Zhang S, Dill BD, Molina H, Tavazoie SF. Modulated Expression of Specific tRNAs Drives Gene Expression and Cancer Progression. Cell **2016**; 165:1416-27.

42. Brubaker PE, Moran JP, Bridbord K, Hueter FG. Noble metals: a toxicological appraisal of potential new environmental contaminants. Environ Health Perspect **1975**; 10:39-56.

43. Ruggero K, Guffanti A, Corradin A, et al. Small noncoding RNAs in cells transformed by human T-cell leukemia virus type 1: a role for a tRNA fragment as a primer for reverse transcriptase. J Virol **2014**; 88:3612-22.

44. Tiku V, Tan MW, Dikic I. Mitochondrial Functions in Infection and Immunity. Trends Cell Biol **2020**; 30:263-75.

45. Ramond E, Jamet A, Coureuil M, Charbit A. Pivotal Role of Mitochondria in Macrophage Response to Bacterial Pathogens. Front Immunol **2019**; 10:2461.

46. Amgalan D, Pekson R, Kitsis RN. Troponin release following brief myocardial ischemia: apoptosis versus necrosis. JACC Basic Transl Sci **2017**; 2:118-21.

47. Porcelli SA, Jacobs WR, Jr. Tuberculosis: unsealing the apoptotic envelope. Nat Immunol **2008**; 9:1101-2.

48. Andreu N, Zelmer A, Fletcher T, et al. Optimisation of bioluminescent reporters for use with mycobacteria. PLoS One **2010**; 5:e10777.

49. Looney MM, Lu Y, Karakousis PC, Halushka MK. Mycobacterium tuberculosis infection drives mitochondria-biased dysregulation of host tRNA-derived fragments. J Infect Dis **2020**.

50. Lu Y, Baras AS, Halushka MK. miRge 2.0 for comprehensive analysis of microRNA sequencing data. BMC Bioinformatics **2018**; 19:275.

51. Huang HY, Lin YC, Li J, et al. miRTarBase 2020: updates to the experimentally validated microRNA-target interaction database. Nucleic Acids Res **2020**; 48:D148-D54.

52. heaks EBELERFEt. gProfiler2. Available at: https://biit.cs.ut.ee/gprofiler/gost.

53. Liis Kolberg UR. gprofiler2: Interface to the 'g:Profiler' Toolset. Available at: https://cran.r-project.org/web/packages/gprofiler2/index.html.

54. Pertea M, Kim D, Pertea GM, Leek JT, Salzberg SL. Transcript-level expression analysis of RNA-seq experiments with HISAT, StringTie and Ballgown. Nat Protoc **2016**; 11:1650-67.

55. Krueger F, Andrews SR. Bismark: a flexible aligner and methylation caller for Bisulfite-Seq applications. Bioinformatics **2011**; 27:1571-2.

56. Feng H, Conneely KN, Wu H. A Bayesian hierarchical model to detect differentially methylated loci from single nucleotide resolution sequencing data. Nucleic Acids Res **2014**; 42:e69.

57. Wu H, Xu T, Feng H, et al. Detection of differentially methylated regions from whole-genome bisulfite sequencing data without replicates. Nucleic Acids Res **2015**; 43:e141.

58. Park Y, Wu H. Differential methylation analysis for BS-seq data under general experimental design. Bioinformatics **2016**; 32:1446-53.

59. Young MD, Wakefield MJ, Smyth GK, Oshlack A. Gene ontology analysis for RNA-seq: accounting for selection bias. Genome Biol **2010**; 11:R14.

60. Fromm B, Domanska D, Hoye E, et al. MirGeneDB 2.0: the metazoan microRNA complement. Nucleic Acids Res **2020**; 48:D132-D41.

61. Uhlen M, Fagerberg L, Hallstrom BM, et al. Proteomics. Tissue-based map of the human proteome. Science **2015**; 347:1260419.

62. O'Brien J, Hayder H, Zayed Y, Peng C. Overview of MicroRNA Biogenesis, Mechanisms of Actions, and Circulation. Front Endocrinol (Lausanne) **2018**; 9:402.

63. Chang L, Zhou G, Soufan O, Xia J. miRNet 2.0: network-based visual analytics for miRNA functional analysis and systems biology. Nucleic Acids Res **2020**; 48:W244-W51.

64. Morales-Nebreda L, McLafferty FS, Singer BD. DNA methylation as a transcriptional regulator of the immune system. Transl Res **2019**; 204:1-18.

65. Pichon X, Lagha M, Mueller F, Bertrand E. A Growing Toolbox to Image Gene Expression in Single Cells: Sensitive Approaches for Demanding Challenges. Mol Cell **2018**; 71:468-80.

66. Risso D, Ngai J, Speed TP, Dudoit S. Normalization of RNA-seq data using factor analysis of control genes or samples. Nat Biotechnol **2014**; 32:896-902.

67. Love MI, Huber W, Anders S. Moderated estimation of fold change and dispersion for RNA-seq data with DESeq2. Genome Biol **2014**; 15:550.

68. Selitsky SR, Sethupathy P. tDRmapper: challenges and solutions to mapping, naming, and quantifying tRNA-derived RNAs from human small RNA-sequencing data. BMC Bioinformatics **2015**; 16:354.

69. Loher P, Telonis AG, Rigoutsos I. MINTmap: fast and exhaustive profiling of nuclear and mitochondrial tRNA fragments from short RNA-seq data. Sci Rep **2017**; 7:41184.

70. Juzenas S, Venkatesh G, Hubenthal M, et al. A comprehensive, cell specific microRNA catalogue of human peripheral blood. Nucleic Acids Res **2017**; 45:9290-301.

71. de Rie D, Abugessaisa I, Alam T, et al. An integrated expression atlas of miRNAs and their promoters in human and mouse. Nat Biotechnol **2017**; 35:872-8.

72. McCall MN, Kim MS, Adil M, et al. Toward the human cellular microRNAome. Genome Res **2017**; 27:1769-81.

73. Baras AS, Mitchell CJ, Myers JR, et al. miRge - A Multiplexed Method of Processing Small RNA-Seq Data to Determine MicroRNA Entropy. PLoS One **2015**; 10:e0143066.

74. Siddle KJ, Tailleux L, Deschamps M, et al. bacterial infection drives the expression dynamics of microRNAs and their isomiRs. PLoS Genet **2015**; 11:e1005064.

75. Liu CH, Liu H, Ge B. Innate immunity in tuberculosis: host defense vs pathogen evasion. Cell Mol Immunol **2017**; 14:963-75.

76. Zhai W, Wu F, Zhang Y, Fu Y, Liu Z. The Immune Escape Mechanisms of Mycobacterium Tuberculosis. Int J Mol Sci **2019**; 20.

77. Finlay BB, McFadden G. Anti-immunology: evasion of the host immune system by bacterial and viral pathogens. Cell **2006**; 124:767-82.

78. Pai AA, Baharian G, Page Sabourin A, et al. Widespread Shortening of 3' Untranslated Regions and Increased Exon Inclusion Are Evolutionarily Conserved Features of Innate Immune Responses to Infection. PLoS Genet **2016**; 12:e1006338.

79. Behr MA, Wilson MA, Gill WP, et al. Comparative genomics of BCG vaccines by whole-genome DNA microarray. Science **1999**; 284:1520-3.

80. Mahairas GG, Sabo PJ, Hickey MJ, Singh DC, Stover CK. Molecular analysis of genetic differences between Mycobacterium bovis BCG and virulent M. bovis. J Bacteriol **1996**; 178:1274-82.

81. Cui Y, Huang Y, Wu X, et al. Hypoxia-induced tRNA-derived fragments, novel regulatory factor for doxorubicin resistance in triple-negative breast cancer. J Cell Physiol **2019**; 234:8740-51.

82. Prosser G, Brandenburg J, Reiling N, Barry CE, 3rd, Wilkinson RJ, Wilkinson KA. The bacillary and macrophage response to hypoxia in tuberculosis and the consequences for T cell antigen recognition. Microbes Infect **2017**; 19:177-92.

83. Fuhrmann DC, Brune B. Mitochondrial composition and function under the control of hypoxia. Redox Biol **2017**; 12:208-15.

84. Hamacher-Brady A, Brady NR. Mitophagy programs: mechanisms and physiological implications of mitochondrial targeting by autophagy. Cell Mol Life Sci **2016**; 73:775-95.

85. Wang TS, Coppens I, Saorin A, Brady NR, Hamacher-Brady A. Endolysosomal Targeting of Mitochondria Is Integral to BAX-Mediated Mitochondrial Permeabilization during Apoptosis Signaling. Dev Cell **2020**; 53:627-45 e7.

86. Hamacher-Brady A, Brady NR. Bax/Bak-dependent, Drp1-independent Targeting of X-linked Inhibitor of Apoptosis Protein (XIAP) into Inner Mitochondrial Compartments

Counteracts Smac/DIABLO-dependent Effector Caspase Activation. J Biol Chem **2015**; 290:22005-18.

87. Gorlewicz A, Krawczyk K, Szczepankiewicz AA, Trzaskoma P, Mulle C, Wilczynski GM. Colocalization Colormap -an ImageJ Plugin for the Quantification and Visualization of Colocalized Signals. Neuroinformatics **2020**; 18:661-4.

88. Jamwal SV, Mehrotra P, Singh A, Siddiqui Z, Basu A, Rao KV. Mycobacterial escape from macrophage phagosomes to the cytoplasm represents an alternate adaptation mechanism. Sci Rep **2016**; 6:23089.

89. Shim D, Kim H, Shin SJ. Mycobacterium tuberculosis Infection-Driven Foamy Macrophages and Their Implications in Tuberculosis Control as Targets for Host-Directed Therapy. Front Immunol **2020**; 11:910.

90. Russell DG, Cardona PJ, Kim MJ, Allain S, Altare F. Foamy macrophages and the progression of the human tuberculosis granuloma. Nat Immunol **2009**; 10:943-8.

91. Menon D, Singh K, Pinto SM, et al. Quantitative Lipid Droplet Proteomics Reveals Mycobacterium tuberculosis Induced Alterations in Macrophage Response to Infection. ACS Infect Dis **2019**; 5:559-69.

92. Polena H, Boudou F, Tilleul S, et al. Mycobacterium tuberculosis exploits the formation of new blood vessels for its dissemination. Sci Rep **2016**; 6:33162.

93. Uusi-Makela M, Ramet M. Hijacking Host Angiogenesis to Drive Mycobacterial Growth. Cell Host Microbe **2018**; 24:465-6.

94. Harding JS, Herbath M, Chen Y, et al. VEGF-A from Granuloma Macrophages Regulates Granulomatous Inflammation by a Non-angiogenic Pathway during Mycobacterial Infection. Cell Rep **2019**; 27:2119-31 e6.

95. Sabir N, Hussain T, Shah SZA, Peramo A, Zhao D, Zhou X. miRNAs in Tuberculosis: New Avenues for Diagnosis and Host-Directed Therapy. Front Microbiol **2018**; 9:602.

96. Etna MP, Sinigaglia A, Grassi A, et al. Mycobacterium tuberculosis-induced miR-155 subverts autophagy by targeting ATG3 in human dendritic cells. PLoS Pathog **2018**; 14:e1006790.

97. Iwai H, Funatogawa K, Matsumura K, et al. MicroRNA-155 knockout mice are susceptible to Mycobacterium tuberculosis infection. Tuberculosis (Edinb) **2015**; 95:246-50.

98. Rothchild AC, Sissons JR, Shafiani S, et al. MiR-155-regulated molecular network orchestrates cell fate in the innate and adaptive immune response to Mycobacterium tuberculosis. Proc Natl Acad Sci U S A **2016**; 113:E6172-E81.

99. Wang J, Jia Z, Wei B, et al. MicroRNA-27a restrains the immune response to mycobacterium tuberculosis infection by targeting IRAK4, a promoter of the NF-kappaB pathway. Int J Clin Exp Pathol **2017**; 10:9894-901.

100. Hussain T, Zhao D, Shah SZA, et al. MicroRNA 27a-3p Regulates Antimicrobial Responses of Murine Macrophages Infected by Mycobacterium avium subspecies paratuberculosis by Targeting Interleukin-10 and TGF-beta-Activated Protein Kinase 1 Binding Protein 2. Front Immunol **2017**; 8:1915.

101. Cui JY, Liang HW, Pan XL, et al. Characterization of a novel panel of plasma microRNAs that discriminates between Mycobacterium tuberculosis infection and healthy individuals. PLoS One **2017**; 12:e0184113.

102. Chen Z, Wang T, Liu Z, et al. Inhibition of Autophagy by MiR-30A Induced by Mycobacteria tuberculosis as a Possible Mechanism of Immune Escape in Human Macrophages. Jpn J Infect Dis **2015**; 68:420-4.

103. Wu Y, Sun Q, Dai L. Immune regulation of miR-30 on the Mycobacterium tuberculosis-induced TLR/MyD88 signaling pathway in THP-1 cells. Exp Ther Med **2017**; 14:3299-303.

104. Harris J. Autophagy and IL-1 Family Cytokines. Front Immunol **2013**; 4:83.

105. Shi CS, Kehrl JH. TRAF6 and A20 regulate lysine 63-linked ubiquitination of Beclin-1 to control TLR4-induced autophagy. Sci Signal **2010**; 3:ra42.

106. Sharbati J, Lewin A, Kutz-Lohroff B, Kamal E, Einspanier R, Sharbati S. Integrated microRNA-mRNA-analysis of human monocyte derived macrophages upon Mycobacterium avium subsp. hominissuis infection. PLoS One **2011**; 6:e20258.

107. Nagpal N, Kulshreshtha R. miR-191: an emerging player in disease biology. Front Genet **2014**; 5:99.

108. Zhao Z, Hao J, Li X, Chen Y, Qi X. MiR-21-5p regulates mycobacterial survival and inflammatory responses by targeting Bcl-2 and TLR4 in Mycobacterium tuberculosis-infected macrophages. FEBS Lett **2019**; 593:1326-35.

109. Jo EK, Silwal P, Yuk JM. AMPK-Targeted Effector Networks in Mycobacterial Infection. Front Microbiol **2019**; 10:520.

110. Singhal A, Jie L, Kumar P, et al. Metformin as adjunct antituberculosis therapy. Sci Transl Med **2014**; 6:263ra159.

111. Degner NR, Wang JY, Golub JE, Karakousis PC. Metformin Use Reverses the Increased Mortality Associated With Diabetes Mellitus During Tuberculosis Treatment. Clin Infect Dis **2018**; 66:198-205.

112. Dubey RK. Assuming the role of mitochondria in mycobacterial infection. Int J Mycobacteriol **2016**; 5:379-83.

113. Jamwal S, Midha MK, Verma HN, Basu A, Rao KV, Manivel V. Characterizing virulence-specific perturbations in the mitochondrial function of macrophages infected with Mycobacterium tuberculosis. Sci Rep **2013**; 3:1328.

114. Abarca-Rojano E, Rosas-Medina P, Zamudio-Cortez P, Mondragon-Flores R, Sanchez-Garcia FJ. Mycobacterium tuberculosis virulence correlates with mitochondrial cytochrome c release in infected macrophages. Scand J Immunol **2003**; 58:419-27.

115. Dallenga T, Repnik U, Corleis B, et al. M. tuberculosis-Induced Necrosis of Infected Neutrophils Promotes Bacterial Growth Following Phagocytosis by Macrophages. Cell Host Microbe **2017**; 22:519-30 e3.

116. Divangahi M, Behar SM, Remold H. Dying to live: how the death modality of the infected macrophage affects immunity to tuberculosis. Adv Exp Med Biol **2013**; 783:103-20.

117. Zorova LD, Popkov VA, Plotnikov EY, et al. Mitochondrial membrane potential. Anal Biochem **2018**; 552:50-9.

118. Samali A, Fulda S, Gorman AM, Hori O, Srinivasula SM. Cell stress and cell death. Int J Cell Biol **2010**; 2010:245803.

119. Yu W, Goncalves KA, Li S, et al. Plexin-B2 Mediates Physiologic and Pathologic Functions of Angiogenin. Cell **2017**; 171:849-64 e25.

120. Stavru F, Bouillaud F, Sartori A, Ricquier D, Cossart P. Listeria monocytogenes transiently alters mitochondrial dynamics during infection. Proc Natl Acad Sci U S A **2011**; 108:3612-7.

121. Hos NJ, Ganesan R, Gutierrez S, et al. Type I interferon enhances necroptosis of Salmonella Typhimurium-infected macrophages by impairing antioxidative stress responses. J Cell Biol **2017**; 216:4107-21.

122. Pliatsika V, Loher P, Magee R, et al. MINTbase v2.0: a comprehensive database for tRNA-derived fragments that includes nuclear and mitochondrial fragments from all The Cancer Genome Atlas projects. Nucleic Acids Res **2018**; 46:D152-D9.

123. Kumar P, Mudunuri SB, Anaya J, Dutta A. tRFdb: a database for transfer RNA fragments. Nucleic Acids Res **2015**; 43:D141-5.

124. Behar SM, Martin CJ, Booty MG, et al. Apoptosis is an innate defense function of macrophages against Mycobacterium tuberculosis. Mucosal Immunol **2011**; 4:279-87.

125. Beckwith KS, Beckwith MS, Ullmann S, et al. Plasma membrane damage causes NLRP3 activation and pyroptosis during Mycobacterium tuberculosis infection. Nat Commun **2020**; 11:2270.

126. Schwebach JR, Jacobs WR, Jr., Casadevall A. Sterilization of Mycobacterium tuberculosis Erdman samples by antimicrobial fixation in a biosafety level 3 laboratory. J Clin Microbiol **2001**; 39:769-71.

127. Chen J, McSwiggen D, Unal E. Single Molecule Fluorescence In Situ Hybridization (smFISH) Analysis in Budding Yeast Vegetative Growth and Meiosis. J Vis Exp **2018**.

128. Zhang X, Tan Y, Ling Y, et al. Viral and host factors related to the clinical outcome of COVID-19. Nature **2020**; 583:437-40.

129. Giamarellos-Bourboulis EJ, Netea MG, Rovina N, et al. Complex Immune Dysregulation in COVID-19 Patients with Severe Respiratory Failure. Cell Host Microbe **2020**; 27:992-1000 e3.

130. Huang C, Wang Y, Li X, et al. Clinical features of patients infected with 2019 novel coronavirus in Wuhan, China. Lancet **2020**; 395:497-506.

131. Chen G, Wu D, Guo W, et al. Clinical and immunological features of severe and moderate coronavirus disease 2019. J Clin Invest **2020**; 130:2620-9.

132. Lucas C, Wong P, Klein J, et al. Longitudinal analyses reveal immunological misfiring in severe COVID-19. Nature **2020**; 584:463-9.

133. Blanco-Melo D, Nilsson-Payant BE, Liu WC, et al. Imbalanced Host Response to SARS-CoV-2 Drives Development of COVID-19. Cell **2020**; 181:1036-45 e9.

134. Kuriakose T, Kanneganti TD. Regulation and functions of NLRP3 inflammasome during influenza virus infection. Mol Immunol **2017**; 86:56-64.

135. Lupfer C, Malik A, Kanneganti TD. Inflammasome control of viral infection. Curr Opin Virol **2015**; 12:38-46.

136. Chattergoon MA, Latanich R, Quinn J, et al. HIV and HCV activate the inflammasome in monocytes and macrophages via endosomal Toll-like receptors without induction of type 1 interferon. PLoS Pathog **2014**; 10:e1004082.

137. Evavold CL, Kagan JC. Inflammasomes: Threat-Assessment Organelles of the Innate Immune System. Immunity **2019**; 51:609-24.

138. Yap JKY, Moriyama M, Iwasaki A. Inflammasomes and Pyroptosis as Therapeutic Targets for COVID-19. J Immunol **2020**; 205:307-12.

139. Rayamajhi M, Zhang Y, Miao EA. Detection of pyroptosis by measuring released lactate dehydrogenase activity. Methods Mol Biol **2013**; 1040:85-90.

140. Liang W, Liang H, Ou L, et al. Development and Validation of a Clinical Risk Score to Predict the Occurrence of Critical Illness in Hospitalized Patients With COVID-19. JAMA Intern Med **2020**; 180:1081-9.

141. Young BE, Ong SWX, Ng LFP, et al. Viral dynamics and immune correlates of COVID-19 disease severity. Clin Infect Dis **2020**.

142. Siu KL, Yuen KS, Castano-Rodriguez C, et al. Severe acute respiratory syndrome coronavirus ORF3a protein activates the NLRP3 inflammasome by promoting TRAF3-dependent ubiquitination of ASC. FASEB J **2019**; 33:8865-77.

143. da Costa LS, Outlioua A, Anginot A, Akarid K, Arnoult D. RNA viruses promote activation of the NLRP3 inflammasome through cytopathogenic effect-induced potassium efflux. Cell Death Dis **2019**; 10:346.

144. Nieto-Torres JL, Verdia-Baguena C, Jimenez-Guardeno JM, et al. Severe acute respiratory syndrome coronavirus E protein transports calcium ions and activates the NLRP3 inflammasome. Virology **2015**; 485:330-9.

145. Chen IY, Moriyama M, Chang MF, Ichinohe T. Severe Acute Respiratory Syndrome Coronavirus Viroporin 3a Activates the NLRP3 Inflammasome. Front Microbiol **2019**; 10:50.

146. Fitzgerald KA, Kagan JC. Toll-like Receptors and the Control of Immunity. Cell **2020**; 180:1044-66.

147. Iwasaki A. A virological view of innate immune recognition. Annu Rev Microbiol **2012**; 66:177-96.

148. Chan AH, Schroder K. Inflammasome signaling and regulation of interleukin-1 family cytokines. J Exp Med **2020**; 217.

149. Schnappauf O, Chae JJ, Kastner DL, Aksentijevich I. The Pyrin Inflammasome in Health and Disease. Front Immunol **2019**; 10:1745.

150. Lieberman J, Wu H, Kagan JC. Gasdermin D activity in inflammation and host defense. Sci Immunol **2019**; 4.

151. Liu X, Zhang Z, Ruan J, et al. Inflammasome-activated gasdermin D causes pyroptosis by forming membrane pores. Nature **2016**; 535:153-8.

152. Swanson KV, Deng M, Ting JP. The NLRP3 inflammasome: molecular activation and regulation to therapeutics. Nat Rev Immunol **2019**; 19:477-89.

153. Frank D, Vince JE. Pyroptosis versus necroptosis: similarities, differences, and crosstalk. Cell Death Differ **2019**; 26:99-114.

154. Takayama K. In Vitro and Animal Models for SARS-CoV-2 research. Trends Pharmacol Sci **2020**; 41:513-7.

155. Botto S, Abraham J, Mizuno N, et al. Human Cytomegalovirus Immediate Early 86-kDa Protein Blocks Transcription and Induces Degradation of the Immature Interleukin-1beta Protein during Virion-Mediated Activation of the AIM2 Inflammasome. mBio **2019**; 10.

156. Karaba AH, Kopp SJ, Longnecker R. Herpesvirus entry mediator and nectin-1 mediate herpes simplex virus 1 infection of the murine cornea. J Virol **2011**; 85:10041-7.

157. Schaecher SR, Mackenzie JM, Pekosz A. The ORF7b protein of severe acute respiratory syndrome coronavirus (SARS-CoV) is expressed in virus-infected cells and incorporated into SARS-CoV particles. J Virol **2007**; 81:718-31.

158. Schaecher SR, Touchette E, Schriewer J, Buller RM, Pekosz A. Severe acute respiratory syndrome coronavirus gene 7 products contribute to virus-induced apoptosis. J Virol **2007**; 81:11054-68.

159. Satis H, Ozger HS, Aysert Yildiz P, et al. Prognostic value of interleukin-18 and its association with other inflammatory markers and disease severity in COVID-19. Cytokine **2021**; 137:155302.

160. Del Valle DM, Kim-Schulze S, Huang HH, et al. An inflammatory cytokine signature predicts COVID-19 severity and survival. Nat Med **2020**; 26:1636-43.

161. Ng DHL, Choy CY, Chan YH, et al. Fever Patterns, Cytokine Profiles, and Outcomes in COVID-19. Open Forum Infect Dis **2020**; 7:ofaa375.

162. Abderrazak A, Syrovets T, Couchie D, et al. NLRP3 inflammasome: from a danger signal sensor to a regulatory node of oxidative stress and inflammatory diseases. Redox Biol **2015**; 4:296-307.

163. Guo H, Callaway JB, Ting JP. Inflammasomes: mechanism of action, role in disease, and therapeutics. Nat Med **2015**; 21:677-87.

164. Mantovani A, Dinarello CA, Molgora M, Garlanda C. Interleukin-1 and Related Cytokines in the Regulation of Inflammation and Immunity. Immunity **2019**; 50:778-95.

165. Karaba AH, Figueroa A, Massaccesi G, Botto S, DeFilippis VR, Cox AL. Herpes simplex virus type 1 inflammasome activation in proinflammatory human macrophages is dependent on NLRP3, ASC, and caspase-1. PLoS One **2020**; 15:e0229570.

166. Allen IC, Scull MA, Moore CB, et al. The NLRP3 inflammasome mediates in vivo innate immunity to influenza A virus through recognition of viral RNA. Immunity **2009**; 30:556-65.

167. Mariathasan S, Weiss DS, Newton K, et al. Cryopyrin activates the inflammasome in response to toxins and ATP. Nature **2006**; 440:228-32.

168. Freeman TL, Swartz TH. Targeting the NLRP3 Inflammasome in Severe COVID-19. Front Immunol **2020**; 11:1518.

169. Zheng M, Williams EP, Malireddi RKS, et al. Impaired NLRP3 inflammasome activation/pyroptosis leads to robust inflammatory cell death via caspase-8/RIPK3 during coronavirus infection. J Biol Chem **2020**; 295:14040-52.

170. Hou YJ, Okuda K, Edwards CE, et al. SARS-CoV-2 Reverse Genetics Reveals a Variable Infection Gradient in the Respiratory Tract. Cell **2020**; 182:429-46 e14.

171. Jain A, Irizarry-Caro RA, McDaniel MM, et al. T cells instruct myeloid cells to produce inflammasome-independent IL-1beta and cause autoimmunity. Nat Immunol **2020**; 21:65-74.

172. Moossavi M, Parsamanesh N, Bahrami A, Atkin SL, Sahebkar A. Role of the NLRP3 inflammasome in cancer. Mol Cancer **2018**; 17:158.

173. Aarreberg LD, Esser-Nobis K, Driscoll C, Shuvarikov A, Roby JA, Gale M, Jr. Interleukin-1beta Induces mtDNA Release to Activate Innate Immune Signaling via cGAS-STING. Mol Cell **2019**; 74:801-15 e6.

174. Huet T, Beaussier H, Voisin O, et al. Anakinra for severe forms of COVID-19: a cohort study. Lancet Rheumatol **2020**; 2:e393-e400.

175. Dimopoulos G, de Mast Q, Markou N, et al. Favorable Anakinra Responses in Severe Covid-19 Patients with Secondary Hemophagocytic Lymphohistiocytosis. Cell Host Microbe **2020**; 28:117-23 e1.

176. Group RC, Horby P, Lim WS, et al. Dexamethasone in Hospitalized Patients with Covid-19. N Engl J Med **2021**; 384:693-704.

177. Shi CS, Nabar NR, Huang NN, Kehrl JH. SARS-Coronavirus Open Reading Frame-8b triggers intracellular stress pathways and activates NLRP3 inflammasomes. Cell Death Discov **2019**; 5:101.

178. Xu H, S.A. Chitre, I.A. Akinyemi, J.C. Loeb, J.A. Lednicky, M.T. McIntosh, and S. Bhaduri-McIntosh. SARS-CoV-2 viroporin triggers the NLRP3 inflammatory pathway. bioRxiv **2020**.

179. V'Kovski P, Kratzel A, Steiner S, Stalder H, Thiel V. Coronavirus biology and replication: implications for SARS-CoV-2. Nat Rev Microbiol **2021**; 19:155-70.

180. Chen W, Xu Y, Li H, et al. HCV genomic RNA activates the NLRP3 inflammasome in human myeloid cells. PLoS One **2014**; 9:e84953.

181. Scully EP, Haverfield J, Ursin RL, Tannenbaum C, Klein SL. Considering how biological sex impacts immune responses and COVID-19 outcomes. Nat Rev Immunol **2020**; 20:442-7.

182. van der Made CI, Simons A, Schuurs-Hoeijmakers J, et al. Presence of Genetic Variants Among Young Men With Severe COVID-19. JAMA **2020**.

183. BETADataLab. How is the federal government funding relief efforts for COVID-19. Available at: https://datalab.usaspending.gov/federal-covid-funding/#:~:text=How%20much%20supplemental%20funding%20has,loan%20and%20loan%20guarantee%20programs.

Vita

Monika Looney

Cell: (301) 938-0045 **Email:** monika.m.looney@gmail.com

Education

Johns Hopkins School of Medicine — **Matriculation: August 2016**
Department of Pathology — Pathobiology PhD Program
Baltimore, MD 21205 — Chief Graduate Student 2018-2019

Johns Hopkins Bloomberg School of Public Health — **August 2018 – October 2020**
Global Health Certificate Program
Department of International Health
Baltimore, MD 21205

University of Maryland — **August 2012 – May 2016**
Integrated Life Sciences Honors College — B.S. Microbiology
Departmental Honors: Cell Biology & Molecular Genetics — B.S. Psychology
College Park, MD 20742

Research Experience

Karakousis Lab — **August – December 2016; June 2017 – Present**
Johns Hopkins School of Medicine
Department of Infectious Diseases, Center for Tuberculosis research

- Investigate regulation of small RNAs (i.e. microRNAs and tRNA-derived fragments in infection with *Mycobacterium tuberculosis* (*Mtb*) and SARS-CoV-2 (SARS-COV-2)
- Study the connection between small RNA dysregulation and mitochondrial distress in *Mtb* infection
- Examine the role of inflammasome activation in modulating host cell outcomes in SARS-COV-2 infection
- **Thesis:** From microRNAs to mitochondria in the macrophage response to *Mycobacterium tuberculosis*: and work on the COVID19 pandemic
- **Skills:** BSL-3 safety and standard operating procedures, mammalian cell culture, bacterial cell culture, SARS-COV-2 viral culture, epithelial and immune cell infection models, RNA extraction, qRT-PCR, ELISA, antibody staining, fluorescent imaging, transfection, RNA and microRNA sequencing analysis, R (working knowledge)
- **Translational rotations:** Non-tuberculosis mycobacteria clinic shadowing (February 2021), COVID19 vaccination clinic volunteer (February 2021)

Roden Lab — **April – June 2017**
Johns Hopkins School of Medicine
Department of Gynecologic Pathology

- Optimized HPV cell culture models and protocols for genetic engineering of MusPV1 genome constructs
- Developed and tested infection and transfection protocols for producing virus-like particles to be used for future vaccine studies
- **Skills:** Fibroblast and epithelial cell culture, production of virus-like particles, mammalian cell culture viral infection, mouse tail viral challenge

Nuermberger Lab **January – April 2017**
Johns Hopkins School of Medicine
Department of Infectious Diseases, Center for Tuberculosis Research

- Characterized *Mtb pks3* mutant strain to investigate the role of pks3 in conferring resistance to bedaqualine, pretomanid, and clofazimine anti-tuberculosis drugs
- **Skills:** Complementation assays in *Mtb*, *Mtb* culture in iron depletion conditions, bacterial mutant screens and selections

Jose Lab **March 2013 – April 2016**
University of Maryland
Department of Cell Biology and Molecular Genetics

- Investigated the relationship between silencing of multicopy DNA and equal cell division
- Researched pathways involved in suppression of silencing of multiocpy DNA in *Caenorhabditis elegans* somatic cells
- **Thesis:** Regulation of RNA-directed silencing of repetitive DNA in *Caenorhabditis elegans*
- **Skills:** Fluorescent imaging, gel electrophoresis, *Caenorhabditis elegans* strain maintenance, bacterial transformation

Publications

Looney MM*, Butscheck G*, Saorin A, Hamacher-Brady A, Karakousis PC. (*in preparation*). *Mycobacterium tuberculosis* disrupts mitochondrial responses to evade host macrophage mediated killing
* Equal first authors

Looney MM, Lorenc R, Halushka MK, Karakousis PC. (*in preparation*). Key macrophage responses to infection with *Mycobacterium tuberculosis* are co-regulated by microRNAs and methylation

Karaba AH*, **Looney MM***, Hsieh L-Y*, Figueroa A*, Massaccesi G, Bullen K, Ordoñez A, Pekosz A, Botto S, DeFilippis VR, Karakousis PC, Cox AL. (*in preparation*). Macrophage sensing of SARS-CoV-2 induces NLRP3-dependent inflammasome activation via MyD88 signaling
* Equal first authors

Looney MM, Lu Y, Karakousis PC, Halushka MK. (2020). *Mycobacterium tuberculosis* infection drives mitochondria-biased dysregulation of host tRNA-derived fragments. *J Infect Dis.* PMID: 32959876

Bullen CK, Hogberg HT, Bahadirli-Talbott A, Bishai WR, Hartung T, Keuthan C, **Looney MM**, Pekosz A, Romero JC, Sillé FCM, Um P, Smirnova L. (2020). Infectability of human BrainSphere neurons suggests neurotrophism of SARS-CoV-2. *ALTEX*. PMID: 32591839

Le HH, **Looney MM**, Strauss B, Bloodgood M, Jose AM. (2016). Tissue homogeneity requires equal inhibition of unequal gene silencing during development. *J Cell Biol,* PMID: 27458132

Published Datasets

Looney MM, Karakousis PC. (2021). RNA sequencing-based analysis of transcriptional reprogramming of primary human monocyte-derived macrophages infected with *Mycobacterium tuberculosis*. NCBI GEO Accession Number: GSE164287

Looney MM, Halushka MK, Karakousis PC. (2020). Differential production of small RNAs in *Mycobacterium tuberculosis* infected primary human monocyte-derived macrophages. NCBI GEO Accession Number: GSE151050

Published Abstracts

Looney MM, Lu Y, Butscheck G, Hamacher-Brady A, Karakousis PC, Halushka MK. (2020). *Mycobacterium tuberculosis* infection drives mitochondria-biased dysregulation of host tRNA-derived fragments. *Keystone Tuberculosis eSymposia: Science Aimed at Ending the Epidemic Abstract Book, ePoster*

Looney MM, Halushka MK, Karakousis PC. (2020). MicroRNA and tRNA fragment dysregulation in the macrophage response to *Mycobacterium tuberculosis*. *Keystone Tuberculosis Meeting: Immunity and Immune Evasion Abstract Book*, 2034

Dutta NK, **Looney MM**, Bruniers N, Pinn ML, Dartois V, Gennaro ML, Karakousis PC. Preclinical testing of statins as adjunctive, host-directed therapy for TB. (2018). *Keystone Tuberculosis Meeting: Translating Scientific Findings for Clinical and Public Health Impact Abstract Book,* 2031

Le HH, Edwards LO, **Looney MM**, Strauss B, Bloodgood M, Jose AM. (2015). Tissue homogeneity requires inhibition of stochastic RNA silencing. *Genetics Society of America Conference Abstract Book*, 1008B

Talks

Pathobiology Recruitment **January 2020**
Johns Hopkins University

tRNA-derived fragments and mitochondrial dysfunction in tuberculosis

Center for Tuberculosis Research Annual Meeting **June 2019**
Johns Hopkins University
Small RNA dysregulation in tuberculosis

Pathology Grand Rounds **July 2018**
Johns Hopkins University
Investigations into the roles of microRNAs in tuberculosis pathogenesis and treatment

Undergraduate Cell Biology and Molecular Genetics **April 2016**
Honors Thesis Defense
University of Maryland, College Park
Regulation of RNA-directed silencing of repetitive DNA in *Caenorhabditis elegans*

Baltimore Worm Club **July 2015**
University of Maryland, Baltimore County
Inhibition of stochastic RNA silencing reduces cell-to-cell variation in *Caenorhabditis elegans*

Posters

Keystone Tuberculosis eSymposia **December 2020**
Science Aimed at Ending the Epidemic
Virtual Symposia
Looney MM, Lu Y, Butscheck G, Hamacher-Brady A, Karakousis PC, Halushka MK. *Mycobacterium tuberculosis* infection drives mitochondria-biased dysregulation of host tRNA-derived fragments.

Keystone Tuberculosis Meeting **January 2020**
Immunity and Immune Evasion
Eldorado Hotel, Santa Fe, New Mexico
Looney MM, Halushka MK, Saorin A, Hamacher-Brady A, Karakousis PC. MicroRNA and tRNA fragment dysregulation in *Mycobacterium tuberculosis*-infected primary human macrophages

Pathobiology Program Retreat **September 2019**
Mount Washington Conference Center, Baltimore, Maryland
Looney MM, Halushka MK, Karakousis PC. The marvelous microcosm of microRNAs (and tRFs) in *Mycobacterium tuberculosis* infected macrophages

Pathology Young Investigators Day **March 2019**
Johns Hopkins University, School of Medicine
Looney MM, Karakousis PC. Combining inflammasome activation with direct antimicrobial activity to enhance killing of *Mycobacterium tuberculosis*

Pathobiology Program Retreat **September 2018**
Mount Washington Conference Center, Baltimore, Maryland
Looney MM, Karakousis PC. The roles of microRNAs in tuberculosis pathogenesis and treatment

Keystone Tuberculosis Meeting **April 2018**
Translating Scientific Findings for Clinical and Public Health Impact
Fairmont Chateau, Whistler, British Columbia, Canada
Dutta NK, **Looney MM**, Bruniers N, Pinn ML, Dartois V, Gennaro ML, Karakousis PC. Preclinical testing of statins as adjunctive, host-directed therapy for TB

Department of Medicine Retreat **April 2018**
Johns Hopkins University, School of Medicine
Looney MM, Karakousis PC. Protocol optimization for tuberculosis miRNA biomarker discovery assays

Pathology Young Investigators Day **March 2018**
Johns Hopkins University, School of Medicine
Looney MM, Karakousis PC. Protocol optimization for tuberculosis miRNA biomarker discovery assays

Pathobiology Program Retreat **September 2017**
Mount Washington Conference Center, Baltimore, Maryland
Looney MM, Karakousis PC. Preliminary investigations into microRNA-mediated modulation of lipogenesis and inflammation in pravastatin adjunctive therapy for active TB

HHMI Undergraduate Research Symposium **March 2016**
University of Maryland, College Park
Le HH[*], **Looney MM**[*], Strauss B, Bloodgood M, Jose AM. Tissue homogeneity requires inhibition of stochastic RNA silencing ([*]Equal Contribution)

International *C. elegans* Meeting **June 2015**
University of California, Los Angeles
Le HH[*], Edwards LO[*], **Looney MM**[*], Strauss B, Bloodgood M, Jose AM. Tissue homogeneity requires embryonic inhibition of stochastically-initiated RNA silencing ([*]Equal Contribution)

Professional Experience and Leadership

Don Amolo Memorial Kid's Ark **January 2015 – Present**
Volunteer Foreign Contact
- Travel to Kenya to assist the Don Amolo Memorial Kid's Ark for children affected by HIV with coordinating free medical camps and conducting community needs assessments
- Facilitate collaborations with The Orphan Grain Train

- Designed and implemented a trackable inventory system for the St. James Memorial Medical Clinic

Pathobiology Graduate Program **July 2018 – June 2019**
Chief Graduate Student
- Coordinated with faculty and administrators to develop and implement program changes aimed at addressing student concerns
- Facilitated expansion of mental health resources for students
- Planned / organized journal club, student lunch meetings, recruitment, and orientation events
- Served as a mentor for lowerclassmen

International Volunteer Headquarters **June 2018 – July 2018**
Imara Foundation HIV/AIDS Support Program Volunteer
- Traveled to Arusha, Tanzania to assist women with HIV/AIDS develop / market income-generating skills
- Facilitated collaborations with The One Acre Fund and the Don Amolo Memorial Kid's Ark

Graduate Student Association **July 2017 – December 2018**
Student Assistance Program Committee Representative
- Coordinated with Student Assistance Program staff members to determine ways to improve graduate student access to psychological health resources
- Coordinated with executive board members of the Graduate Student Association to facilitate discussion about the importance of psychological health on campus and in the community
- Wrote and distributed to the Johns Hopkins School of Medicine graduate students a monthly Wellness Newsletter that provides information and tips for maintaining psychological, physical, and social wellness

Teaching and Mentoring Experience

Tender Bridge **January 2021 – Present**
Mountain biking program and COVID19 safety coordinator
- Coordinate mountain biking focused sports-mentoring program for at risk Baltimore youth
- Develop a COVID19 response strategy to encourage adherence to public health guidelines and vaccine uptake amongst mentors and mentees

Karakousis Lab **September 2017 – Present**
Graduate Student Mentor
- Train junior lab members on laboratory techniques and biosafety level 3 standard operating procedures
- Teach trainees to conceptualize independent research projects
- Assist trainees in the process of applying for independent research funding
- **Current Trainees:** Harley Parker (junior PhD student, Pathobiology Program, Johns Hopkins School of Medicine), Samuel Ayeh (clinical fellow), Pranita Neupane (clinical fellow)

- **Former Trainees:** Rachel Lorenc (undergraduate, Johns Hopkins University), Grace Ren (undergraduate, Johns Hopkins University), Nathan Crilly (rotation PhD student, Johns Hopkins School of Medicine)

Pathobiology PhD Program **September 2017 – June 2019**
Big Sibling
- Assist lowerclassmen in the Pathobiology PhD Program with their transition into graduate school

Graduate Infectious Disease and Immunology **April 2018, 2019**
Teaching Assistant
- Scheduled faculty lectures
- Assisted students with course content during class and review sessions
- Taught lecture on Zika, Dengue, and Yellow Fever

Graduate Basic Mechanisms of Disease **August-September 2017, 2018**
Teaching Assistant
- Helped re-design course material
- Served as lead TA for content related to infectious disease and immunology
- Taught lecture on fundamental immunology

Johns Hopkins Peer Mentoring Committee **August 2017 – January 2018**
Peer Mentor
- Participated as a mentor for other graduate students during scheduled group discussion about stressful situations students may experience
- Assisted in planning group discussions and peer mentoring events
- Served as a liaison to the Student Assistance Program

Professional Societies

American Society for Microbiology **February 2018 – Present**
American Association for the Advancement of Science **February 2018 – Present**
American Institute of Biological Sciences **February 2018 – Present**

Grants and Funding

Keystone Tuberculosis Meeting Scholarship **December 2020**
Eukaryotic Tissue Core Facility Core Coins **December 2017**
Howard Hughes Medical Institute Undergraduate Research Fellowship **May 2015 – May 2016**
Howard Hughes Medical Institute Capstone Travel Award **June 2015**

Awards and Honors

Johns Hopkins Pathobiology Chief Graduate Student **May 2018**
Omicron Delta Kappa National Leadership Honor Society **May 2016**
Primannum Honors Society **May 2013**
Alicia Betancourt Scholarship **April 2012**
National Order of the Elks Scholarship **May 2012**